Searching for Extra-Terrestrial Intelligence Through Multi-wavelength Observations

M.Sc Thesis

By

Priyatam Kumar Mahto

Department of Astronomy, Astrophysics and Space Engineering

INDIAN INSTITUTE OF TECHNOLOGY INDORE

May, 2023

Searching for Extra-Terrestrial Intelligence Through Multi-wavelength Observations

M.Sc Thesis

Submitted in partial fulfillment of the requirements for the awards of the degree
of
Master of Science in Astronomy

by

Priyatam Kumar Mahto

Department of Astronomy, Astrophysics and Space Engineering

INDIAN INSTITUTE OF TECHNOLOGY INDORE

May, 2023

INDIAN INSTITUTE OF TECHNOLOGY INDORE

CANDIDATE'S DECLARATION

I hereby certify that the work which is being presented in the thesis entitled **Searching for Extra-Terrestrial Intelligence Through Multi-wavelength Observations** in the partial fulfilment of the requirements for the award of the degree of **MASTER OF SCIENCE** and submitted in the **DISCIPLINE OF ASTRONOMY, ASTROPHYSICS AND SPACE ENGINEERING, Indian Institute of Technology Indore**, is an authentic record of my own work carried out during the time period from June 2022 to May 2023 under the supervision of Dr. Suman Majumdar, Associate Professor, Department of Astronomy, Astrophysics and Space Engineering, Indian Institute of Technology, Indore and Dr. Erik Zackrisson, Associate Professor, Department of Physics and Astronomy, Uppsala University Sweden.

The matter presented in this thesis has not been submitted by me for the award of any other degree of this or any other institute.

3 May 2023

Signature of the student with date
Priyatam Kumar Mahto

This is to certify that the above statement made by the candidate is correct to the best of my/our knowledge.

03 May 2023
Signature of the Supervisor of
M.Sc. thesis #1 (with date)
Dr. Suman Majumdar

04 May 2023
Signature of the Supervisor of
M.Sc. thesis #2 (with date)
Dr. Erik Zackrisson

Priyatam Kumar Mahto has successfully given his M.Sc. Oral Examination held on **24 April 2023**.

Dr. Manoneeta Chakraborty
Signature of PSPC Member #1
Date: 06/05/2023

Prof. Subhendu Rakshit
Signature of PSPC Member #2
Date: 06/05/2023

1. 03 May 2023
2. 04 May 2023
Signature(s) of Supervisor(s) of MSc thesis
Date: 1. 2.

Signature of M.Sc. Co-Ordinator
Date: 06/05/2023

Convener, DPGC
Date: 02/06/2023

Signature of HoD (Officiating)
Date: 06/06/2023

ACKNOWLEDGEMENTS

I would like to express my deep appreciation to my supervisors, Dr. Suman Majumdar and Dr. Erik Zackrisson, for granting me the privilege to work on this project and providing me with exceptional guidance. Their unwavering support, motivation, and belief in me have been invaluable, particularly during challenging times. My collaborator, Mr. Matías Suazo, deserves special recognition for his constant support throughout this project. His valuable insights and contributions have been crucial in helping me achieve my research goals. I would also like to extend my gratitude to my labmates, Mr. Chandra Shekhar Murmu and Mr. Saswata Dasgupta, for their invaluable guidance and assistance throughout the course of this project in helping me to overcome any obstacles I encountered. I am immensely grateful to the Department of Astronomy, Astrophysics and Space Engineering for allowing me to make a contribution to this vibrant field. I would also like to extend my heartfelt gratitude to my friend Pranjali for her unflinching support, encouragement, and unwavering belief in me. Her support and motivation have been invaluable throughout this project. I would also like to express my gratitude to my classmates, especially Ved, for their continuous inspiration and encouragement, which has motivated me to strive for excellence in all aspects of this project. Finally, I am indebted to my mother, father, and brother for their encouragement and support, which have given me the courage to venture into this entirely new field.

Dedicated

to

my mother and father

“Two possibilities exist: either we are alone in the Universe or we are not. Both are equally terrifying.”

- Arthur C. Clarke, 1999

Abstract

The Copernican principle states that the Earth is not a special location in the Universe. However, so far this is the only planet known to humankind which can support life. This is why we have always been curious to know whether intelligent life exists in some other parts of the universe or not. Humans have collectively spent 60-plus years in Searching for Extraterrestrial Intelligence (SETI), without any success so far. This is known as the Fermi paradox.

Many efforts have been made throughout history to resolve this paradox in several ways. One such approach is to search for Dyson Spheres (Dyson, 1960), a hypothetical megastructure built by advanced extraterrestrial civilizations around their host star for harvesting its radiation energy. The aim of SETI is to search for observational signatures of Dyson spheres, which are marked by a change in the spectrum of the star. This change is expected to be in the form of waste heat from the absorbing structure (radiation emitted in the infrared) and obscuration of direct starlight. Suazo et al. (2022) had identified a tentative list of DS candidates in the Milky Way by fitting Spectral Energy Distribution (SED) based model of DS with observed data through GAIA, SDSS, DSS in the optical band and 2MASS, WISE in the infrared band.

It has been observed, though very rarely, that some stars do exhibit the spectral energy distributions of the type predicted for Dyson spheres. In most cases, there may be astrophysical explanations for this behaviour. In this category, we primarily find Young Stellar Objects (YSOs), which are mostly located in nebular regions.

Suazo et al. 2023 (in prep.) have developed a Convolution Neural Network (CNN) based image classifier to classify stars into two categories depending on whether they belong to a nebular or non-nebular region by analyzing W3 images of sources in WISE survey. However, this algorithm fails sometimes to detect any nebular feature surrounding a star having the signature of a Dyson sphere even though literature surveys indicate that the star is very young.

In this thesis, we present a technique, which can further filter out the false-positive Dyson sphere candidates using the phenomenon of dust reddening. This happens due to the fact that the shorter wavelength lights get absorbed and scattered by dust particles from the surrounding nebula of a target star while longer wavelength lights pass through it. This results in a higher fraction of red stars in a nebular region than in a non-nebular region within a certain angular radius around the target star. We use this as the basic principle for our filtration technique.

Our analysis shows that the fraction of neighbouring red stars for YSOs (like Herbig Ae/Be and T-Tauri star) around a search radius of 6 arc minutes is greater than

that of the randomly chosen main sequence star. Using a sample of 218 randomly chosen main sequence, Herbig Ae/Be and T-Tauri stars, we find that the average fraction of red stars for Herbig Ae/Be is 0.681 ± 0.259 and T Tauri star is 0.871 ± 0.063 while the average fraction of neighbouring red stars for a randomly chosen main sequence star is 0.340 ± 0.292. By analyzing the fraction of neighboring red stars for all 302 DS candidates, we were able to distinguish between Dyson Sphere candidates located within nebular regions and those outside. This parameter, combined with manual inspection of DS candidates across multiple databases, led us to discard 136 contaminated candidates out of the original 302. These were eliminated due to factors such as blending with nearby sources, irregular structure in the WISE data, and faintness. We are planning to conduct detailed follow-up observations on the remaining 166 candidates, focusing on our best Dyson Sphere candidates.

Contents

List of Figures

List of Tables

CHAPTER 1

Introduction

Humans have spent thousands of years looking at the stars in the night sky and thinking about them. Many questions must have come to their mind about the bright objects of the night sky, but one specific question that they surely have come across is that "Do lives exist outside the Earth?". We, humans, are always curious and have been searching for the answer to that question.

Until the late 1540s, humans believed that the Earth is the centre of the universe and that everything orbits around the Earth. It was only in 1548 that the Copernican theory emerged, which led us to believe that the Earth is not the centre of the universe. Earth is just another planet in the solar system like Venus, Mars, Jupiter, Saturn etc and revolves around the Sun along with these other planets. Therefore, it can be safely said that the Earth is not a special planet in the universe. Humans got the idea that there are possibilities of having millions of Earth-like planets in the universe, which revolve around some stars and some of them might have the suitable condition to grow life on them. There is also a finite possibility that some of these planets which have sustainable conditions for life to form may actually have some form of life on them. Out of all of these planets in which lives exist, some of them might even have intelligent life on them. For several millennia we have asked our philosophers and priest the question "Do lives exist outside the Earth?". Several religions and branches of philosophy had tried to provide answers to this question as well (Dick, 1998). However, a scientific answer to the same requires verifiable evidence, which makes it a more difficult task due to the following reasons: Whether there are extraterrestrial intelligent lives exist or not, depends on the criteria of intelligence that are set by us. Further, the signature of their intelligence will be reflected via their advancement in science and technology. Additionally, our own technological development has to be also good enough to be able to build sensitive enough instruments that can detect the signature of such intelligent lifeforms via our observations of the cosmos.

In the second half of the 20th century, the rules for searching for intelligent lifeforms saw a significant change due to the development of radar technologies. In 1961, for the first time in the history of humanity, scientists and engineers were able to plan and conduct experiments/observation e.g. Project Ozama - which could provide a solution to this crucial and age-old question (Tarter, 2001). Radio telescopes were one of the scientific tools employed in this initial quest for extraterrestrial intelligence. In this period Karl G. Jansky's contributions to the domain of radio astronomy led to the significant advancement of radio communication technologies which allowed scientists to utilise them to search for intelligent extraterrestrial life. Once the technology to search for intelligent extraterrestrial life was in hand, there was a need to formulate an efficient method to conduct these searches effectively. At this point in time, there was a lack of sufficient understanding of the universe, including its sizes and structures, distributions of planets around stars, chances of discovering planets like Earth, size of the solar system, distances between stars, the arrangement of stars in galaxies, and many other such crucial factors. As humans began learning more and more about the cosmos via observations at different wavelengths, it became clear that the answer to the question of whether there is intelligent extraterrestrial life in the Universe is not going to be very simple. However, by knowing the history of our own civilization's gradual development in science and technology, we now have a better understanding of how technological development may progress in an extraterrestrial intelligent civilization. Through the study of our own civilization's history, we have also understood the vital role that energy (and various utilization of it) and its sources play in the progress and sustainability of civilization.

The continuous and sustainable flow of energy is crucial for the survival and progress of a civilization and its advancement in science and technology. Therefore we can assume that a sufficiently intelligent civilization must have figured out the efficient ways of collecting, distributing and storage of energy that is necessary for its survival and progress. This by definition makes them intelligent. Based on this idea, in 1964, Kardashev concluded that, if intelligent civilizations do exist in the universe, their energy consumption may be used as a measure of their intelligence.

1.1 Kardashev Scale

Energy is the fundamental requirement for any civilisation to grow and the amount of energy used by the civilisation also represents the intelligence of that civilisation. Energy consumption is also a measure of "how much a civilisation is technologically developed". Kardashev (1964) gave a classification of technologically developed ETI civilisations based on their energy consumption. The proposed scale by Kardashev (1964) is presented below -

1. **Kardashev Type I civilisation**: Kardashev defined Type I civilisation as - A civilisation whose energy consumption is about the same as the energy consumption of all humans in the 1960s ($\approx 4 \times 10^{12}\ \ W$). They are at the same level of technological advancement as the Earth attended in the 1960s.

But a Type I civilization is typically defined as one that can harness all of the energy that its home planet receives from its parent star (for Earth, this amount is approximately $2 \times 10^{16}\ \ W$), which is four orders of magnitude more than what is currently attained on Earth, with energy consumption at $2 \times 10^{13}\ \ W$ as of 2020 (Ritchie et al., 2022).

2. **Kardashev Type II civilisation**: A civilisation that is capable of harvesting all the radiation energy of its host star. The energy consumption of the ETI is comparable with the luminosity of the Sun ($\approx 4 \times 10^{26}\ \ W$).

3. **Kardashev Type III civilisation**: A civilisation that is capable of harvesting and controlling all the energy at the scale of its host

galaxy. The energy consumption of such ETI is comparable with the luminosity of their galaxy ($\approx 4 \times 10^{36}$ W).
Figure 1.1 describes the visual representation of all three Kardashev-type civilisations and their energy consumption.

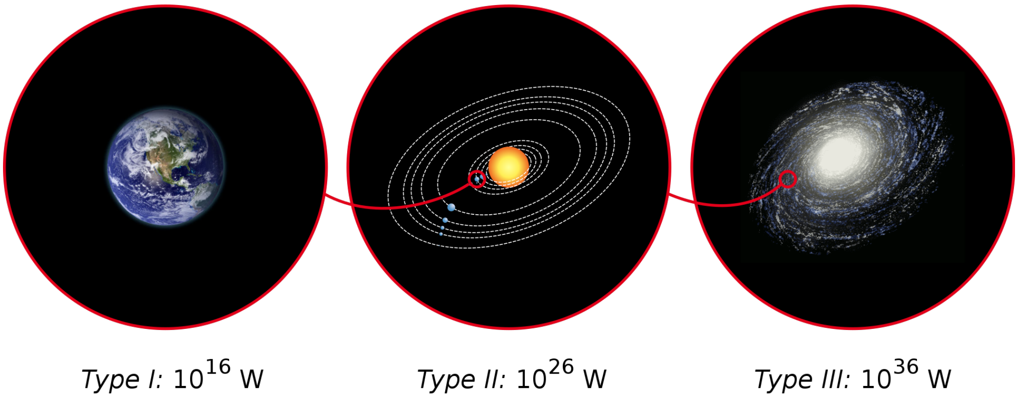

Figure 1.1: Representative figure of Kardashev Scale. Image Credit: Indif

Numerous modifications have been proposed since the Kardashev scale was first introduced. Sagan (1973) proposed replacing Roman numbers with Arabic numbers to take into consideration intermediate values. In addition, Sagan proposed altering the Type I civilization's energy requirements significantly, contending that Kardashev (1964) estimate was out of date. Gray (2020) also suggested using Arabic numerals with 10^{10} intervals to accommodate decimal fractions for finer precision, drawing inspiration from Sagan's viewpoint. According to Sagan (1973) and Gray (2020), the Kardashev scale is best understood as -

$$K = \frac{\log 10(P) - 6}{10} \tag{1.1}$$

Where K is the scale value, and P is power in Watts.

Gray (2020) also referred to the existence of Type 0.0 and Type 4.0 civilizations by extrapolating the energy consumption required by Equation 1.1 to obtain these K values. The civilization Type 0.0 would have a power level compared to the metabolic power of the largest terrestrial animals and groups of animals on Earth. In contrast, a type 4.0 civilization would control a power close to the current estimates for the luminosity of the observable universe (Wijers, 2005).

Table 1.1: Civilization Type by Power, Extended and Updated Scale by Gray (2020)

Type	Civilisation Description	Power(W)	Example	Example Power (W)
0.0	Biological	10^6	Maximum for terrestrial organisms	4.6×10^5
1.0	Planetary	10^{16}	Insolation of a planet like Earth	1.7×10^{17}
2.0	Stellar	10^{26}	Luminosity of a star like Sun	3.8×10^{26}
3.0	Galactic	10^{36}	Luminosity of a galaxy like Milky Way	1.2×10^{37}
4.0	Observable Universe	10^{46}	Luminosity of observable universe	$\sim 10^{48}$

The original Type I civilization that Kardashev (1964) proposed would yield a $K = 0.67$ according to equation 1.1. In contrast, our civilization would yield $K = 0.73$ if we consider the world energy consumption during 2020 provided by Ritchie et al. (2022).

Extraterrestrial life might be in any stage of evolution, from simple single-celled life to extremely intelligent life. But our current technologies confined us to search only those extraterrestrial lives which are intelligent and ahead of us in technological developments or at least equal to us.

The probability of intelligent life in the cosmos is a crucial question we must answer before searching for it in interstellar space. Frank Drake provided a crucial equation in 1961 that attempts to quantify this possibility, which is described in the section below.

1.2 Drake Equation

One of the most important questions to us is “how many civilisations in the Milky Way are capable of communicating with us?”. This number is a very important parameter to get an idea of how often we will encounter extraterrestrial intelligence lives in our search programs. To calculate this number, Frank Drake gave an equation in 1961. He presented this equation as a basis for discussion at the first SETI conference. The equation is -

$$N = R_{\star} \times f_p \times n_e \times f_1 \times f_i \times f_c \times L \tag{1.2}$$

Where,

N = Number of intelligent civilisation in our galaxy with which communication might be possible,

$R_{\star}$= the average rate of solar-type star formation per year in our galaxy

f_p = the fraction of these stars that host planetary systems

n_e = the number of planets in each system that are potentially habitable

f_l = the fraction of habitable planets where life originates and becomes complex

f_i = the fraction of life-bearing planets that bear intelligent civilisation

f_c = the fraction of civilizations that develop a technology that releases detectable signs of their existence into space, and

L = the length of time for which such civilizations release detectable signals into space.

From the equation, 1.2, $N >> 1$ suggests that there are numerous civilizations that we might receive communication signals from, whereas $N << 1$ suggests that we are likely alone in the Galaxy and would need to search across several galaxies to identify our closest radio-communicating partners. Depending on the assumptions made, N can vary widely (e.g, Wilson, 2001).

Modern astronomy can provide the estimates of the first three parameters of the Drake equation (1.2) $R_{\star}$, f_p and n_e but it doesn't have much information about the rest of the parameters f_l, f_i, f_c and L.

What do you mean when you say "intelligent life"? You are free to ask me this query. Different suppositions concerning the intelligence of life have been made by SETI. In contrast to Radio SETI, a civilization that can send and receive radio signals is considered intelligent, Artefact SETI has a different presumption.

We now have a rough estimate from Drake equation (1.2) of how many ETI (extraterrestrial intelligence) there may be in space. We established a dedicated program called SETI to look for them.

1.3 SETI

Humankind had started searching for evidence of extraterrestrial intelligence (ETI) using the scientific approach. They found a program named "Search for Extra-Terrestrial Intelligence" (SETI). There are two approaches to searching for intelligent life.

1. **Communication SETI**
2. **Artefact SETI**

1.3.1 Communication SETI

The size of the cosmos is enormous. The distances between the stars are vast, even inside the Milky Way. Any civilisation will wish to employ long-wavelength electromagnetic radiation as a communication signal since it can travel farther without being absorbed by interstellar dust and can pierce any solid object in the interstellar medium. Additionally, humans use longer wavelengths to communicate and transmit information across vast distances on Earth and beyond. Searching for them at greater wavelengths in the spectrum is an appropriate strategy. There are two wavelength regimes in which we could search them for their communication signal from the Earth- the optical band and radio band of the electromagnetic spectrum because, for radio wavelengths, the atmosphere of the Earth is transparent as shown in the figure 1.2. This is the reason radio SETI has become one of SETI's most well-liked branches. Also, Optical SETI (OSETI) is a promising approach for communication with extraterrestrial intelligence, in addition to traditional radio SETI. The transparency of Earth's atmosphere to optical wavelengths (1.2) makes it possible to search for signals in the visible and near-infrared bands from the surface of the Earth. OSETI offers advantages over radio SETI in terms of higher data rates, smaller antennas, and lower interference from natural sources. OSETI is also more resistant to man-made interference, as laser light can be easily distinguished from natural sources, and can be highly directional, reducing the likelihood of interference with other systems.

Finding ETI communication signals—either deliberate messages or deliberate "leaking" of signals not intended for humanity—is the primary goal of communication SETI (Wright et al., 2014). Theoretically, any ET with equally advanced technology as ours could use radio transmission to communicate with other types of civili-

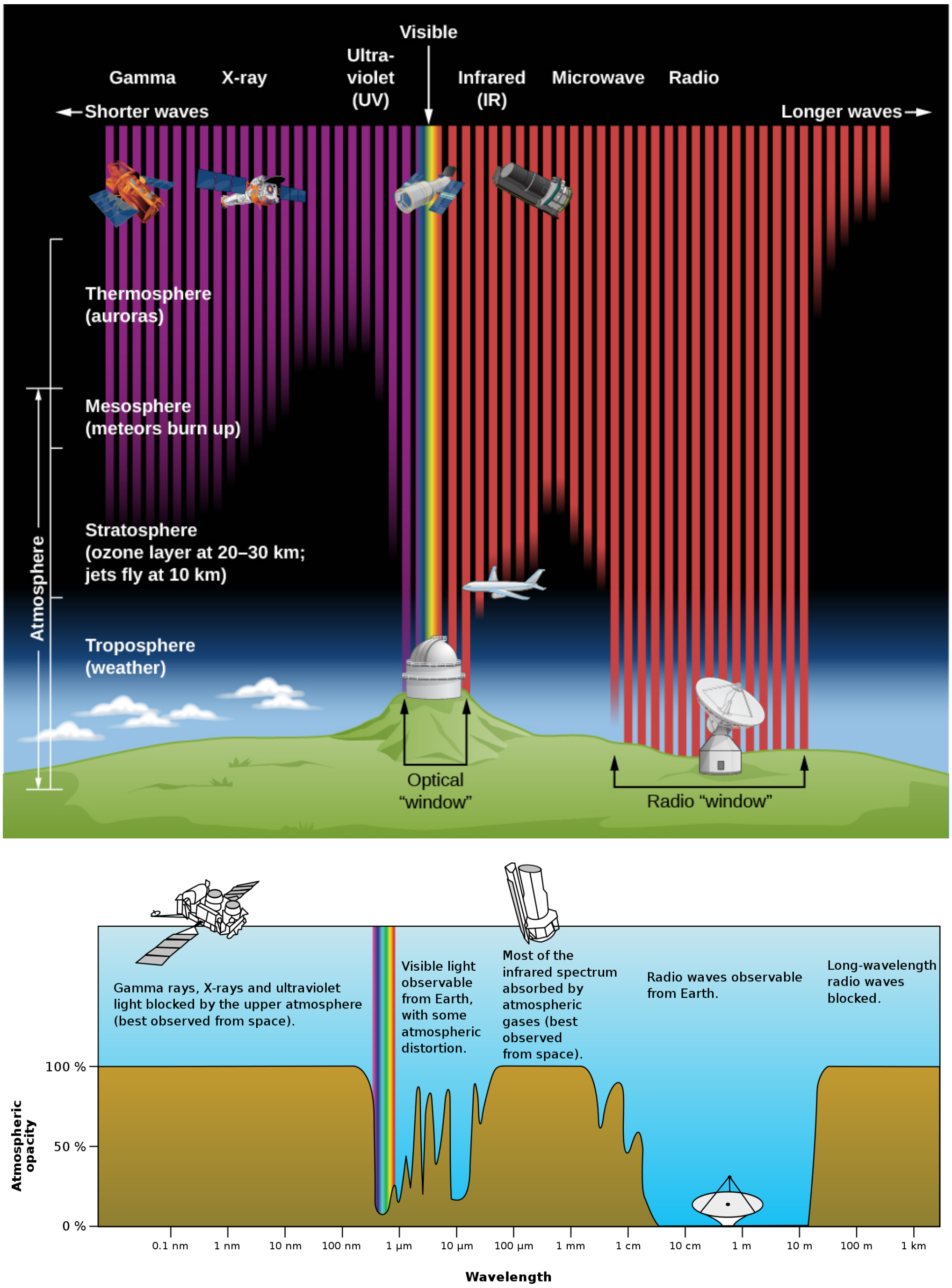

Figure 1.2: Top: This figure shows the electromagnetic spectrum's bands and how effectively the Earth's atmosphere transmits each one;
Bottom: Earth's atmospheric opacity to various wavelengths of the electromagnetic spectrum. Image credit: NASA and OpenStax, Rice University, modification of work by STScI/JHU/NASA.

sation.

1.3.1.1 Radio SETI

Radio SETI had to wait for the development of radio astronomy as a field (Jansky, 1933), a major technological advance from World War II radar investigations, and the finding of the 21-cm emission line.

Cocconi and Morrison (1959) ushered in the scientific era of radio SETI by recognizing that our technology had advanced to the point that a signal could be transmitted at the "universal" frequency of HI (the most abundant element in the universe) and that signal would be detectable over interstellar distances against the relatively low natural background of the astrophysical universe.

Cocconi and Morrison (1959) published the 1st paper written in the field of SETI. They argued that the optimum channel for communication should minimize the stellar background as well as the Galactic background, ending up with the radio region of the electromagnetic spectrum. In particular, they proposed the 1.42 GHz line (21 cm) of neutral hydrogen, since it would be known to all technologically sophisticated societies and would constitute a universal frequency. In addition to this line, the fact that the Earth's atmosphere is transparent to radio waves 1.2 made radio SETI one of the most popular branches.

1.3.1.2 Optical SETI

Since in the 1960s, the majority of SETI searches have been conducted in the radio regime. However, the discovery of laser by Maiman in 1960 and the proposal of interstellar optical communication by Schwartz and Townes (1961) opened a new window into SETI. Although we refer to optical and laser SETI as equivalent concepts, it operates from ultraviolet to near-infrared. The feasibility of optical communication was initially questioned by Project Cyclops due to the challenge of developing a laser powerful enough to avoid being obscured by the host star's light, but later, a detailed follow-up study by Townes in 1983 proved this to be true, and further research supported the hypothesis by Ekers in 2002.

1.3.2 Artifact SETI

In the early 1960s, Freeman Dyson proposed a new strategy for searching for signs of extraterrestrial life. He postulated that any advanced civilisation will look for energy sources outside of those provided by their planet to run its civilisation. The technologically advanced civilization is not able to function on the host planet's energy resources alone. It would be logical to assume that they can construct a structure that would capture the stellar energy of their host star assuming the timescale for technological progress is significantly shorter than the lifetime of a star. Dyson hypothesised that the leftover energy—often referred to as waste heat—emitted by these massive structure would radiate in the infrared spectrum (Dyson, 1960). So we could look for the infrared radiation signature of the Dyson sphere at the wavelength around $10\ \mu m$ in the outer space(Dyson, 1960). One potential megastructure is a spherical structure surrounding the host star comprised of material that can absorb radiation energy. Dyson spheres is the term given to these structures in honour of Dyson's key research. Only K-II and K-III types of civilizations are capable of constructing these structures. The illustration below (figure 1.3) depicts an artistic interpretation of the construction of a Dyson sphere by dismantling a planet.

Figure 1.3: A artistic representation of construction of Dyson sphere around a star. Image Credit: Adam Burn

One possible megastructure is the Dyson Sphere (Dyson, 1960), a hypothetical megastructure built by advanced extraterrestrial civilizations to harvest radiation energy from stars.

Artefacts SETI involves the search for evidence of technology beyond our solar system, including not only Dyson spheres but also other structures such as Bracewell probes. These probes are hypothetical autonomous spacecraft that could potentially be stationed in the solar system to communicate with other civilizations.

1.4 Dyson Spheres

Dyson (1960) discussed the Dyson sphere, an engineering megastructure built by the ETI to harvest the energy of their host stars. The civilisation gets advanced, its energy requirements increase exponentially. To fulfil this energy requirement, the planet's resources are not enough for it, So they can harvest the energy of their host star by constructing a sphere built of solar energy-absorbing materials like - solar cells. The Dyson sphere is a sphere which will cover the star partially or fully and absorb radiation. It would eventually emit a black body in the infrared between 200 and 300 K. According to Dyson, stars with these structures would glow as infrared beacons.

Furthermore, using the Solar System as an example, Dyson (1960b) predicted that it would only take a few thousand years to complete the construction of such an artificial biosphere. In this illustration, Dyson recognised the necessity of dismantling neighbouring planets to obtain the building materials. He thought a mass about equal to Jupiter's ($\sim 2 \times 10^{27}$ kg) should be sufficient to make a solid shell having a thickness of 2 to 3 meters (depending on the density) around the sun at the distance of 2 AU (Dyson, 1960).

1.4.1 Construction of Dyson Sphere

A monolithic Dyson sphere would be unstable, as Dyson (1960a) noted. Applying Gauss' law, we may say that the net gravitational force acting on a completely spherical shell is zero. The

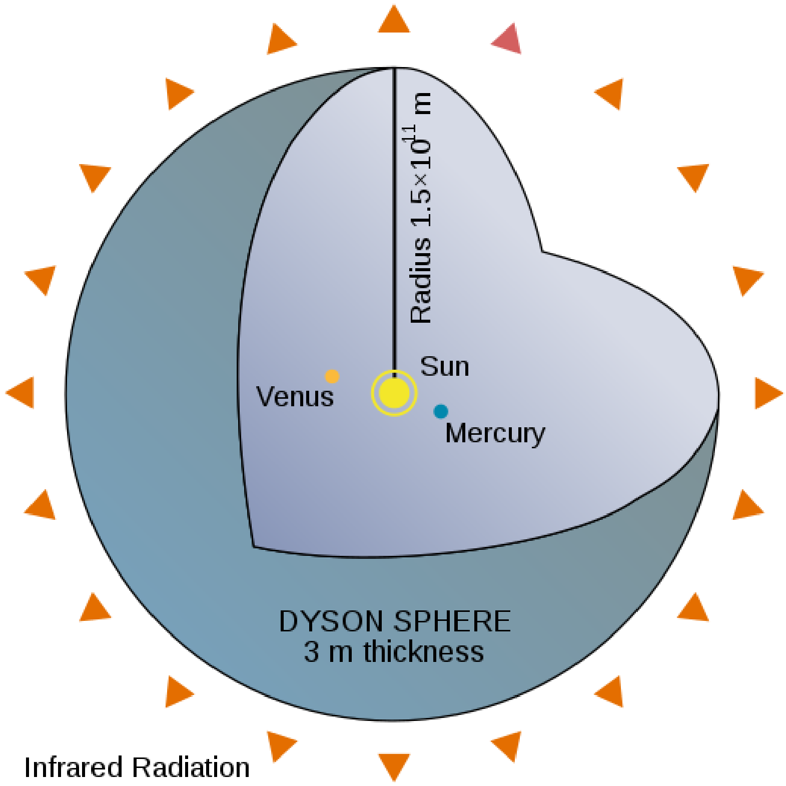

Figure 1.4: Dyson sphere

structure falls into the star, though, if symmetry is lost. However, Wright (2020) demonstrated that radiation pressure remains neutrally stable and provides support independent of the geometry of the structure. He also observed that conservation of momentum would cause the DS's location to recenter if photons were to escape for whatever reason.

The initial artificial biosphere has been proposed in several different forms. A Dyson sphere is now thought of as a collection of panels that may be built gradually and either orbit the star or remain stationary. The "Dyson Bubble" scenario is one in which these panels remain stationary in the star's frame. Each panel in this array employs radiation pressure to resist the gravitational attraction of the star. Such constructions wouldn't be at risk of running into one another or covering an adjacent panel. Such panels might even change how far away from their star they are.

On the other hand, the "Dyson Swarm" refers to the system of panels in orbit around the stars. In this instance, the panels circle the star in a tight arrangement. This variety is the one that people typically think of when discussing Dyson spheres, therefore we will view them from this angle for the remainder of this chapter. The below figure 1.5 shows some proposed designs of the Dyson sphere - Dyson shell, Dyson bubble and Dyson ring.

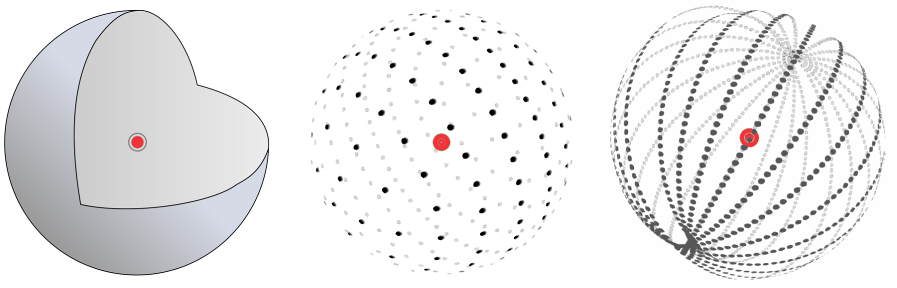

Figure 1.5: Illustration of a few of the Dyson sphere design plans. A Dyson shell, a Dyson bubble, and a Dyson swarm are shown from left to right. Image: Wikipedia

1.5 Major Milestone in the history of SETI

There are some events in the history of SETI which acts as a milestones.

Year	Milestone
1959	The first modern SETI article is published (Cocconi and Morrison, 1959).
1960	Frank Drake conducts the first SETI search, Project OZMA. The results are published the following year (Drake, 1961).
1960	Searching for interstellar probes is proposed as an alternative SETI strategy (Bracewell, 1960).
1960	The possibility of searching for megastructures based on their infrared waste heat signature is presented (Dyson, 1960b)
1961	The search for continuous optical wave laser beacons is proposed (Schwartz & Townes, 1961)
1961	The first SETI Conference, Order of the Dolphin, takes place. Frank Drake introduces what is now known as the Drake Equation.
1964	The Kardashev scale is introduced (Kardashev, 1964).
1972 - 1973	The Pioneer Plaques, containing a message about our planet are launched on the Pioneer 10 and Pioneer 11 space probes.
1973	Francis Crick and Leslie Orgel evaluate the possibility of life on Earth originating elsewhere in the Universe.
1975	Michael H. Hart publishes a detailed examination of the Fermi paradox and argues for the non-existence of other civilizations (Hart, 1975).
1977	The Ohio State Big Ear telescope detects the famous “Wow!” signal, a narrowband signal from the constellation Sagittarius.
1977	Voyager 1 and Voyager 2 space probes launched. They carry gold-plated records containing images and sounds of Earth.
1979	The Planetary Society is founded by Drs. Carl Sagan, Bruce Murray and Louis Friedman.
1981	The Proxmire Amendment kills congressional support of NASA SETI.
1981	The Planetary Society begins strong advocacy for NASA to conduct searches for extraterrestrial signals. Dr. Sagan, then-president of the Society, persuades Senator Proxmire to stop opposition.
1983	The International Astronomical Union establishes Commission 51, dedicated to astrobiology and the search for extraterrestrial life.
1984	The SETI Institute is founded as a home for research, investigating all aspects of life in the Universe. Initially, its activities were supported by NASA.
1995	51 Pegasi B is detected – the first confirmed planet around a nearby Sun-like star (Mayor & Queloz, 1995).
1998	The SETI Institute and The Planetary Society now support searching for optical laser signals.

Table 1.2: Timeline of some of the milestones in SETI history until 2000. Credit: Matias and Robert M. Owen

1.5.1 Major Searches

Several searches were done in the history for searching ETIs. In this section, we will discuss a few of them in briefly.

1.5.1.1 Project Ozma

The first contemporary effort to find interstellar radio broadcasts was made by radio astronomer Frank D. Drake in 1960 at the National Radio Astronomy Observatory (NRAO) in Green Bank, West Virginia. The picture 1.6 shows Frank in front of the Green Bank radio telescope. Project Ozma was named after the queen of L. Frank Baum's imaginary land of Oz – a place "very far away, difficult to reach, and populated by strange and exotic beings." Drake picked two stars for the initial SETI search that were each around eleven light-years (64 trillion miles) away: Tau Ceti in the constellation Cetus (the Whale) and Epsilon Eridani in the constellation Eridanus (the River). Both stars, which are almost the same brightness as the Sun, were formerly thought to have planets but this was not known. While Epsilon Eridani is considerably younger than the Sun, Tau Ceti is somewhat older.

The 85-foot antenna's receiver was set to the frequency of interstellar hydrogen's 21-centimetre emission line from April to July 1960, six hours a day. It was assumed that every technologically advanced culture would be aware of this frequency, 1420 MHz and that it would serve as a global "hailing frequency."

A chart recorder and a loudspeaker were employed by the small Ozma crew to keep track of any signal entering the antenna. Only static could be heard coming from the loudspeaker, and aside from an early false alert that was likely brought on by high-altitude airplane, there were no discernible bumps overlaid on the wiggles recorded on the chart recorder (Shuch, 2011).

1.5.1.2 The Wow Signal

In 1977 a telescope called Big Ear operated by Ohio State University, which had been carrying out an all-sky SETI survey since 1974, picked up a signal that appeared to have all the right characteristics. The signal was coming from the constellation of Sagit-

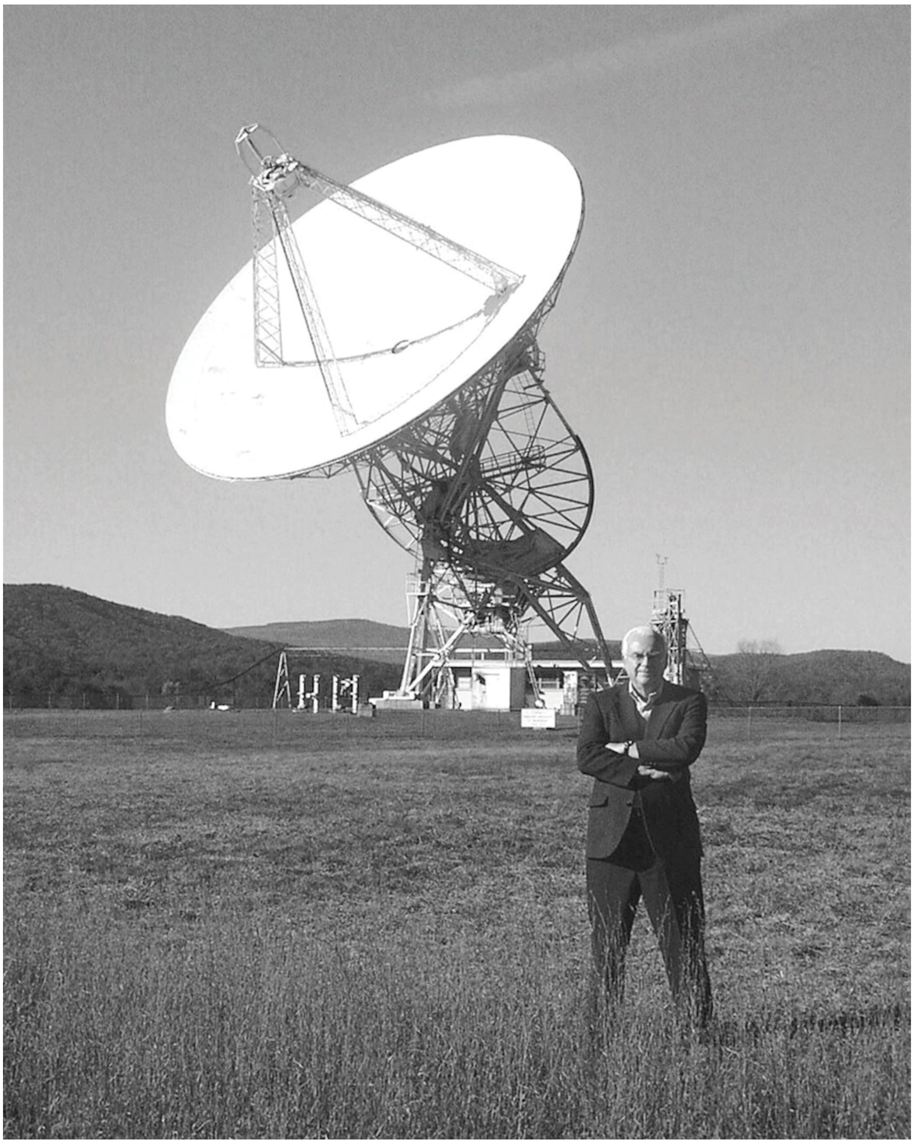

Figure 1.6: Frank D. Drake with first radio telescope at the National Radio Astronomy Observatory. Credit: NRAO/AUI/NSF

tarius and the signal was observed at a frequency close to 1.42 GHz. This signal lasts for 72 seconds (The time for which the telescope could track the sources). It is called the "Wow" signal because that is what the astronomer analyses the data written in the margin of the computer printout (1.7). Sadly, in follow-up observations, no signal has ever been picked up from the same region of the sky. The origin of this strong radio signal is still unknown.

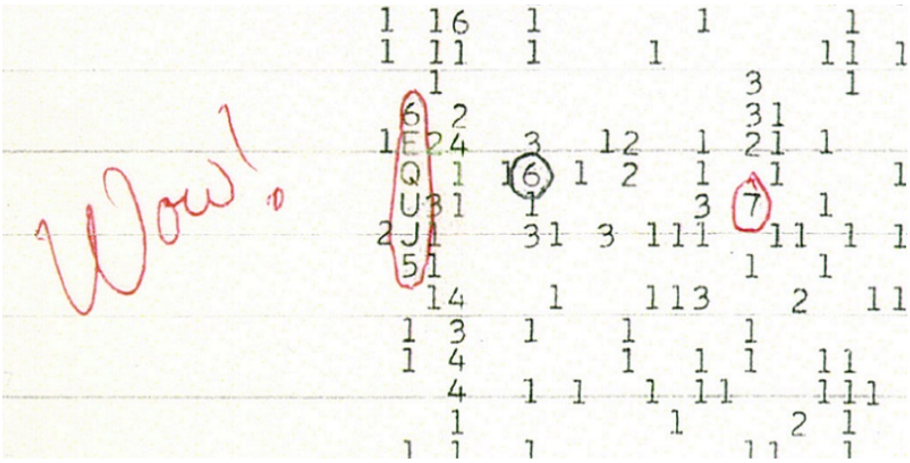

Figure 1.7: The Wow Signal observed by Big Ear antenna (The Ohio State University Radio Observatory).

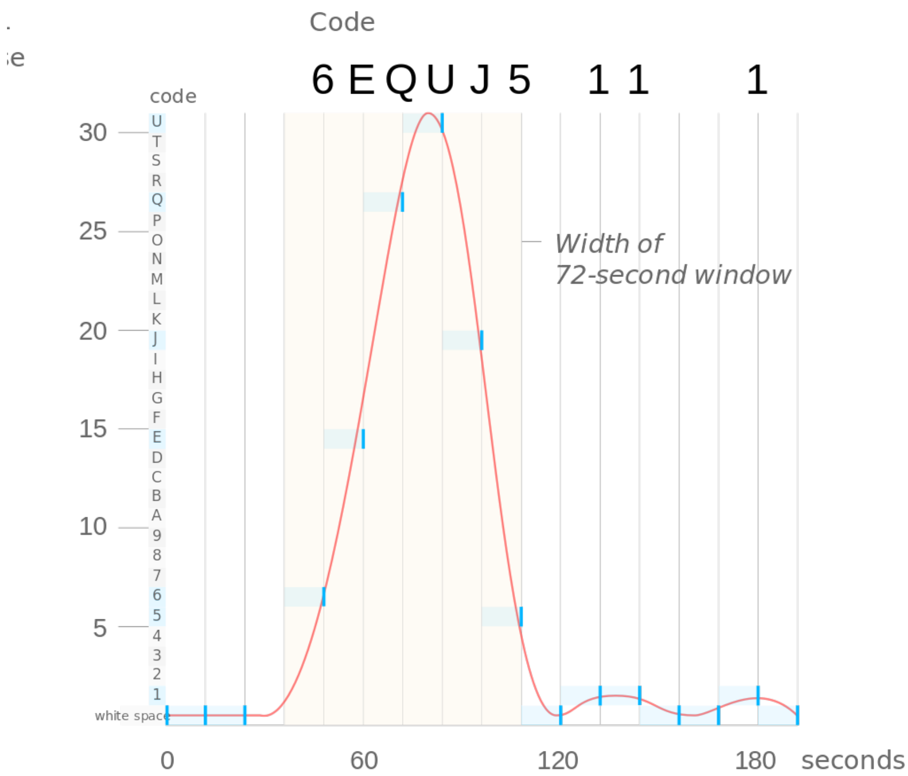

Figure 1.8: Plot displaying the Wow! signal's strength

1.5.1.3 Project Phoenix

Up until around 2015, Project Phoenix was the most sensitive and thorough search for alien intelligence yet undertaken. By keeping an eye out for radio signals that were either accidentally or purposefully being blasted our way from another planet, scientists were trying to find extraterrestrial civilizations. Phoenix was the replacement for the ambitious NASA SETI program that was cancelled in 1993 by a money-conscious Congress. Phoenix started making observations in February 1995 using the Parkes 210-foot radio telescope in New South Wales, Australia. This is the biggest single-dish radio telescope in the southern hemisphere. About 200 stars that are hidden from northern hemisphere observatories were studied by Phoenix over a sixteen-week timeframe. The study then focused on star systems in the north after this southern effort. With the help of this phase, SETI was able to return to its beginnings at the National Radio Astronomy Observatory in Green Bank, West Virginia. The antenna used by Frank Drake for Project Ozma is not far from the 140-foot telescope utilised for these observations. In Green Bank, Project Phoenix ran from September 1996 until April 1998. Since the 140-foot was the observatory's main instrument at the time, it was also utilised for other radio astronomy studies. About half of the time, Phoenix used the antenna. In August 1998, Project Phoenix moved to Arecibo and it continued its observations of the sky.

Phoenix did not look across the entire sky. Instead, it examined the areas around neighbouring stars that resembled the Sun. These stars are thought to be the most likely to have habitable, long-lived planets. Naturally, planet-bearing stars are also included. All of the 800 star systems identified by Project Phoenix were located within 200 light-years from 1995 - 2004. Phoenix was concurrently monitoring millions of radio stations, therefore the majority of the "listening" was carried out by computers. Phoenix looked for signals between 1,200 and 3,000 MHz. Signals that are at only one spot on the radio dial (narrow-band signals) are the "signature" of an intelligent transmission. The spectrum searched by Phoenix is broken into very narrow 1 Hz-wide channels, so nearly two billion channels were examined for each target star.

Figure 1.9: Upper: Arecibo Observatory, Caribbean, Bottom: Parkes Observatory, Australia.

1.6 Project Hephaistos

One of the most intriguing missions that humanity has ever engaged in is the search for sentient life in the universe. Astronomers have found several exoplanetary systems in recent years, and if one entertains the idea that intelligent life could not just exist on Earth, the Search for Extra-Terrestrial Intelligence (SETI) would seem to be a promising endeavour. Astronomers have been looking up at the stars for more than 60 years, but so far they have not seen any signs of extraterrestrial civilizations sending out any kind of communication. While signal-based searches should undoubtedly continue when new and improved telescopes (like the Square Kilometer Array) go online, alternative strategies should also be taken into consideration.

What if the closest alien culture is too far away to communicate with us? What if we are only seen as being too primitive to merit contact? Then, would it be possible for us to still discover the presence of other civilizations? Possibly. Searching for signs of alien technology, such as elaborate engineering feats, interstellar propulsion systems, and industrial pollution in the atmospheres of exoplanets offers an alternative to the conventional, signal-based method. This type of search makes no assumptions about alien civilizations' readiness to communicate with us directly. In addition, non-detections from properly planned searches of this kind can provide substantial upper bounds on the number of civilizations employing the presumed technology.

Figure 1.10: Logo of Project Hephaistos. Credit: Hephaistos Team

Project Hephaistos, which takes its name from the Greek god of blacksmiths who created many of the magnificent items used by the Olympian gods (such as chariots, weapons, and even automatons), is a member of this new SETI endeavour class that focuses on the search for signs of extraterrestrial technology like- Dyson Sphere rather than looking for signals that are purposefully sent to Earth. This project is led by Dr. Erik Zackrisson along with his colleagues Matías Suazo and Andreas Korn from Uppsala University.

Suazo et al. (2022) has developed a Spectral Energy Distribution (SED) model for Dyson sphere based on the observational signatures of it, which includes dimming in the optical band due to the obscuration of starlight and brightening in the infrared due to the release of waste heat from the structure. He uses this model to fit the SED of stars observed by the GAIA mission and identify a tentative list of potential Dyson sphere candidates. Suazo et al. 2023 (in prep.) have used a Convolution Neural Network (CNN) based image classifier to classify stars into two categories depending on whether they belong to a nebular or non-nebular region by analysing ALLWISE images of the stars. Sometimes, this algorithm fails to detect any nebular feature surrounding a star having the signature of a Dyson sphere even though literature surveys indicate that the star is very young. My aim for this project is to develop a filtration technique which can further filter out the false Dyson sphere candidates using the phenomenon of interstellar reddening from the nebula. This method is based on the astrophysical phenomenon of interstellar reddening, where dust particles absorb and scatter shorter wavelength light, while longer wavelength light can pass through unaffected. As a result, objects in nebular or dusty regions appear redder. We utilize the fact that there are higher fractions of red stars in the nebular region compared to the non-nebular region within a certain angular radius around a star. This is the basis for our filtration technique.

CHAPTER 2

Astrophysical Parameters of Stars

The most well-known astronomical object is a star, which also serves as one of the basic components of galaxies. A galaxy's history, dynamics, and evolution can be traced by the age, distribution, and composition of its stars. Additionally, stars produce and distribute heavy elements like carbon, nitrogen, and oxygen, and their features are closely related to those of the planetary systems that may form around them. These heavy elements are the basic important requirement for forming life on a planet surrounding a star. So, the study of stars will help us to find civilisation. Energy is an important ingredient to form life in any place in the universe. Starlight is another important ingredient for forming life in the universe. The surrounding space of a star is a suitable place to host lives. Before understanding what sort of lives exist surrounding a star, Let's first understand, how these stars form in the galaxies.

2.1 Formation of stars

The most massive reservoirs of interstellar matter—and some of the most massive objects in the Milky Way Galaxy (or any galaxy)—are the giant molecular clouds. These clouds have cold interiors with characteristic temperatures of only 10–20 K; most of their gas atoms are bound into molecules (e.g.- H_2, **CO**). These clouds called nebulae turn out to be the birthplaces of most stars in our Galaxy. Also, these areas of space are sometimes known as 'stellar nurseries' or 'star-forming regions. In most galaxies, stars are created amid dust clouds and dispersed throughout them. The Orion Nebula is a well-known illustration of one of these dust clouds. Deep within these clouds, turbulence produces knots of sufficient mass that the gas and dust can start to collapse under its gravitational pull. The cloud's centre material starts to heat up as it breaks up. This heated core at the centre of the collapsing cloud is known as a protostar, and it will eventually become a star.

Molecular clouds have masses that range from a few million solar masses to 10,000 times the mass of the Sun (Krumholz, 2015). Although far less dense than cirrus clouds in Earth's atmosphere, molecular clouds contain a complex filamentary structure. The filaments of the molecular clouds can span up to 1000 light-years. We refer to the cold, dense regions that make up the clouds as clumps; these regions typically have masses between 50 and 500 times that of the Sun. There are cores—smaller, even denser regions—within these aggregates.

The cores are the embryos of stars. Low temperature and high density are the ideal circumstances for star formation in these cores. Keep in mind that gravity and pressure's constant struggle for dominance is at the heart of every star's life story. The gravitational pull of a star inward attempts to cause it to collapse. The movements of the gas atoms create internal pressure that pushes outward and seeks to enlarge the star. Low temperature (and hence low pressure) and high density (and so stronger gravitational pull) both contribute to gravity having the upper hand when a star is early developing. We require a typical core of interstellar atoms and molecules to undergo a factor of approximately 10^{20} increase in density and a radius reduction to form a star, that is, a dense, hot ball of matter capable of igniting nuclear processes deep inside. It is the force of gravity that produces this drastic collapse.

There are various parameters which characterise a star- Brightness, Surface Temperature, Colour, Mass, Size, Metallicity and so on (Salaris and Cassisi, 2005).

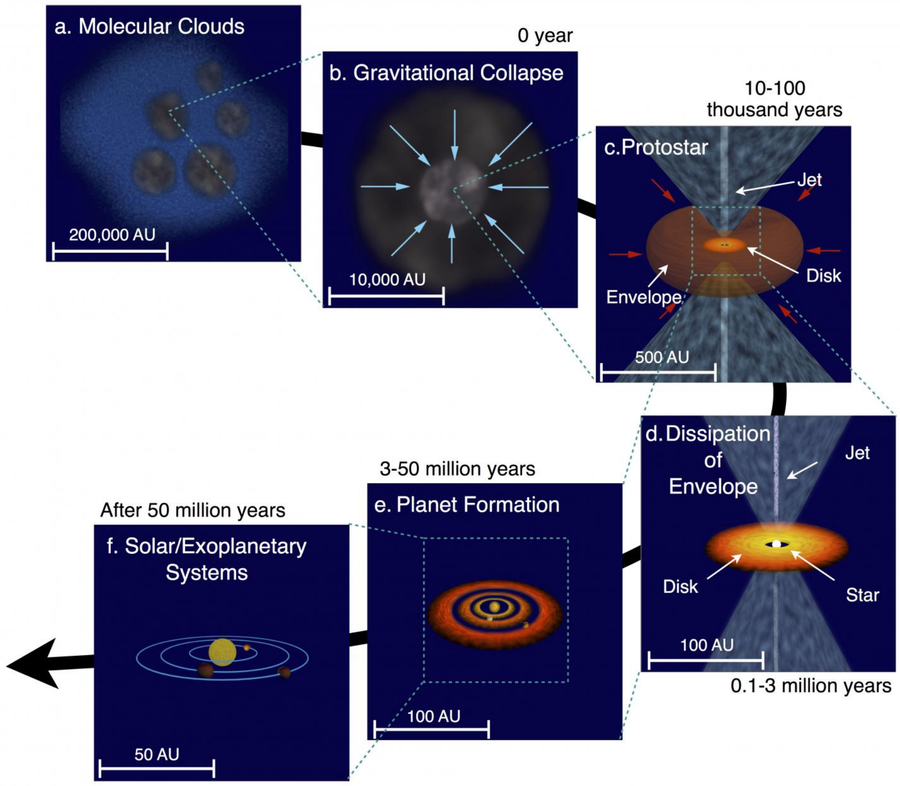

Figure 2.1: An artistic imagination of star formation from a molecular cloud. Image Credit: ASIAA

2.1.1 Apparent Magnitude and Absolute Magnitude

Apparent magnitude, m of a star is a number that tells how bright that star appears in the night sky to us at its great distance from Earth. It is a relative measure of the brightness of that star relative to a star. The scale is "backward" and logarithmic. Brightness is another way to say the flux of light, in Watts per square meter, coming towards us.

$$m_2 - m_1 = -2.5 \log_{10} \left(\frac{B_2}{B_1} \right) \tag{2.1}$$

Where, m_1 is the apparent magnitude of star 1 (reference star) having brightness (or measured flux from the Earth) B_1 and m_2 is the apparent magnitude of star 2 having brightness (or measured flux from the Earth) B_2.

The brightness of a source having distance d from the Earth and luminosity L (It is the measure of the amount of energy coming from the source per second, Watts) is defined as the energy flux received by the observer on the Earth.

$$B = \frac{L}{4\pi d^2} \tag{2.2}$$

The brightness of a star depends on two factors -

- The amount of light it emits
- Its distance from the Earth
- Obscuration of intervening dust

From equations 2.1 and 2.2,

$$m_2 - m_1 = -2.5 \log_{10}\left(\frac{\frac{L_2}{4\pi d_2^2}}{\frac{L_1}{4\pi d_1^2}}\right)$$

$$\Rightarrow \quad m_2 - m_1 = -2.5 \log_{10}\left(\frac{L_2 d_1^2}{L_1 d_2^2}\right) \tag{2.3}$$

Instead of comparing the intensities and magnitudes of two different stars, we will compare the intensities and magnitudes of the same star at two different distances.
So, $L_1 = L_2$, then equation 2.3 becomes-

$$m_2 - m_1 = -2.5 \log_{10}\left(\frac{d_1^2}{d_2^2}\right)$$

$$\Rightarrow \quad m_2 - m_1 = -2.5 \log_{10}\left(\frac{d_1}{d_2}\right)^2$$

$$\Rightarrow \quad m_2 - m_1 = -5 \log_{10}\left(\frac{d_1}{d_2}\right) \tag{2.4}$$

Absolute Magnitude, M is the measure of the magnitude a star would have if it were placed to a distance of 10 parsecs from the Earth.

Suppose a star having real distance d and apparent magnitude m is placed at a distance of 10 parsecs (pc) away from the observer then its absolute magnitude M will be -
Using $m_1 = m$, $d_1 = d$, $m_2 = M$ and $d_2 = 10 \ \ parsec$

$$M - m = -5 \log_{10}\left(\frac{d}{10}\right)$$

$$\Rightarrow \quad M = m - 5 \log_{10}\left(\frac{d}{10}\right) \tag{2.5}$$

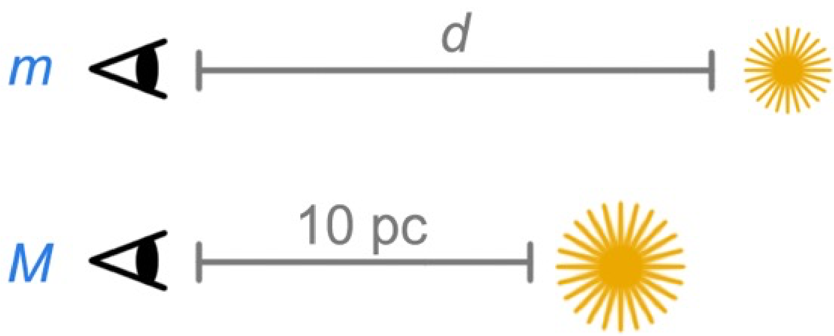

Figure 2.2: Figure describing the measured apparent magnitude (m) and absolute magnitude (M) of star.

$$\Rightarrow \quad m - M = 5\log_{10}\left(\frac{d}{10}\right)$$

Here, d must be in parsec. This $\mu = \mathrm{m} - \mathrm{M}$ is known as distance modulus. Also, we can find the distance of the star having distance modulus -

$$d = 10^{(m-M+5)/5} \quad parsec \tag{2.6}$$

2.1.2 HR Diagram and Color Magnitude Diagram

One of the most crucial tools for studying star evolution is the HR diagram, often known as the Hertzsprung-Russell diagram (HR diagram). It was independently created by Ejnar Hertzsprung and Henry Norris Russell in the early 1900s. The theoretical HR diagram is a plot of surface or effective temperature ($\mathrm{T_{eff}}$) of stars against their luminosity (**L**) -

$$\mathrm{L} = 4\pi \mathrm{R}_\star^2 \mathrm{T}_{\mathrm{eff}}^4$$

Here, $\mathrm{R}_\star$ is the radius of the star.

The locations of the stars seem to be divided into four distinct regions in the HR diagram:

1. The main sequence is a line of stars that runs diagonally from bright blue stars to dim red stars. In this stage, stars spend about 90% of their lives fusing hydrogen into helium at their cores.

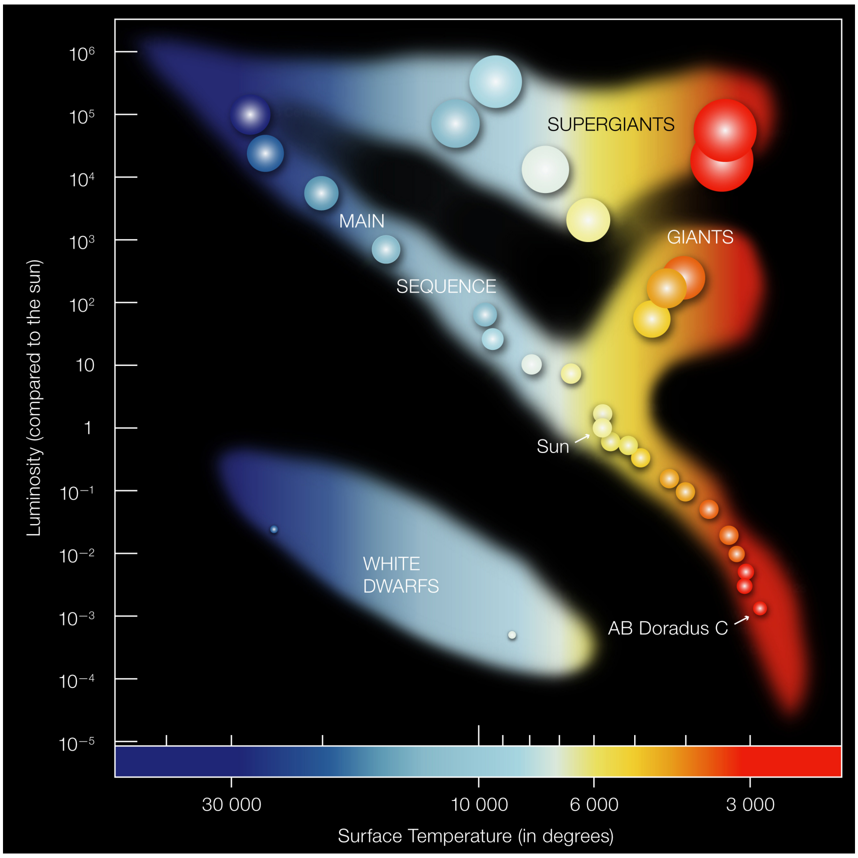

Figure 2.3: The Hertzsprung-Russell diagram shows the various stages of stellar evolution. Image Credit: ESO.HR Diagram

2. Supergiants are a horizontal band of incredibly brilliant stars that range in colour from blue to red (signifying a range of temperatures from hot to cool).

3. Red giants are a collection of red stars that may be found above (and hence brighter than) and to the right of the main sequence.

4. A collection of white dwarfs, which are extremely faint stars that are typically (but not always) blue or blue-white. These stars are frequently discovered in the heart of stunning structures called planetary nebulae.

Where as the observational HR diagram is a plot between the colour of stars (or Spectral Type) against their absolute magnitude, it is also known as a color-magnitude diagram (CMD).

2.1.3 Color of Stellar Objects

Color is an essential aspect of optical astronomy, allowing astronomers to study and understand the properties of celestial objects. When steallar objects observed through telescopes, they exhibits a range of colors that can provide crucial information about their physical characteristics, such as temperature, composition, and distance. The colors has a different meaning for an optical astronomers than it does for the majority of humans. The "colour" of stars is determined using the approach of measuring magnitudes at two separate wavebands. Astronomers refer to the colour of a star as its colour index rather than using terms like red or orange to describe it.

The color index or CI is defined as the difference between the magnitude of a star in one passband and the magnitude of the same star in a different passband and It is simply expressed in a number.

$$\mathbf{CI = m_1 - m_2} \tag{2.7}$$

Here, m_1 and m_2 are the apparent magnitude of star in passband 1 and passband 2 respectively.

The most common used passbands are the Johnson-Cousins B and V. The color index in B-V band is -

$$\mathbf{(B - V) = m_B - m_V} \tag{2.8}$$

Here, m_B and m_V are represents the apparent magnitude of star in B band (corresponding to wavelength around $440nm$) and the apparent magnitude of the same star in V band (corresponding to the wavelength around $550nm$) respectively.

The star Vega is the basis for color scale. Vega has $m_V = 0$ and $m_B = 0$, so obviously its color index is $(B - V) = 0.0$. Therefore,

- a star is redder than Vega if its $(B - V) > 0$.
- a star is bluer than Vega if its $(B - V) < 0$.

The color of an object is determined by its spectral energy distribution, which describes the intensity of radiation emitted or reflected by the object at different wavelengths. A typical star's spectrum can be approximated as a Planck curve, which describes the intensity of emitted energy as a function of wavelength. This means that the distribution of energy emitted by a star varies with wavelength, with hot stars ($15000\ K$) emitting relatively more energy at blue wavelengths than at red, while cool stars ($3000\ K$) emit more energy at red wavelengths as shown in the figure 2.4.

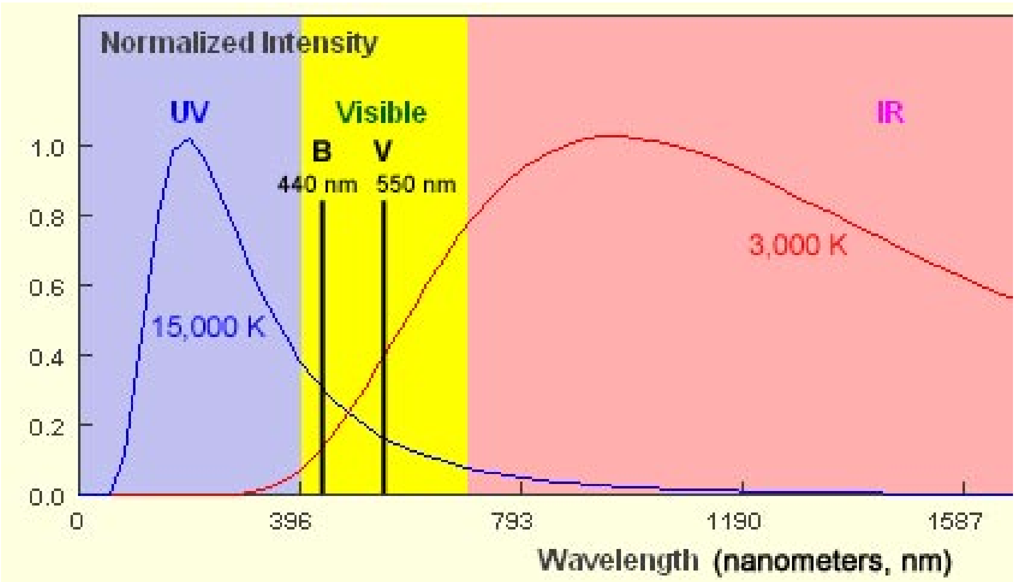

Figure 2.4: The 15,000 K star in the blue curve produces more energy in the B waveband than the V waveband, and the 3,000 K star in the red curve emits more energy in the V waveband than the B waveband. Image Credit: M. Guidry

The apparent magnitude of a star is proportional to negative logarithm of its brightness or flux as described in relation 2.1. As a result, if a star produces more radiation in one band, its apparent magnitude in that band will be lower, and if it emits less radiation in another, its apparent magnitude in that band will be greater.

Figure 2.5a depicts the optical blackbody radiation distribution of a star having temperature $15000\ K$; as can be seen, it is brighter in the B band than the V band, hence its apparent magnitude (m_B) in B will be less than its apparent magnitude (m_V) in V. This suggests that this star's Color Index (B-V) is less than zero, or negative. That is, star is bluer than Vega.

Similarly, figure 2.5b depicts the optical blackbody radiation distribution of a star having temperature $3000\ K$; as can be seen, it is brighter in the V band than the B band, hence its apparent magnitude (m_V) in V will be less than its apparent magnitude (m_B)

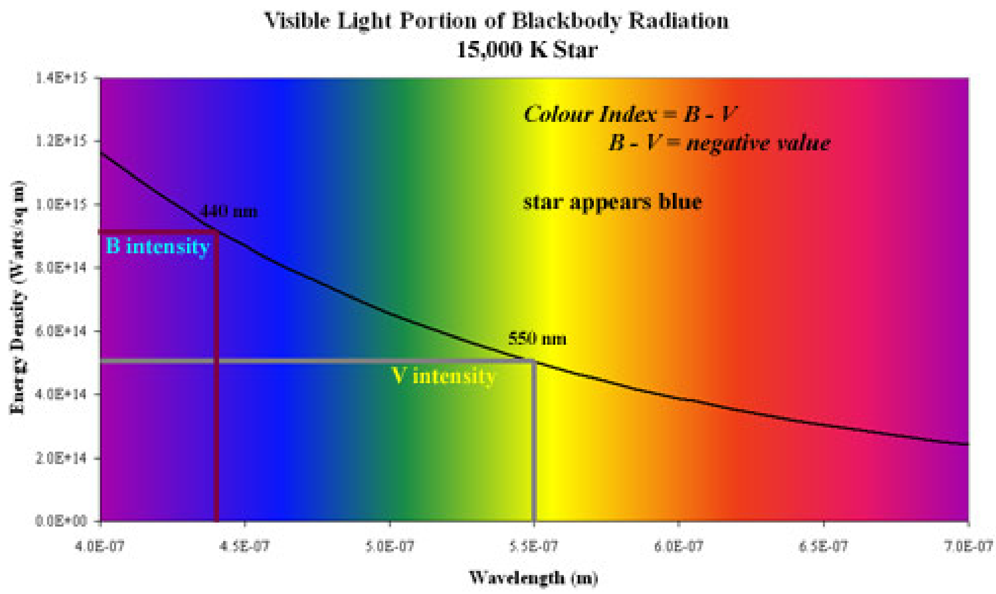

(a)

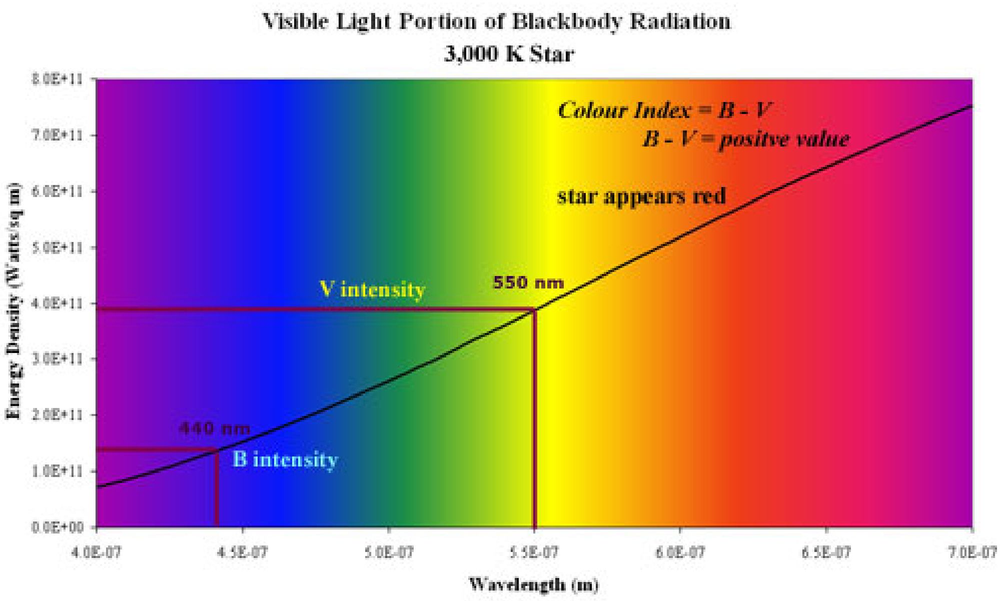

(b)

Figure 2.5: Explain the process of measurement of colour index through black-body radiation of a hot star 2.5a and cool star 2.5b. Image Credit: M. Horrell

in B. Therefore, the colour index (B-V) of this star is greater than zero or positive. Hence, the star is redder than Vega.

The (B-V) color index is widely used in astronomy as it has a long history and practical reasons behind it. Photographic plates used in the past were more sensitive to blue light, making the (B-V) index a popular choice. Additionally, this combination of colors is a good indicator of temperature, making it a useful tool for studying the physical properties of celestial objects.

But one can also define the color index of any pair of pass-bands. Some of the most common are:

- (V-I) is often used by HST observers, and in studies of other galaxies
- (V-K) combines an optical magnitude (V) with an infrared magnitude (K) to provide a very long "baseline" of wavelength

Our upcoming work, finding fraction of red star around a star, will utilize the G-K color index.

2.2 Effects of Extinction

Interstellar space is not empty but is permeated by the Interstellar Medium (ISM). Gas and dust make up the majority of the ISM. The ISM affects starlight which passes through it. The star radiation will tend to be scattered by dust and absorbed by interstellar gas (and re-radiated in a new wave band). These effective losses are collectively described as **Interstellar Extinction**. The average size of dust particles in the interstellar medium is equivalent to the wavelength of blue light. As a result, dust strongly absorbs and scatters blue light from distant objects, thereby eliminating it from the light that reaches us and giving the impression that the objects are redder than they are, as shown in figure 2.6.

Astronomers must take into consideration this interstellar reddening when analysing data captured at optical wavelengths in particular. The reddening of an object is inversely proportional to the wavelength of optical light, so shorter wavelengths (blue) are more heavily reddened than longer (red) wavelengths.

By measuring the object's colour index $(B-V)$ and comparing it to its real colour index $(B-V)_0$ using the following equation, we may determine the degree of reddening:

$$\mathbf{E(B-V) = (B-V) - (B-V)_0}$$

Since starlight interactions with dust grains cause both interstellar reddening and extinction, the two phenomena are intimately related. As a result, we can anticipate that the more dust

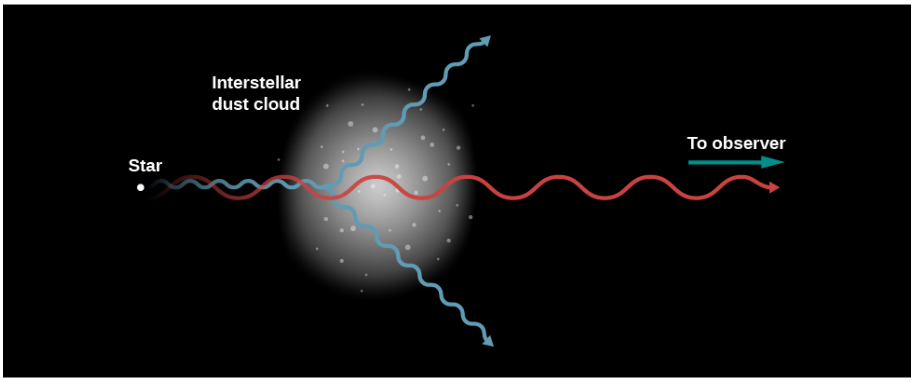

Figure 2.6: Blue light is scattered by interstellar dust more effectively than red light, giving clouds of dust near stars a bluish colour and making distant stars look redder. In this image, a red starlight beam strikes the observer directly, while a blue ray is shown scattering. Similar scattering is what gives the blue colour to Earth's sky. Image Credit: https://phys.libretexts.org/

in the line of sight, the more prominent the reddening and the greater the extinction. This is what is found, with the equation connecting extinction and reddening

$$\mathbf{A_V = R_V E(B - V)}$$

Where A_V is the extinction and Rv is the ratio of total extinction to selective extinction, which depends on the properties of the interstellar dust grains.

Apart form interstellar extinction, there is another type of extinction, **circumstellar extinction**, caused by the presence of dust or gas in the vicinity of the stars that are embedded in molecular clouds or surrounded by a circumstellar or protoplanetary disk as shown in figure 2.1 and 2.7.

The extinction of starlight can be measured by comparing the observed brightness of the star to its intrinsic brightness. The ratio of the observed brightness to the intrinsic brightness is known as the extinction factor, denoted as A_λ. The extinction factor varies with wavelength, and hence the extinction curve can be obtained by measuring A_λ at different wavelengths.

The extinction curve is often modeled as a power-law, with the form

$$\boldsymbol{A_\lambda \propto \lambda^{-\alpha}}$$

Where, λ is the wavelength of light and α is the extinction coef-

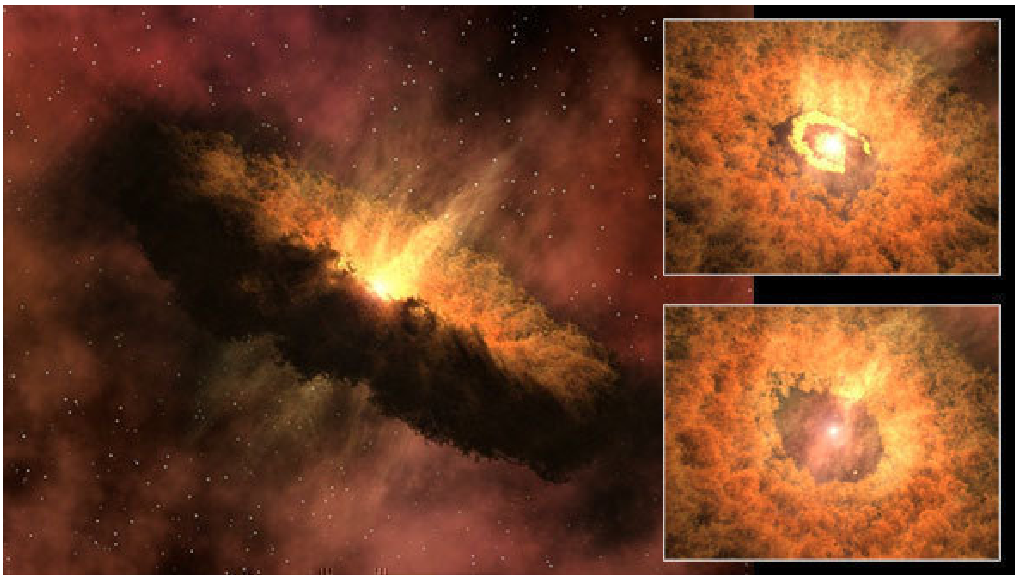

Figure 2.7: This illustration depicts a young star encircled by a dusty protoplanetary disk, which contains the fundamental material necessary for the development of planets as the star system progresses. Circumstellar extinction is caused by the dust present within the circumstellar disk. Image Credit: NASA/JPL-Caltech/R. Hurt (SSC/Caltech)

ficient. The value of α depends on the properties of the dust or gas causing the extinction. In general, α is larger at shorter wavelengths, indicating that shorter wavelength light is more strongly attenuated. The total amount of extinction is often quantified by the visual extinction, denoted as A_V.

The distance equation 2.6 must be expanded to the following form to get the accurate distance (in parsecs) of an object taking into consideration interstellar extinction and circumstellar extinction:

$$d = 10^{(m-M+5-A_V)/5} \quad parsec$$

To compensate for the loss of light, we brighten the magnitude of this equation by subtracting the extinction from the exponent.

Young stellar objects (YSOs) are commonly found in nebular regions that contain large amounts of dust particles, as well as in regions where circumstellar disks are present. Due to the cumulative effect of both interstellar and circumstellar extinction, YSOs appear reddened, falling within the region of the redder stars when plotted on a color-magnitude diagram

2.3 Dyson Sphere Models

In order to predict the observational features of a composite system consisting of a star and its Dyson Sphere, we utilize a model where the stellar component is assumed to be an obscured version of its original spectrum, while the Dyson Sphere component is modeled as a blackbody with its brightness being dependent on the amount of radiation it collects.

The AGENT formalism mentioned in Wright et al. (2014) offers a practical method for parameterising the various energy inputs and outputs of a Dyson sphere. The benefit of it is that it does not assume anything about the engineering or nature of extraterrestrial civilizations.

This formalism divides the energy supply into two parts: stellar energy (α) and other parts (ϵ), which include things like fossil fuels, nuclear energy, etc. The disposal of energy is further classified into two categories: radiation waste energy (γ) and other losses (ν), such as neutrinos or gravitational waves. The waste energy (γ) can be associated with a blackbody temperature (T_{waste}), so AGENT is a mnemonic for $\alpha\gamma\epsilon\nu T_{\mathrm{waste}}$. The definitions of each element in the AGENT formalism are compiled in table 2.1.

Parameters	**Meaning (All Powers are Normalized by Available Starlight)**
α	Power of intercepted starlight
ϵ	Power of non-starlight energy supply (e.g., fossil fuel use, zero-point energy, nuclear energy)
γ	Power of waste heat in the form of thermal radiation of photons
ν	Power of other waste disposals (e.g., neutrino radiation, non-thermal emission, kinetic energy, energy-to-mass conversion)
T_{waste}	Characteristic color temperature of thermal waste photons

Table 2.1: Definitions of Parameters in the AGENT Formalism (Wright et al., 2014)

According to the principles of energy conservation and steady state, energy collected or produced by a civilization must be equal to energy released as waste heat or disposed by the civilisation. This implies that,

$$\alpha + \epsilon = \gamma + \nu$$

To better understand these parameters, let's calculate them for humanity. Around 1.7×10^7 Megawatts, or 1.4×10^5 TW hr per year, of energy are provided to humanity, primarily by fossil fuels (Kleidon 2010). Since the total amount of sunlight incident on the Earth is 1.7×10^{11} MW. We parameterize humankind as having the numbers shown in table 2.2.

Parameters	Value	Notes
α	$\sim 10^{-7}$	Counting only photovoltaic generation (ignoring passive heating, agriculture, etc.)
ϵ	$\sim 10^{-4}$	Mostly fossil fuel, some nuclear
γ	$\sim 10^{-4}$	$\sim \epsilon$
ν	Negligible	Radio transmission and radar, neutrino losses in nuclear reactors, kinetic and potential energy in spacecraft
T_{waste}	$\sim 285K$	Typical operating/ambient temperature

Table 2.2: Approximate Values for Humanity in the AGENT Formalism (Wright et al., 2014)

During my thesis research, we have made the assumption that the primary source of energy input for the civilization is through the captured stellar radiation by the Dyson Sphere, ($\epsilon \ll \alpha$). Furthermore, we have assumed that the primary method of energy dissipation is through thermal photons, ($\gamma \gg \nu$). This leads to

$$\alpha = \gamma$$

We also consider that Dyson Spheres behave as gray absorbers and that their thermal losses can be described by a blackbody with a temperature between 100-1000 K. This temperature range is determined by the detectability of the excess infrared radiation emitted by the Dyson Sphere in the mid-IR wavelength range, which is the range where WISE operates. If the temperature is lower than 100 K, the excess would be in the far-IR, and if the temperature is higher than 1000 K, the excess would shift to the near-IR.

Using these presumptions, only two parameters - the effective temperature of the DS (T_{DS}) and the luminosity of the thermal radiation it emits (L_{DS}) - are necessary to simulate the spectra of stars surrounded by DS. To make things more straightforward, we redefine γ as the normalised DS energy output:

$$\gamma = \frac{L_{DS}}{L_*}$$

Where, L_{DS} is the brightness of the DS and L_* is the brightness of the host star before the DS was veiled. According to this definition, γ may have values ranging from 0 to 1. In the case of an isotropically emitting star, γ also denotes the level of completeness of the DS or, in more colloquial words, the fractional solid angle of the outgoing radiation intercepted by the DS (the covering factor). Because of this, we use γ and covering factor interchangeably throughout this analysis.

2.4 Spectrum of Dyson Sphere

We can simulate the photometric and spectroscopic characteristics of an obscured star and its DS using the above assumptions. We lay forth a fundamental spectral model for this compound system in this section.

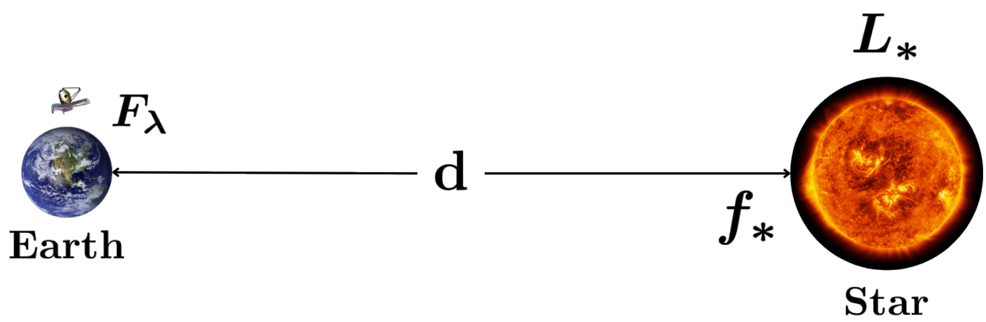

Consider a simple model in which a star at distance d has a stellar luminosity L_* and a flux density (Wm^{-2}/m) received across wavelength λ at Earth F_λ then

$$\lambda F_\lambda = f_* \frac{L_*}{4\pi d^2} \tag{2.9}$$

Here, f_* represents the fractional energy distribution of star across wavelength. It is a function of wavelength $f_* = f(\lambda)$ and It is defined as -

$$f(\lambda) = \lambda \frac{B_\lambda(T)}{L}$$

Where, $L = \dfrac{\sigma T^4}{\pi}$ is the radiance from a specified angle of view (watts per square metre per steradian).

$$f(\lambda) = \lambda \frac{\pi B_\lambda(T)}{\sigma T^4}$$

Suppose this star hosts a civilisation with a Dyson sphere around it of temperature T_{DS} and blocking a fraction α of the stellar luminosity. As we assumed primary method of energy dissipation is through thermal photons of temperature $T_{DS} = T_{waste}$. The spectrum received at Earth will be altered, to first order, by the presence of the civilisation and become,

$$\lambda F_\lambda = [(1-\alpha)f_* + \gamma f_{DS}]\frac{L_*}{4\pi d^2}$$

Here, f_{DS} represents the fractional energy distribution of DS across wavelength.

$$\lambda F_\lambda = \left[(1-\alpha)\frac{\lambda\pi B_\lambda(T_*)}{\sigma T_*^4} + \gamma\frac{\lambda\pi B_\lambda(T_{DS})}{\sigma T_{DS}^4}\right]\frac{L_*}{4\pi d^2} \tag{2.10}$$

Where, $B_\lambda(T_{DS})$ is the specific intensity of the Dyson Sphere of temperature T_{DS}.

If we roughly approximate a star as a blackbody with temperature T_* then the estimated SED can be rewritten as follows -

$$F_\lambda \approx \left[(1-\gamma)B_\lambda(T_*) + \gamma B_\lambda(T_{DS})\left(\frac{T_*}{T_{DS}}\right)^4\right]\frac{\pi}{\sigma T_*^4}\frac{L_*}{4\pi d^2} \tag{2.11}$$

Then Specific luminosity of the combined system (DS+Star) becomes,

$$L_\lambda \approx \left[(1-\gamma)B_\lambda(T_*) + \gamma B_\lambda(T_{DS})\left(\frac{T_*}{T_{DS}}\right)^4\right]\frac{\pi}{\sigma T_*^4}L_* \tag{2.12}$$

Using Rayleigh-Jeans limit as $\lambda \gg hc/(kT_*)$ *i.e.* $B_\lambda(T) = \dfrac{2ckT}{\lambda^4}$, we can approximate above expression more realistically,

$$L_\lambda(\lambda \gg hc/(kT_*)) \approx \left[(1-\gamma) + \gamma\left(\frac{T_*}{T_{DS}}\right)^3\right]\frac{2\pi ck}{\lambda^4\sigma T_*^3}L_* \tag{2.13}$$

$$\approx \left[(1-\gamma) + \gamma\left(\frac{T_*}{T_{DS}}\right)^3\right]L_\lambda(\gamma = 0) \tag{2.14}$$

This above expression emphasises the important benefit of looking for high γ civilizations using the mid-infrared (MIR) wavelength region. A high MIR flux will result from the waste heat from these civilizations, which is mostly controlled by the factor $(\frac{T_*}{T_{DS}})^3$. This term has the ability to increase the MIR flow by a factor of 10^3 even for moderate γ values. For a civilisation having $\gamma = 0.15$, $T_* = 4000\ K$ and $T_{DS} = 255\ K$, this causes the MIR flux to increase by nearly 7 magnitude. Because the $255K$ waste heat would predominate the MIR colour temperature, it would stand out from other astronomical sources in terms of colour and brightness.

In contrast, the optical and near-infrared (NIR) dimming effects are significantly less pronounced and only perceptible for α or γ values close to 1.

The figure 2.8 provides illustrative examples of the impact of a Dyson sphere (DS) on a Sun-like blackbody spectrum with $T_* = 5778\ K$ and $L_* = 1L_\odot$. The modifications in the blackbody spectrum are shown under various assumptions concerning the DS temperature and coverage factor in the above equation 2.14. Both panels in the figure exhibit a Sun-like blackbody spectrum. We show how a DS with a fixed temperature of 300 K and a covering factor of either = 0.1, 0.5, or 0.9 alters the compound spectrum in the top panel 2.8a. As can be observed, the DS results in an increase in the mid-infrared and a decrease in the stellar component's brightness. It depends on the DS covering factor for both features. In the optical and near-infrared spectrums, the decrease is dominating. In the bottom panel 2.8b, we demonstrate how the spectrum changes when we use DS models with a fixed covering factor of 0.5 and DS temperatures of 100, 300, and 600 K. The signatures—a decrease in stellar flux and an increase in the mid-infrared—that were previously stated are restored. The mid-infrared blackbody peak shifts in wavelength when DS temperature changes since we are taking a variety of DS temperatures into account.

In this analysis, the temperature range of DS was chosen such that the excess in IR, should be within the WISE mission's observable wavelength window.

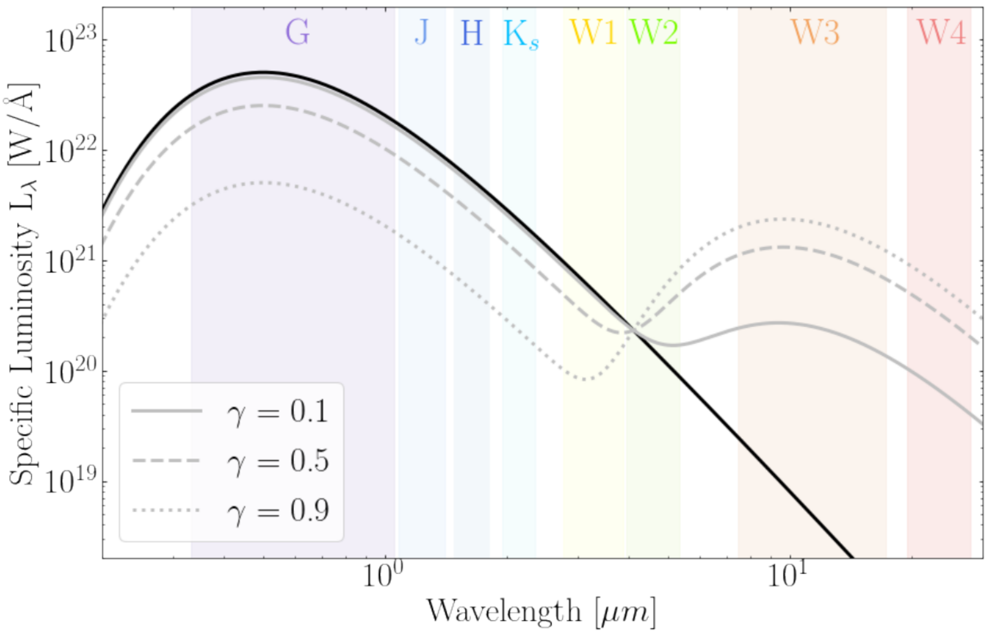

(a)

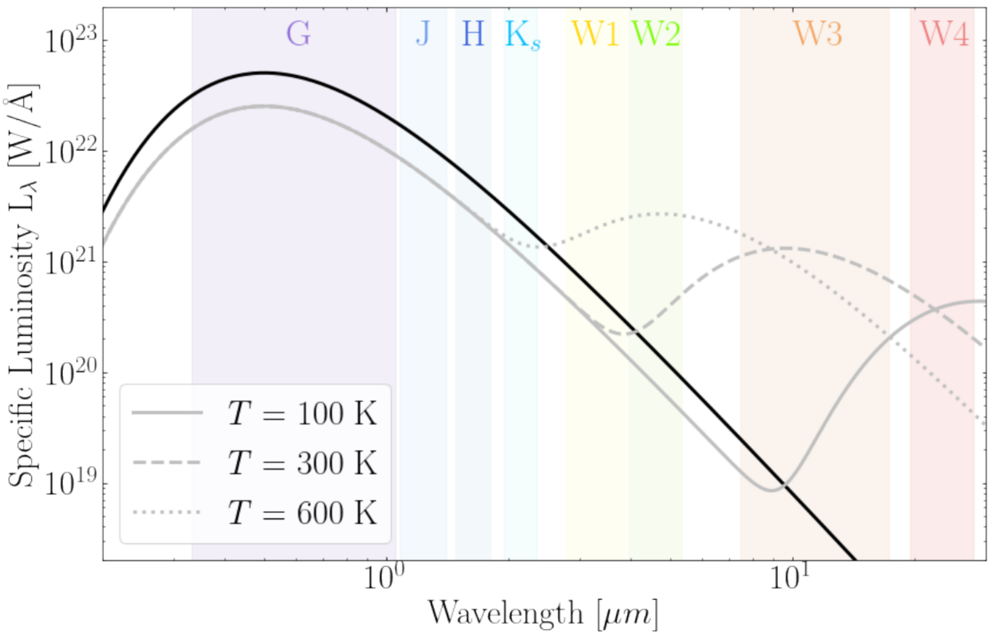

(b)

Figure 2.8: These figures represents the modified blackbody spectra of the Sun as a result of the presence of Dyson spheres having different combination of γ & T_{DS}. The unmodified blackbody ($T_* = 5778K, L_* = 1L_\odot$) is shown by the solid black line in both panels. In the top panel, grey solid, dashed, and dotted lines, respectively, represent DS models with $T = 300K$ and covering factors of 0.1, 0.5, and 0.9. On the bottom panel, grey dotted, dashed, and solid lines, respectively, represent DS models with a covering factor of 0.5 and temperatures of 100, 300, and $600K$. The coloured bands correspond to the wavelength ranges of the Gaia, 2MASS, and WISE missions. Image Credit: Matias Suzao from his paper (Suazo et al., 2022).

CHAPTER 3

Analysis of red fraction of stars

Colour magnitude diagrams(CMDs) are an important tool to study stars. Dyson sphere candidates appear slightly dim in the optical spectrum but luminous in the infrared when viewed via telescopes. There are several astrophysical sources, like- YSOs, that exhibit the same characteristics - dim in the optical band and bright in the infrared as genuine Dyson sphere candidates. These YSOs appear redder due to interstellar reddening and are placed in the HR diagram or CMD just right above the main sequence. When we do a colour-magnitude analysis of these Dyson sphere candidates to further confirm them, we find that they are located in the region of YSOs in CMDs. Using the astrophysical properties of these YSOs, we are trying to filter the false-positive Dyson sphere candidates.

3.1 CMD of GAIA DR2 Sources

I plotted the colour-magnitude diagram of 152879 sources from the GAIA DR2 keeping the Y-axis as the Absolute Magnitude of the G band and the X-axis as $G_{BP} - G_{RP}$ as shown in the figure 3.1.

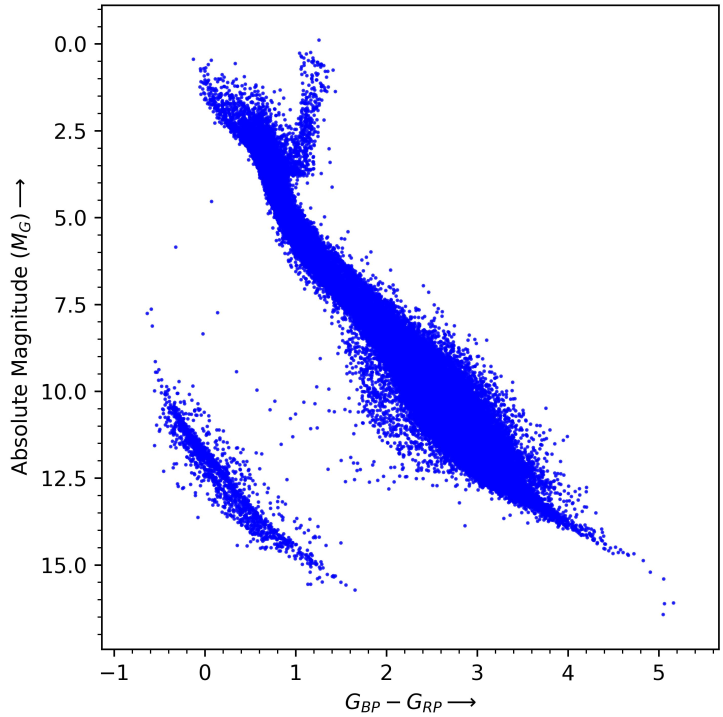

Figure 3.1: Color Magnitude Diagram (CMD) of 152879 sources from the GAIA DR2

3.2 Red Fraction Analysis

Since the dust clouds are so huge (generally light-years across), the whole cloud tends not to collapse into one star. Instead, it appears that different portions of a vast cloud can collapse toward different gravitational centres, with the result that one giant cloud light-years across can produce several stars (and presumably planetary systems). These pre-main sequence stars are located within dust clouds, and when we study them in the visible range, not just interstellar but also circumstellar extinction and reddening lead them to look redder. A star is born when the core temperature of a pre-main star reaches millions of Kelvin and begins fusing hydrogen with helium. All of the dust particles spread out in interstellar space as a result of the star's radiation pressure, and the disc that surrounds the star develops into a planetary system. Those stars which lie within the nebula will appear more redden, while those stars which lie outside appear less redden. These characteristics of the nebular region will help us classify whether a star belongs to the nebular region or not.

For our analysis, we will be utilizing the (G-K) color index against the absolute magnitude in the G band of the GAIA (i.e. M_G) color-magnitude plot. The color-magnitude diagram will assist us in determining whether a star falls into the category of being red or not. A star will be classified as red if its color index (G-K) value is greater than that of corresponding main sequence stars with the same absolute magnitude. Our definition of a red star is straightforward, which means any star that appears to the right of the main sequence star boundary (represented by the golden line) in the color-magnitude diagram of (G-K) vs. M_G. This classification is illustrated in figure 3.2.

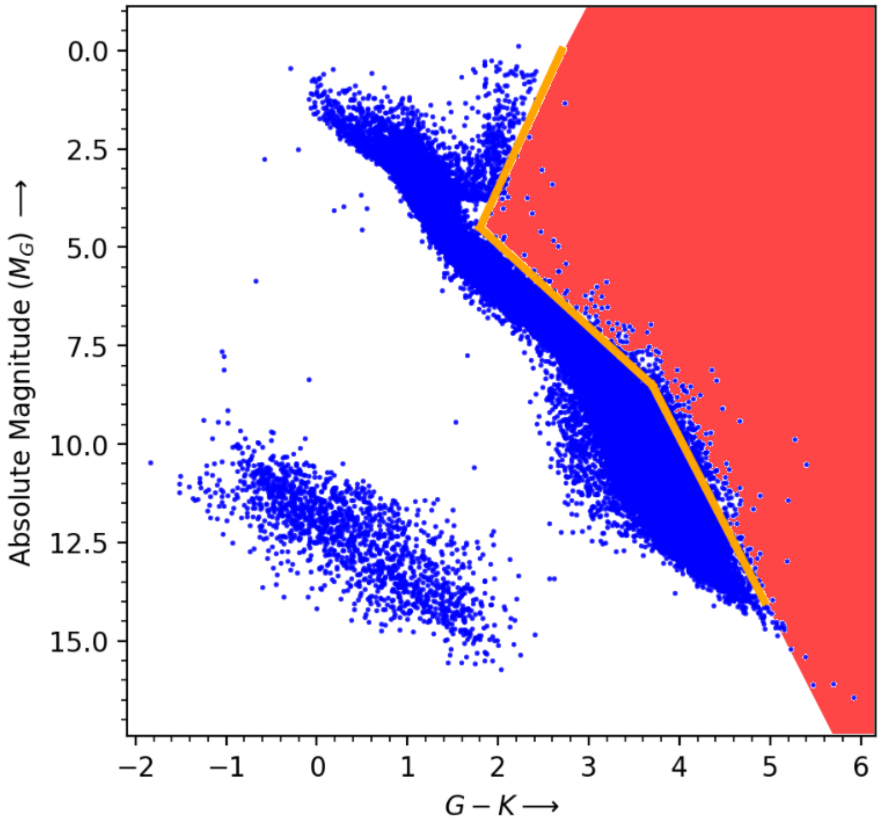

Figure 3.2: Any star that is located in the plot's red area is referred to as a red star.

3.2.1 Boundary Lines

In the (G-K) vs M_G plot, we define the boundary line by choosing arbitrary points on it which will separate the main sequence stars and red stars. The arbitrary points in the (G-K) vs M_G plot are A$(2.5, 1)$, B$(1.8, 4.5)$, C$(3.7, 8.5)$ and D$(4.6, 12.5)$. Depending on the value of absolute magnitude (M_G) of the star, we divide the boundary line into three segments AB, BC and CD. We have two individual straight-line equations as shown in the figure below 3.3.

Case I: $M_G \leq 4.5$

From the definition of the straight line equation

$$\frac{y - y_0}{x - x_0} = \frac{y_1 - y_0}{x_1 - x_0}$$

Using points A and B, we can find the equation of boundary line -

$$x = 2.5 - \frac{(y - 1)}{5}$$

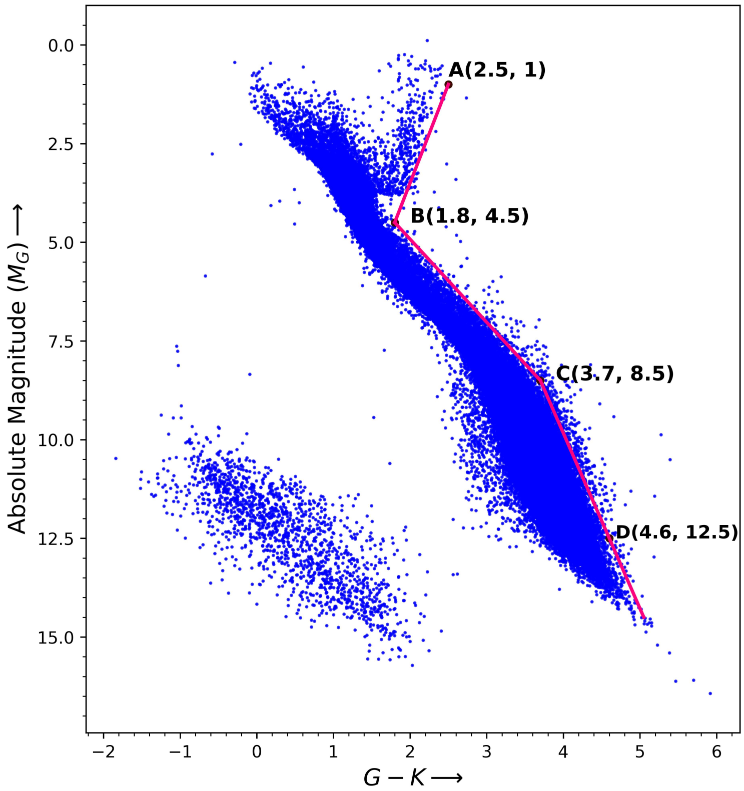

Figure 3.3: Defining arbitrary boundary equation

Similarly for other,

Case II: $4.5 < M_G \leq 8.5$

Using points B and C,

$$x = 1.8 + \frac{1.9 \times (y - 4.5)}{4.0}$$

Case III: $M_G > 8.5$
Using points B and C,

$$x = 3.7 + \frac{9 \times (y - 8.5)}{40.0}$$

Here, x and y stand for the G-K and M_G value of the star.

3.2.2 Search Radius

The size of the nebular region in interstellar space varies significantly. Stars are born collectively in the nebular cloud. As time progresses, some of these stars undergo evolution and eventually become main-sequence stars. These stars are then dispersed throughout the nebular cloud. The angular search radius is a crucial factor in our analysis of the red fraction of stars around a source, whether it is a main sequence star or a YSO. As the angular search radius increases, more stars are included in our search sample, which can affect the calculated red fraction. This is demonstrated in the image below 3.4, where an increase in the angular search radius results in a larger number of stars being included in our search result.

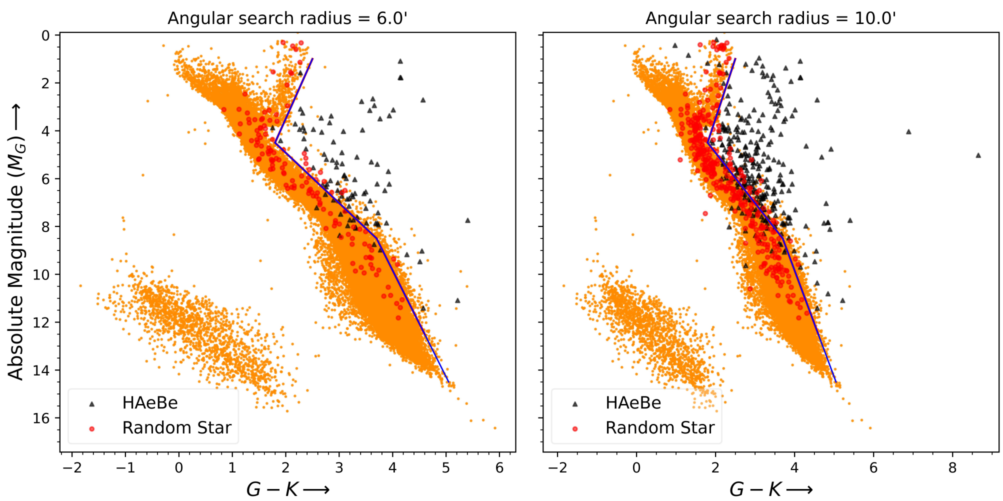

Figure 3.4: Placing all neighbouring stars of a Herbig Ae/Be star and Random star in CMD for two different radii 6' and 10'.

3.2.3 Work flow for finding the fraction of red star around a source

The process of determining the fraction of red stars surrounding a target source involves various steps, including selecting the right ascension and declination of the target source, accessing data from the GAIA database, and analyzing it. The flow chart depicted in Figure 3.5 outlines the process of determining the red fraction of stars around a target star/candidate.

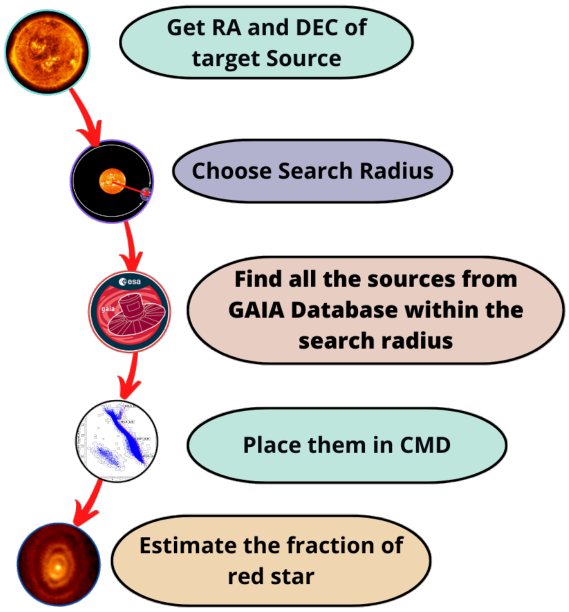

Figure 3.5: Describing the process of finding the red fraction of stars around a target source.

3.3 Analysis for Herbig Ae/Be and Random stars

For the initial analysis of this technique, I randomly chose 20 well-known Herbig stars from a catalogue of Vioque et al. and the 20 random stars from GAIA DR3 and find the fraction of red stars around them within the search radius of 5 arcminutes. We can clearly see that the average fraction of red stars for the 20 Herbig Ae/Be stars is about 0.72 and 0.17 for the 20 randomly chosen main sequence stars. These findings indicate that the average red star fraction for the Herbig Ae/Be stars is higher than that of the randomly chosen main sequence stars. The plot in figure 3.6 shows the red star fraction values for the 20 random randomly chosen main sequence stars and 20 Herbig Ae/Be stars.

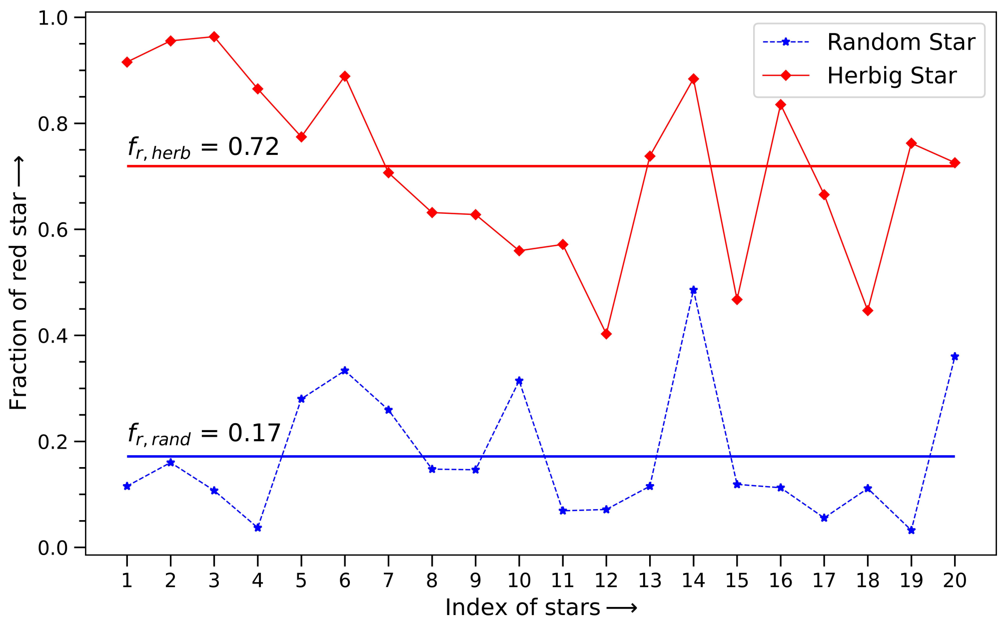

Figure 3.6: This graph represents the fraction of red stars of 20 Herbig Ae/Be and 20 randomly chosen main sequence stars within 5 arc-minutes.

There are some cases where the individual red fraction for a main sequence star is higher than that of a Herbig Ae/Be star. In the above plot, it is clear that the main-sequence star (index 14) has a higher red fraction value than the Herbig Ae/Be star. The distribution of dust is non-uniform throughout the Milky Way. During the evolutionary process of stars in nebular regions, some of them move out of the nebular clouds while others remain in them. Stars that leave the nebular regions may enter into dusty regions where the density is higher than that of the interstellar medium. Light from those stars that remain inside the nebular regions or in higher-density dust regions encounters more reddening due to the higher amount of dust. This leads to a higher red fraction around these stars.

The fraction of red stars around a target source depends on the search radius. To see the dependency of the fraction of red stars on the search radius, I calculated the red fraction of these stars with different search radii around them. The average fraction of red stars around Herbig Ae/Be stars is 0.72 ± 0.16 whereas the average fraction of red stars around a Random star is 0.15 ± 0.12. I observed that the red fraction of these stars almost remains constant for all radii as shown in figure 3.7

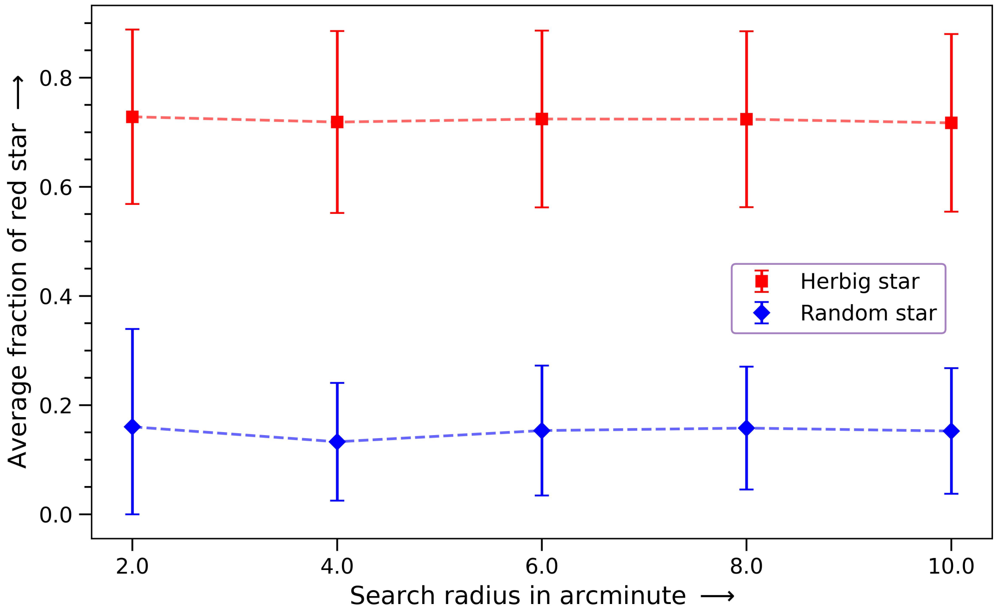

Figure 3.7: Variation of fraction of red stars with radius around 20 Herbig Ae/Be stars (Vioque et al., 2020) and 20 Random stars

We have a total of 218 well-verified examples of Herbig Ae/Be star from Vioque et al.. Further, I tried to calculate the average red fraction of the star for all these Herbig Ae/Be stars simultaneously. The distance distribution of HerbigAe/Be stars is shown in figure below 3.8. To address distance distribution biases, we chose 218 main sequence stars with a similar distance distribution as the Herbig Ae/Be stars as shown in figure 3.8.

So now, we have sampled 218 random stars with the same distance distribution as Herbig Ae/Be stars. I estimate the fraction of red stars among all sources in the Herbig Ae/Be and random star catalogues for an angular search radius of 6'. The variation of the fraction of red star for both Herbig and Random star with the distance of the source is shown below in figure 3.9. The average fraction of a red star for a Herbig Ae/Be star is 0.669 ± 0.262 while the average fraction of a red star for a random star is 0.330 ± 0.283. The **red line** represents the average fraction of the red star for Herbig Ae/Be while the **blue line** represents the average fraction of the red star for the random star.

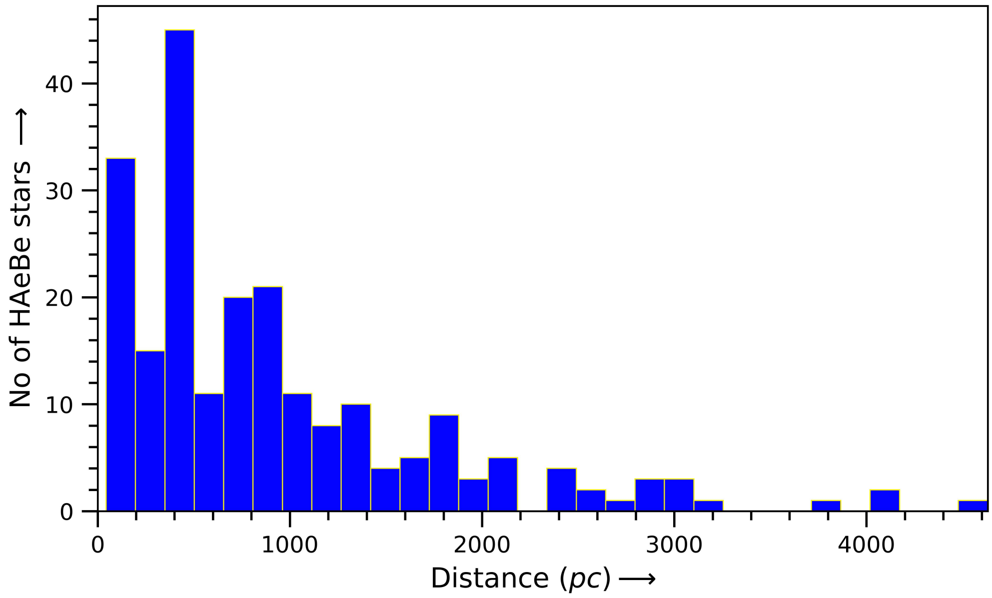

Figure 3.8: Distance distribution of all 218 Herbig Ae/Be (HAeBe) stars from (Vioque et al., 2020)

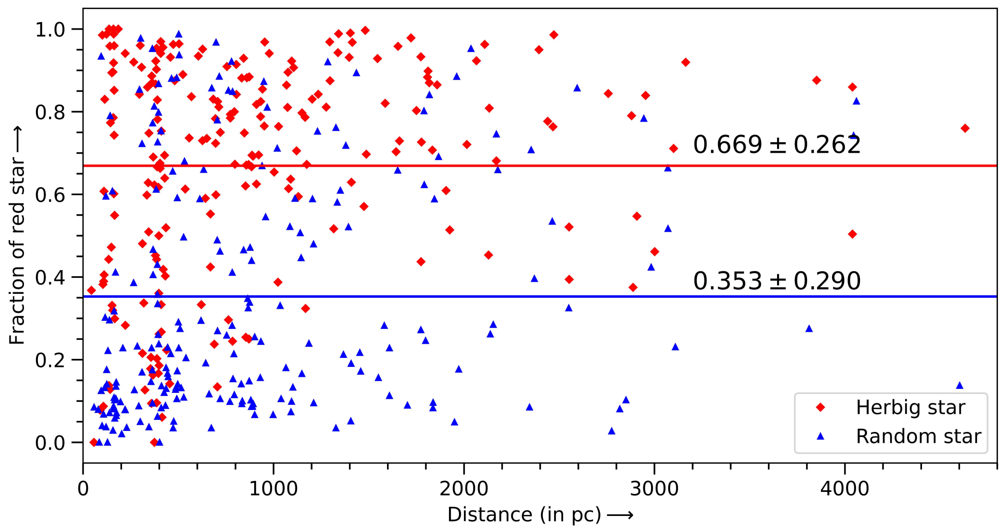

Figure 3.9: This plot shows their distances vs the red fraction for all 218 Herbig Ae/Be stars and 218 random stars having **angular search radius = 6'**.

We also plotted the probability distribution of the fraction of red stars for both Herbig Ae/Be stars and random stars in the figure below 3.10.

The plot indicates that a star with a lower red fraction value is more likely to be located in a non-nebular region than in a nebular region. Conversely, a star with a higher red fraction value is more likely to be situated in a nebular region, which suggests that the star may actually be a young star. Therefore, determining the red

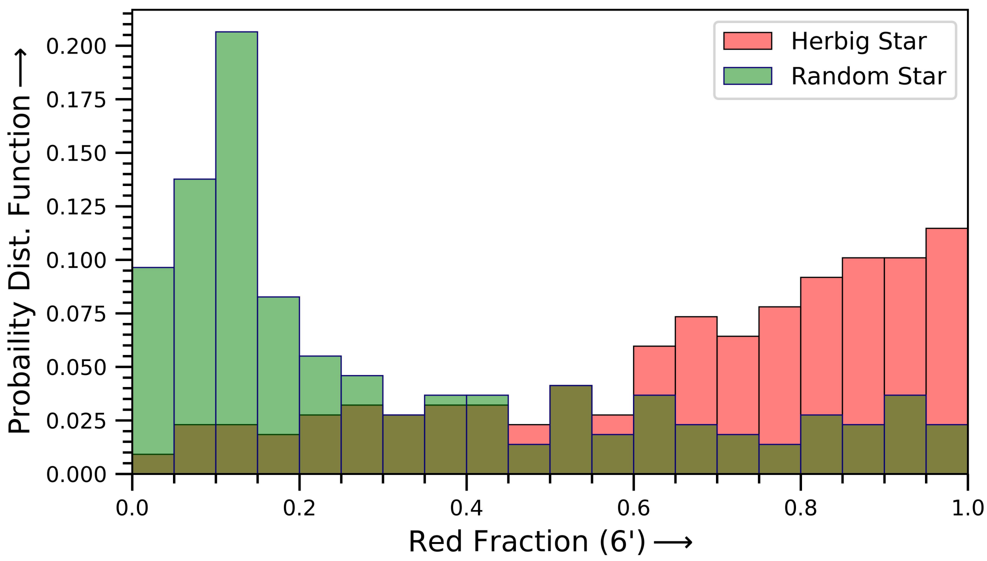

Figure 3.10: Top: Probability distribution of fraction of red star within the search radius $6'$ for Herbig Ae/Be star and Random chosen main sequence star. Bottom: Cumulative distribution function of corresponding above PDF.

fraction parameter value for all Dyson sphere candidates can aid in classifying as truly DS candidates or a young star.

3.4 Analysis for T Tauri stars

To check the robustness of our method, we extended this analysis to the T Tauri Star, which is another sort of YSO. T Tauri stars are sampled from the four different catalogues of Nebulae - **Orion Nebula** (Szegedi-Elek et al., 2013), **Lagoon Nebula** (Kalari et al., 2015), NGC 2264 (Barentsen et al., 2013) and IC 1396 (Barentsen et al., 2011). Taking into account the same distance distribution as Her-big Ae/Be stars (3.8), I selected 218 T-Tauri stars from these four catalogues mentioned above. We find the fraction of neighbouring red stars for T Tauri within the search radius of $6'$ and comparing with Herbig Ae/Be and random stars as shown in figure 3.11 and plotted the corresponding pdf of all three sources as shown in the figure 3.12.

It is clear that the neighbouring fraction of red stars around T Tauri stars is 0.871 ± 0.063, which is greater than that of randomly chosen main sequence stars. These results tell that the neighbouring fraction of red stars around a YSO (T Tauri and Herbig

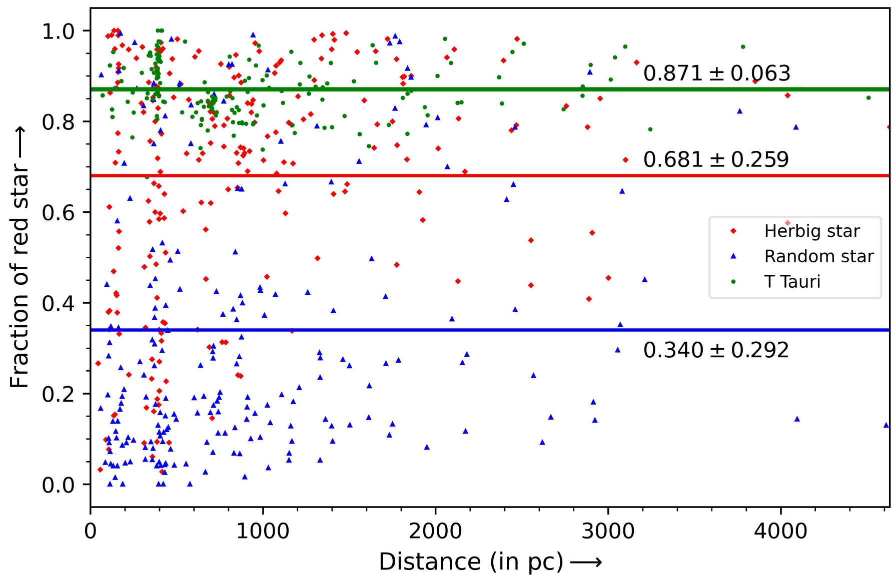

Figure 3.11: The red fraction for T Tauri, Herbig Ae/Be and Random star for angular search radius = $6'$.

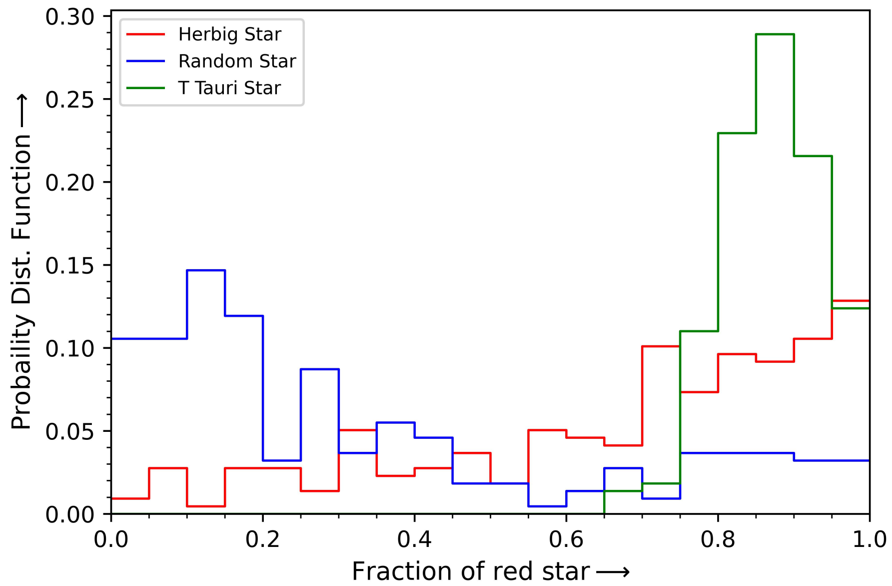

Figure 3.12: The corresponding pdf for the fraction of Herbig Ae/Be, T-Tauri, and randomly selected stars with an angular search radius of $6'$.

Ae/Be stars) is greater than that of main sequence stars. So, we can use this parameter to describe whether a star lie in a nebular region (dusty region) or not. If the neighbouring fraction of red star around a DS candidate is high then we can simply say that the chances of being this candidate in the nebular region are high, and then we can discard this candidate from our catalogue.

CHAPTER 4

Dyson Sphere Candidates

The search for extraterrestrial intelligence has been a topic of fascination for scientists and the general public alike for decades. One potential solution to the problem of finding intelligent life is the concept of searching a Dyson sphere (DS), a hypothetical megastructure that surrounds a star and captures all of its energy output. However, the vastness of space and the limitations of human technology made identifying potential Dyson spheres a daunting task in the past, but with today's advancements in technology and algorithm, we are now able to search for observable signatures of potential Dyson Sphere candidates, dim in the optical band and bright in the infrared, in our Milky Way. This observational signature of DS is described in chapter 2, section 2.3.

4.1 Identifying Dyson Sphere Candidates from GAIA

To identify potential Dyson Sphere candidates in the Milky Way, my collaborator, Matías Suazo in his paper Suazo et al. (2022) has developed a Spectral Energy Distribution (SED) based model of combined system (DS + Star) based on the observational signatures of a Dyson sphere, dimming in the optical band due to the obscuration of starlight and brightening in the infrared due to the release of waste heat from the structure. The theory behind the model is described in the section 2.3. There are two main parameters which are optimised to fit the observational data - the covering factor of the DS (γ) and the temperature of the Dyson Sphere (T_{DS}). The model is used by Matias to fit the spectral energy distribution (SED) of stars that have been observed by the GAIA mission. The observed spectrum data for these stars are collected from various missions, such as optical photometry data from DSS, SDSS, and GAIA, and infrared photometry data from 2MASS and ALLWISE. To identify potential Dyson sphere candidates, the model is fitted to the observed data of stars, and the best-fit parameters γ and T_{DS} are determined. These parameter values are then assigned to the DS candidate for further verification. This process is carried out for all IR excess sources in GAIA, resulting in a tentative list of potential Dyson sphere candidates being selected. This process of selecting DS candidates is described in figure 4.1.

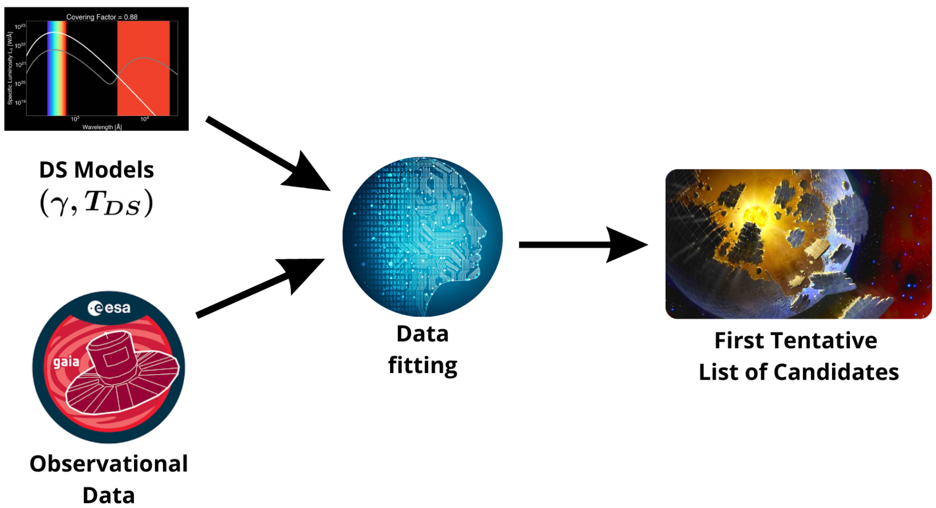

Figure 4.1: The figure explains the flow of selecting first tentative list of potential DS candidates from the GAIA database by fitting model with observational data.

The below figure 4.2 shows two potential Dyson Sphere candidates selected using this model fitting method corresponding to the best parameters values. The best parameter value corresponding to the candidates shown in figure 4.2a and 4.2b are ($\gamma = 0.10$ & $T_{DS} = 100.0\ K$) and ($\gamma = 0.10$ & $T_{DS} = 125.0\ K$) respectively.

However, there are other sources that can mimic these signatures, such as young stellar objects (YSOs). To filter out these YSOs from our potential DS candidate list, we have taken use of the natural habitat of YSOs, which means that these YSOs are

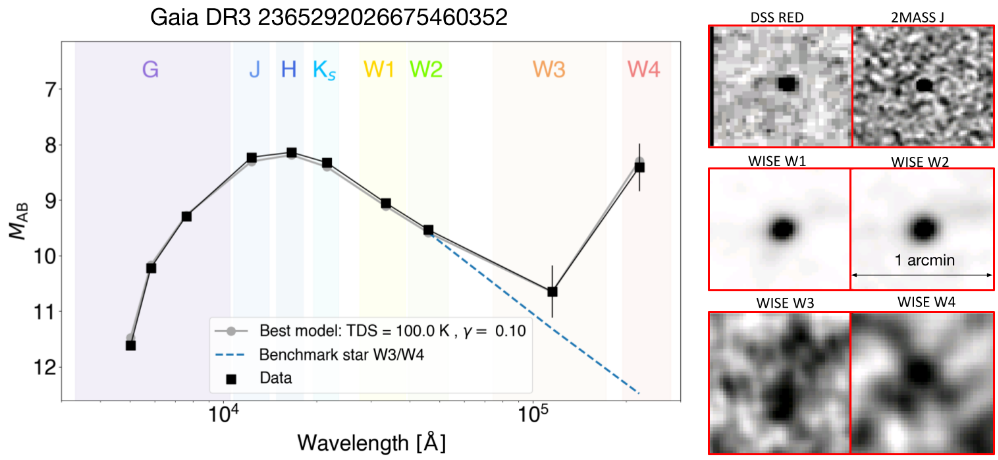

(a)

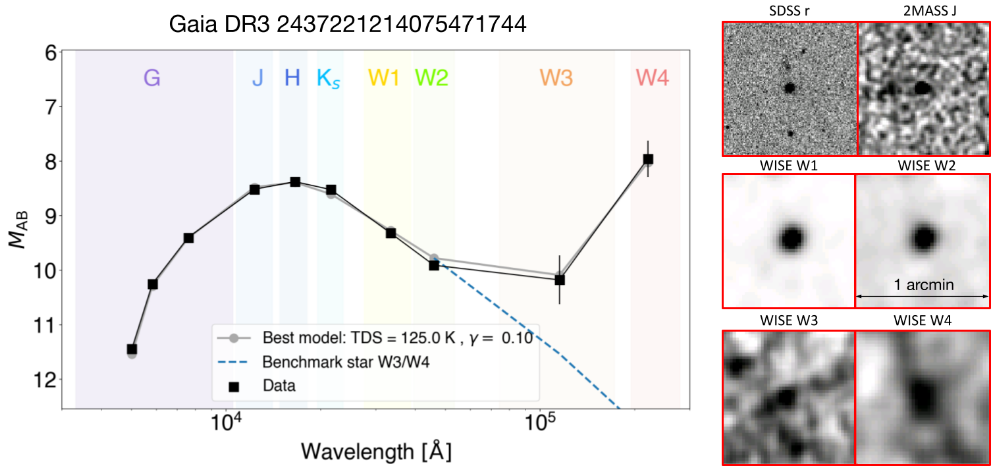

(b)

Figure 4.2: The best parameters γ and T_{DS} obtained by fitting the model with observed data are used to select potential Dyson sphere candidates. The top candidate has $\gamma = 0.10$ and $T_{DS} = 100.0\ K$, while the bottom candidate has $\gamma = 0.10$ and $T_{DS} = 125.0\ K$. Image Credit: Matias Suzao

typically found within nebular regions. It is unlikely that our Dyson sphere candidates would be found in such regions since they are known to be chaotic and violent in terms of energy phenomena. Suazo et al. (2023) (In Prep.) utilized a Convolution Neural Network (CNN) image classifier to differentiate between stars in nebular and non-nebular regions by analyzing ALLWISE W3 (corresponding to wavelength $12.0\ \mu$m) images of sources from the IRSA database. If the image classifier detects nebular features around the candidate, it discards that candidate from our list. However, there are instances where the CNN nebulae classifier failed to detect any nebular features around the potential Dyson sphere candidates, but further literature surveys have revealed that these candidates are located in the nebular region. This discrepancy is due to the limitations of our detection instruments, which can only detect nebular features within a certain range. The figure 4.3 below summarizes the above process. Nonetheless, this highlights the importance of combining automation with human expertise and knowledge to ensure the accuracy of our findings.

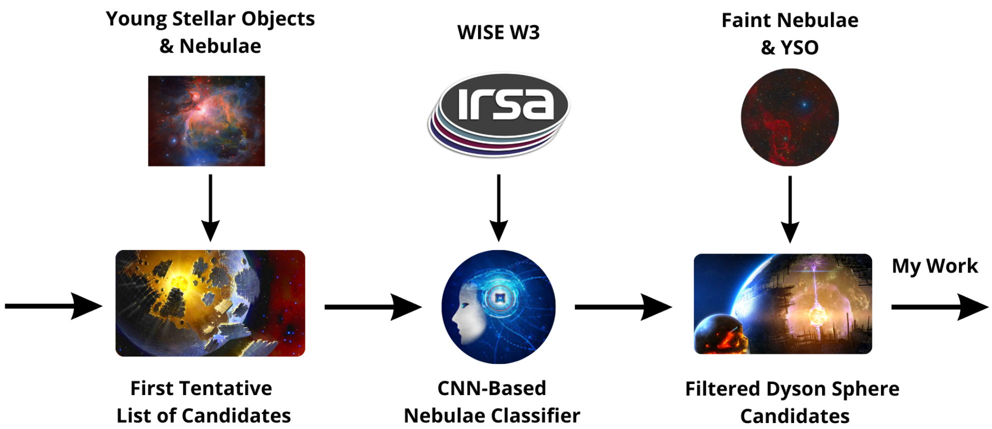

Figure 4.3: This figure represents the flow of filtering out YSOs by looking at nebular features around it using the Machine Learning Algorithm in IRSA database.

Matias Suzao has provided a list of 302 potential candidates for Dyson spheres, which were identified after filtering out false-positive candidates using a CNN image classifier as shown in Appendix A. However, these candidates need to be further verified. In my master's thesis, I aim to verify these candidates by developing the red fraction, which quantifies the dust around the candidates, and finding it for all the candidates. Additionally, I plan to cross-verify them across multiple databases.

4.2 Finding another parameter

In addition to the fitting model with observed data and the CNN Nebulae classifier, I have also developed another parameter to filter out false positive Dyson sphere candidates. This parameter is called the "red fraction" described in chapter 3 and it is based on the astrophysical phenomenon of interstellar and circumstellar dust reddening, when light passes through dust particles, the shorter wavelengths are blocked, allowing only the longer wavelengths to pass through. This leads to the reddening of light, which is an observable effect in astrophysics.

By examining the red fraction around our Dyson sphere candidates, we can determine whether they are located within a nebular region or not. If the candidate is within a nebular region, the red fraction will be higher due to the presence of more circumstellar and interstellar dust. Conversely, if the red fraction is low, it indicates that the candidate is not located within a nebular region.

The histogram shows the distribution of the red fraction of all the DS candidates in figure 4.4.

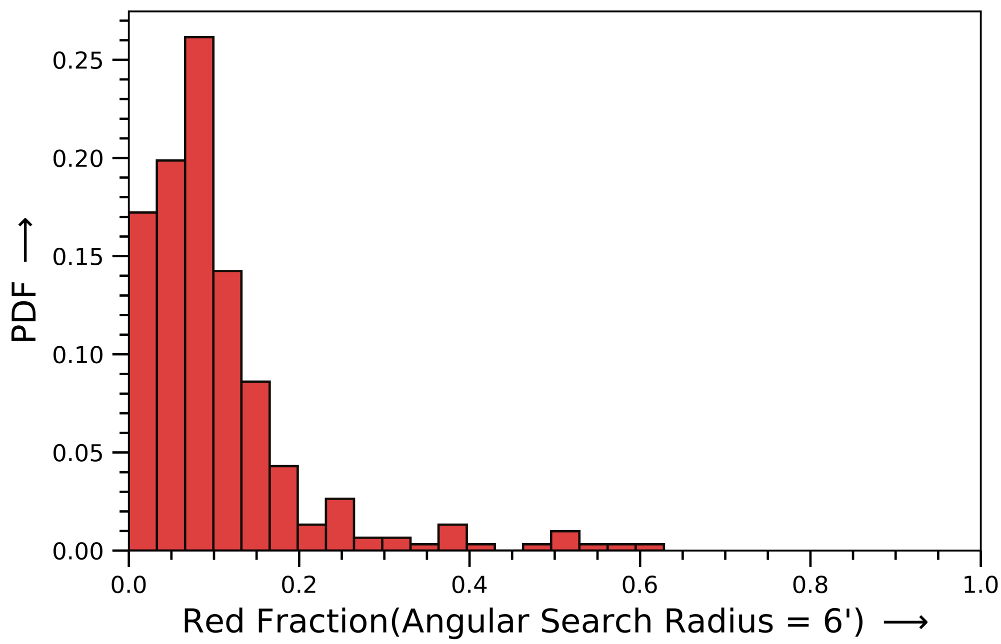

Figure 4.4: This plot shows the red fraction distribution of all DS candidates.

The majority of DS candidates have red fraction values below 0.20, while only a few have values exceeding 0.45. This suggests that most of the candidates are unlikely to belong to nebular regions, but a small number have a higher probability of being found there due to their higher red fractions. Nonetheless, we are not excluding candidates with higher red fractions since our analysis indicates that some main sequence stars also exhibit this trait, even though they are not as numerous.

By incorporating this additional parameter, we can further refine our selection process and reduce the number of false positive Dyson sphere candidates. The combination of model fitting, CNN nebular feature analysis on images, and the red fraction parameters allow us to accurately identify potential Dyson spheres and increase the likelihood of discovering extraterrestrial intelligence.

To ensure the quality of observed sources, we considered several parameters, including Gvar, RUWE, Astrometric Excess Noise (AEN), WISE ph_qual, and WISE var_flag. The Gvar parameter provides information on the variability of a source in the optical band, while RUWE and Astrometric Excess noise help to determine the accuracy of the parallax and proper motion measurements in the Astrometric solution. WISE ph_qual parameter indicates the quality of photometry in the MID-infrared band, and the WISE var_flag parameter informs about the variability of the source in the MIR, with some limitations in the W3 and W4 bands.

4.3 Verification of DS candidates across different databases

In the search for potential Dyson spheres, my collaborator and I utilized a combination of model fitting, nebular feature analysis using CNN, and the red fraction parameter to accurately identify 302 potential candidates. The list of all DS candidates is shown in Appendix A. It is important to note that these candidates are still just - candidates. We must have to conduct further investigations to confirm their nature and distinguish them from natural astronomical phenomena. Importantly, the limited capabilities of our instruments may introduce potential errors in data about sources. This potential error in sources may lead to a Dyson Sphere candidate in our list. So, we have to get rid of these candidates. Therefore, we conducted manual inspections across various databases, including Aladin Lite, VizieR, and IRSA, to look for other types of anomalies, for instance - Aladin Lite is used to see the DS candidates in different wavelength regimes, IRSA database is used to inspect the photometric anomalies, especially in ALLWISE and VizieR database is used to inspect the source across the past literature surveys whether this source is classified as YSO, main sequence star, QSO or other interstellar objects.

By looking across these databases, we filtered out 136 candidates due to bad photometric data quality and low angular resolution of ALLWISE, leaving us with 166 positive potential Dyson Sphere candidates for further possible verification.

4.3.1 Contaminated Sources

Contaminated sources are those which show anomalous features that are not consistent with the expected observational signature of Dyson spheres The IR photometry data from ALLWISE plays an important role in selecting Dyson Sphere candidates. We are expecting excess IR radiation from these sources (why described in expression 2.14) but it is possible that excess IR radiation can get from various other reasons also. So we have to look at images of DS candidates carefully across the observing bands of ALLWISE. The AllWISE measured sources in four passbands, $W1$, $W2$, $W3$ & $W4$, covering near- and mid-IR wavelengths centred at $3.4, 4.6, 12$, and $22\mu m$ with an angular resolution of the filters of $6.1'', 6.4'', 6.5''$, and $12.0''$ respectively. In our list of 136 false-negative DS candidates, which we eliminated, there are primarily three categories of contaminated sources. To get a better idea about the distribution of contaminated DS candidates, a pie chart is shown below 4.5.

The first category consists of sources that are blended with nearby sources due to low angular resolution, while the second category includes irregular sources around it in ALLWISE band caused by low SNR. The third category comprises faint sources, which were also discarded. Two sources have been removed from the list of Dyson sphere candidates. One source has UV emission, which are not expecting from our DS candidates, while the other star was classified as a Herbig Ae/Be star in a study by Vioque et al. (2020). More detailed explanations of each category are provided below.

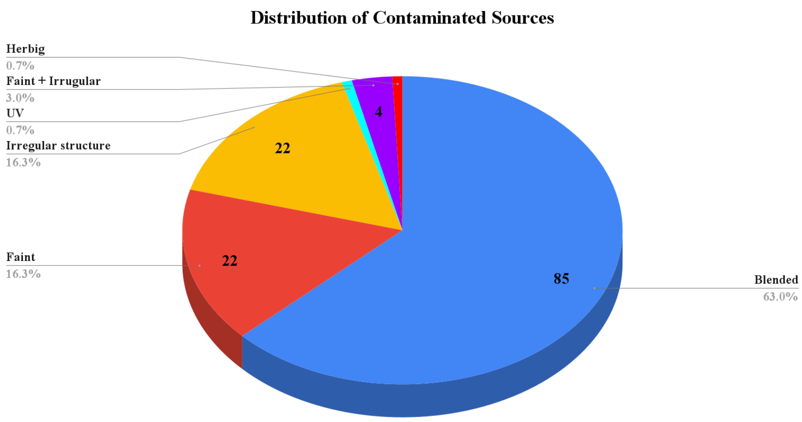

Figure 4.5: Distribution of discarded sources due to contaminated

1. Blended

Due to the limited angular resolution of the ALLWISE photometry, it is often unable to resolve very close sources. Consequently, a significant number of our target DS candidates were found to be blended with nearby sources. An example of such a structure is shown in the figure 4.6.

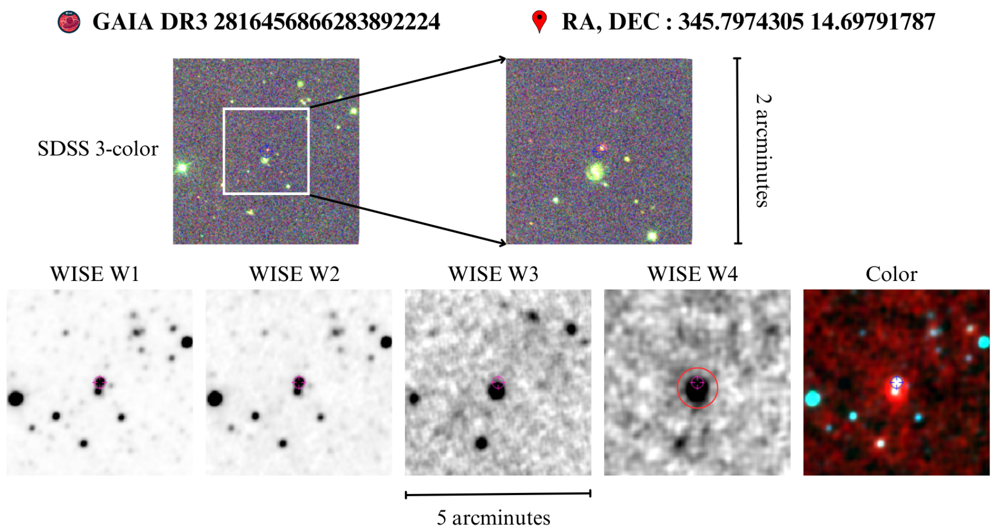

Figure 4.6: The image illustrates a DS candidate that is blended with a nearby galaxy in the WISE observation, whereas it is easily distinguishable in the SDSS observation. This blending is a result of the limited angular resolution of WISE.

In such cases, the photometry data for the target source is a summed value of the blended sources, leading to inaccurate results. During my manual inspection of these sources, I found evidence of this blending and that lead to irregularity in the photometry data. To achieve reliable analysis, these sources were eliminated.

2. Irregular Structure

During the inspection of our potential Dyson Sphere (DS) candidates, we came across some sources with an extended irregular structure in the ALLWISE W4 passband. We rejected such candidates from our DS candidate list. An example of such a structure is shown in the figure below 4.7.

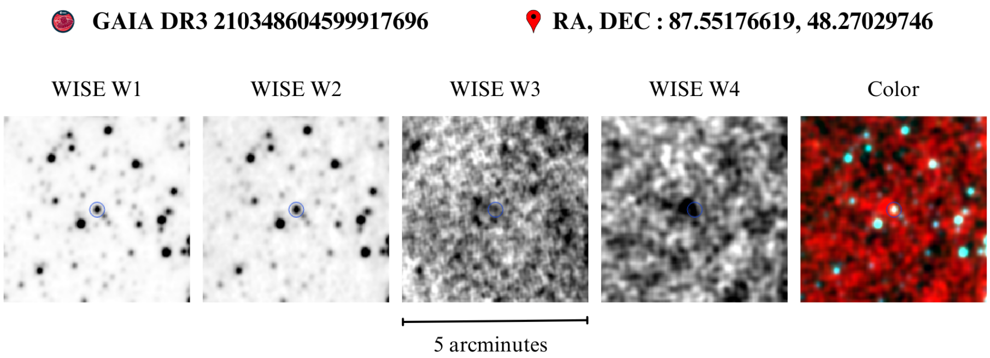

Figure 4.7: The images of a DS candidates illustrates the irregular structure around it in WISE W3 & W4 bands.

One possible explanation for these structures could be the presence of dust surrounding the target candidates. Dusty nebular regions emit prominently in W3 and W4, and the overall effect can mimic a DS candidate. Hence, we excluded these sources to ensure the accuracy of our DS candidate list.

3. Faint Source

During the inspection process of potential Dyson Sphere candidates, some sources were found to have an extended irregular shape in the ALLWISE W4 passband, but were very faint in the other passbands. As a result, we decided to exclude these candidates from our list. An example of such a candidate is shown in figure 4.8.

The most plausible explanation for these irregular structures is the presence of dust surrounding the target candidates, which

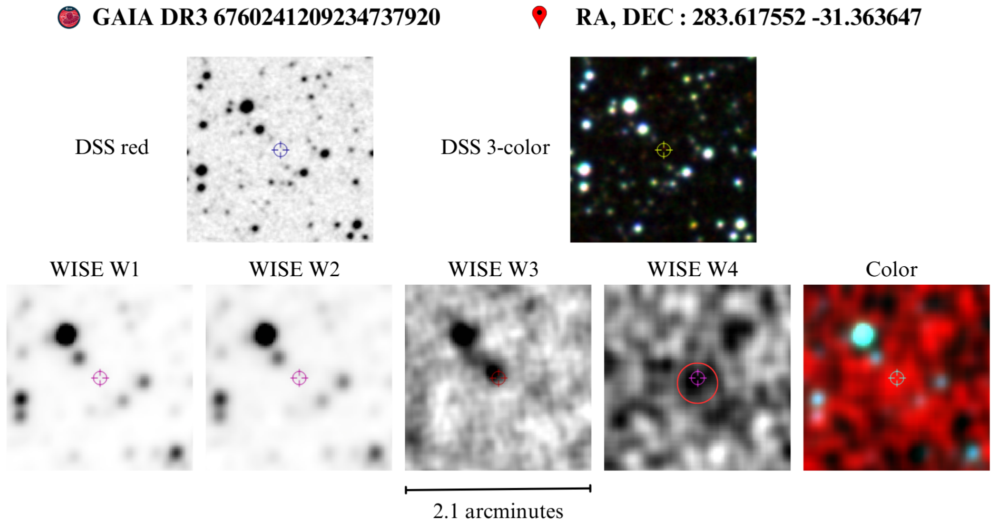

Figure 4.8: Irregular structure around it in W4.

can emit strongly in the W3 and W4 passbands. This effect can potentially mimic a Dyson Sphere candidate, but upon closer inspection, these sources were found to be too faint and lacked the necessary characteristics to be considered as legitimate candidates.

4.4 Verified Potential DS Candidates

Once we removed the contaminated sources from the Dyson Sphere candidates list using manual inspection, now we have 166 potential DS candidates mentioned in appendix B that need to investigate further by cross-referencing with the SDSS database, which provided access to photometric and spectroscopic data along with the class assigned to the sources, to enhance the reliability on our candidates. This additional step would allow us to rule out any instrument biases causing excessive infrared emission and provide further insight into the classification of these sources in SDSS. Our analysis showed that only 62 out of 166 candidates were observed through SDSS and have photometry data in u, g, r, i & z bands. All of them were classified as stars.

The general characteristic of these potential Dyson sphere candidates are described below.

4.4.1 Position of DS candidates in the Galactic plane

The position of the identified Dyson Sphere candidates in the galactic plane is depicted in Figure 4.9. As evident from the figure, these candidates are distributed both above and below the galactic plane. This observation suggests that the candidates are less likely to be located in the nebular regions as the presence of dust and gas is more prominent in the galactic plane.

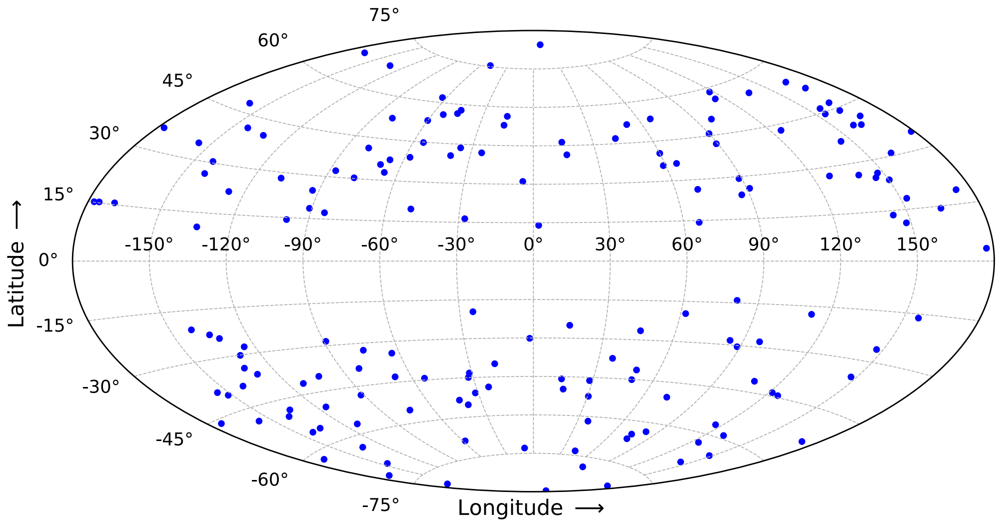

Figure 4.9: Position of filtered potential DS candidates in the Galactic plane. Here, each blue dot represents a potential DS candidate.

4.4.2 Red Fraction Distribution

The red fraction distribution of filtered positive Dyson sphere (DS) candidates is presented in Figure 4.10. The top figure shows the red fraction distribution of DS candidates in the galactic plane, while the bottom figure shows the probability distribution of red fraction for filtered positive DS candidates. The results suggest that the red fraction of our filtered DS candidates is generally less than 0.3, with only a few candidates having a higher red fraction. This indicates that our filtered DS candidates are less likely to be found in the nebular region. Interestingly, the DC candidates with higher red fraction, shown in green dot, are mainly located near the galactic plane, as seen in Figure 4.10a.

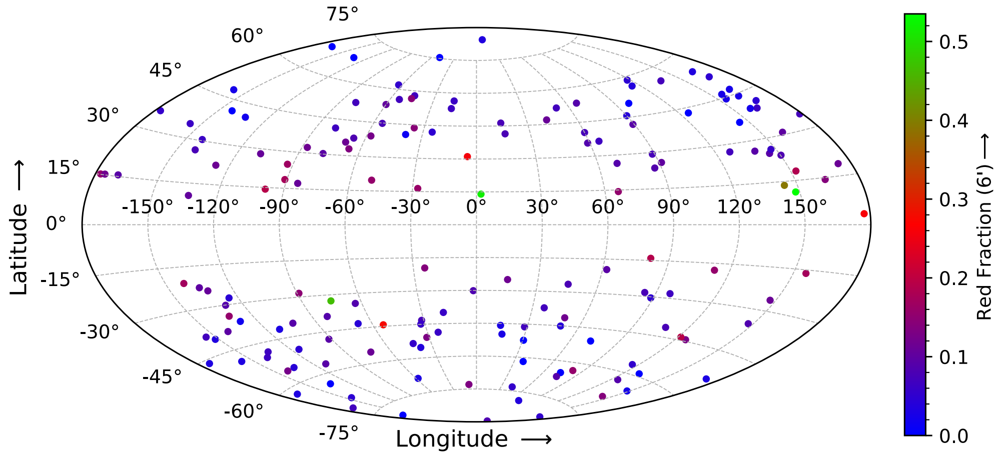

(a)

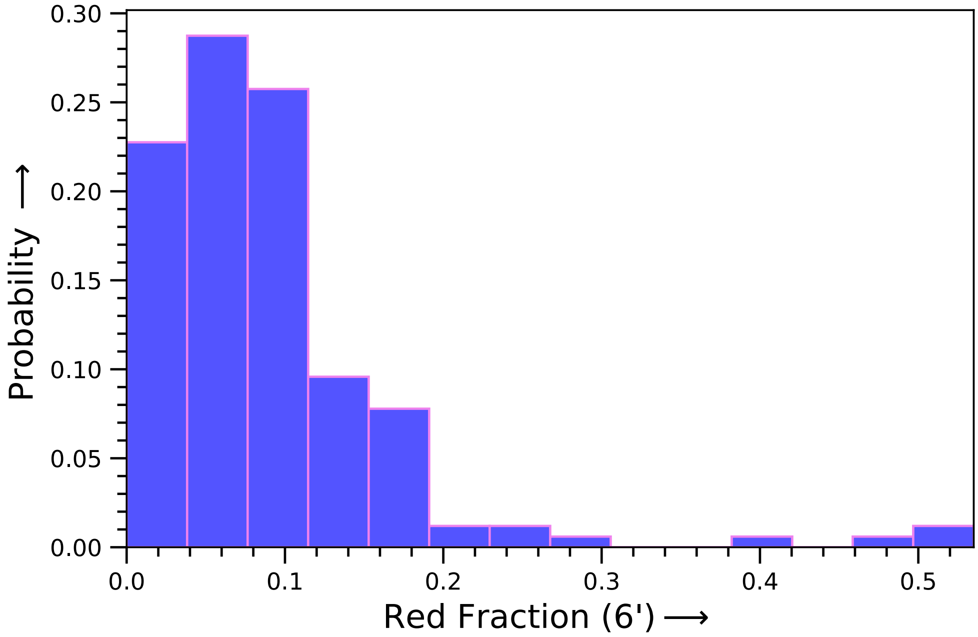

(b)

Figure 4.10: Position and Red fraction

4.4.3 Brightness Distributions

The brightness distribution of DS candidates in both bands, the optical g band and infrared j band, are shown below. I also showed the brightness distribution of DS candidates in the galactic coordinate. The figure 4.11 shows the g-magnitude distribution of all filtered DS candidates.

The j-band brightness distribution of DS candidates is shown in figure 4.12

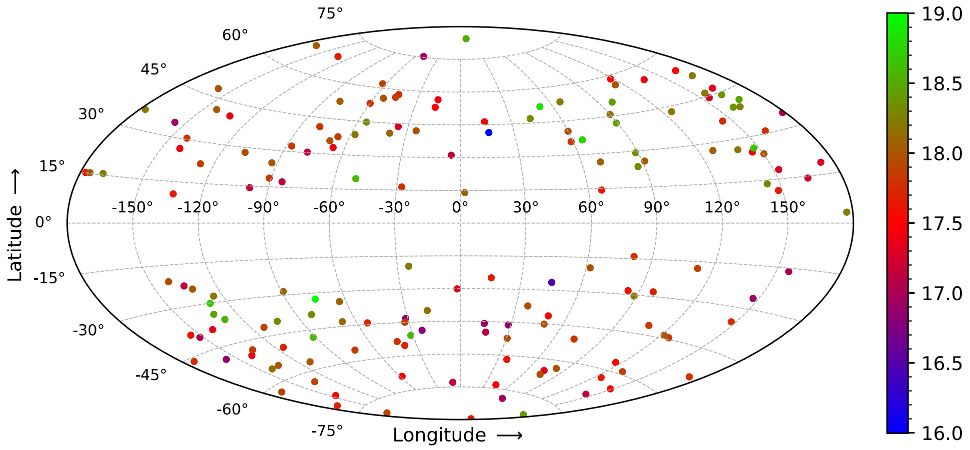

(a)

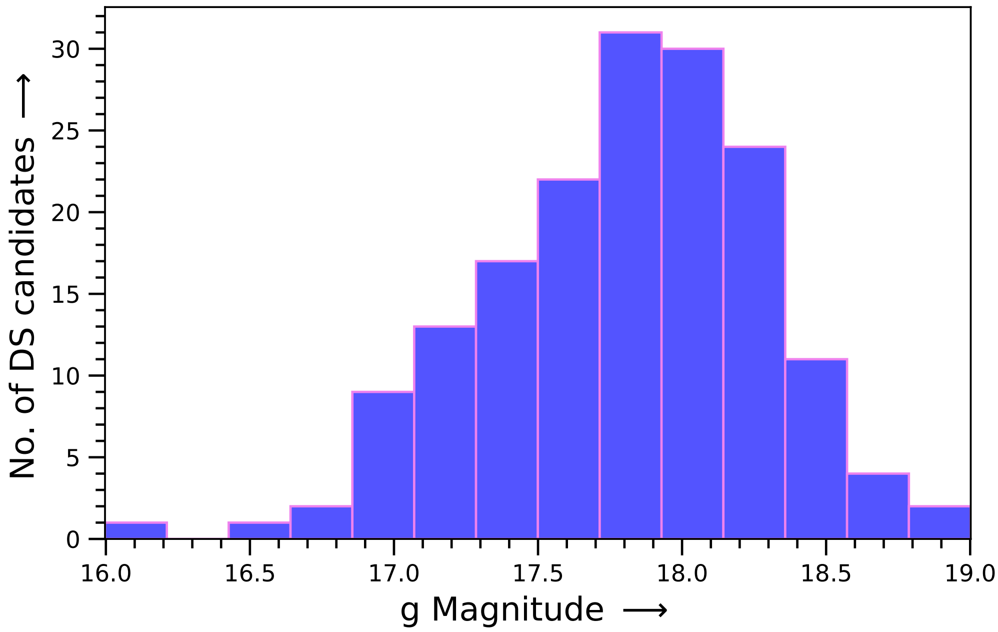

(b)

Figure 4.11: Top: Position of sources in galactic coordinate and the corresponding g magnitude. Bottom: Distribution of g magnitude of sources

The analysis of magnitude in both the g-band and j-band of our sources revealed that three candidates, which appeared bright in the g-band, also showed a high level of brightness in the j-band in the same order. These three sources are marked in the hexagonal shape and are illustrated in Figure 4.13.

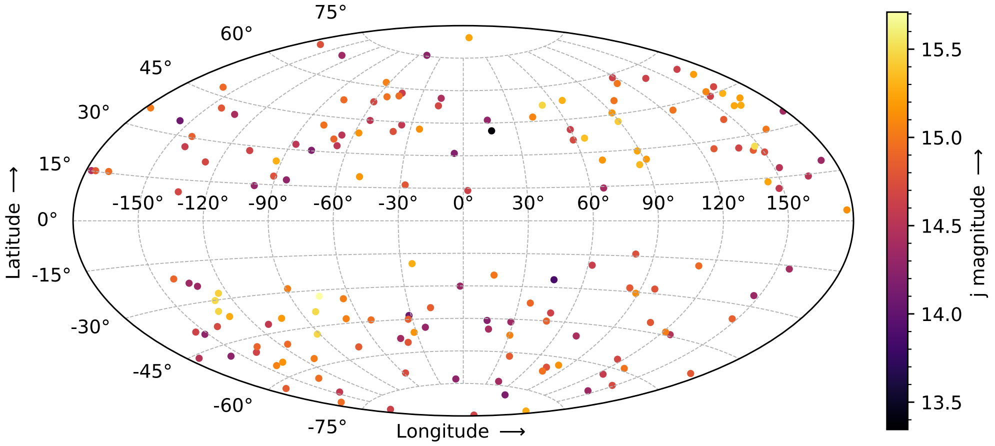

(a)

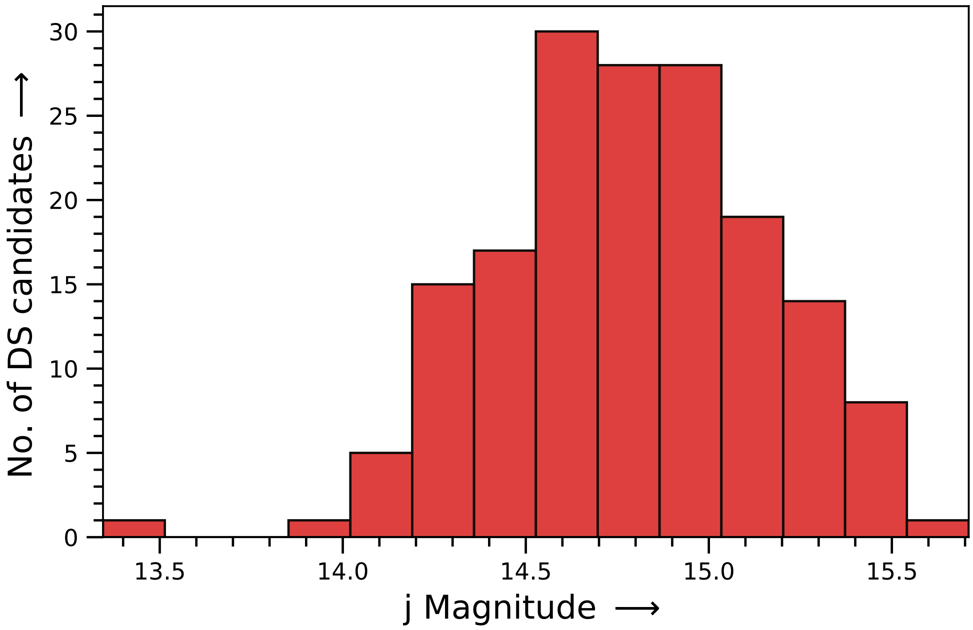

(b)

Figure 4.12: Top: Position of sources in galactic coordinate and the corresponding j magnitude. Bottom: Distribution of j magnitude of sources

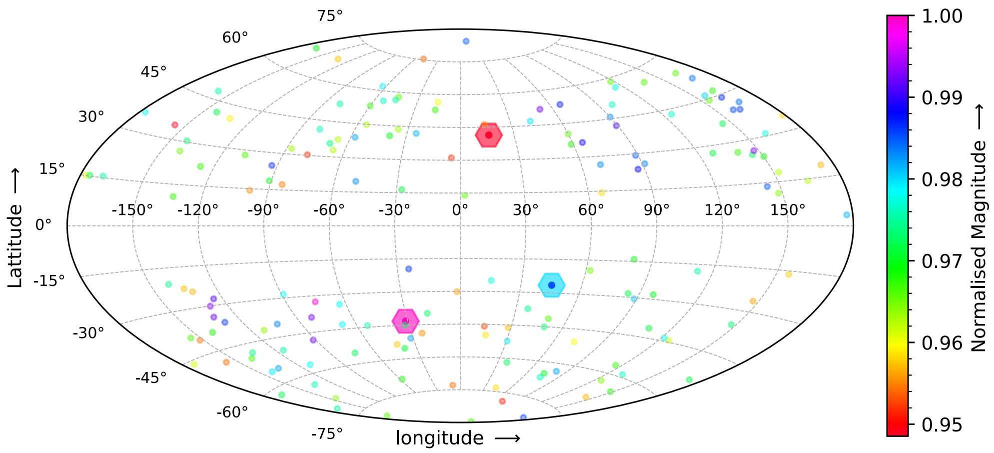

Figure 4.13: The hexagonal shape shows DS candidates which are brightest in both band together. The magnitude in both bands are normalised.

CHAPTER 5

DISCUSSION

The goal of my thesis was to investigate the potential Dyson Sphere candidates identified through an ML algorithm by my collaborator, Matias Suzao from Uppsala University using various methods, such as - calculating red fraction, cross-referencing with multiple databases and conducting a comprehensive literature survey across the past research on the target candidates.

The first objective of my thesis was to develop the "red fraction" parameter, which quantifies the presence of dust around a target candidate within a search radius. To achieve this, I analyzed the red fraction for YSOs (such as Herbig Ae/Be and T-Tauri stars) and randomly chosen main sequence stars. The results showed a significant difference between the two groups, with YSOs having a higher average value of neighbouring red stars (Herbig Ae/Be: 0.681 ± 0.259 and T-Tauri: 0.871 ± 0.063) compared to randomly chosen main sequence stars (0.340 ± 0.292). This difference in neighbouring fraction of red star is utilised as a parameter to distinguish whether a target source lies in nebular region or not.

I calculated this parameter for all 302 potential DS candidates, and I have found that the red fraction for all of our potential DS candidates is within the range of the main sequence star, except for a few candidates with a neighbouring fraction above 0.5. These results suggest that the majority of our DS candidates are not young stars, indicating that the excessive infrared emission observed in these candidates is likely due to Dyson Sphere other than dust and gas in the nebular region. However, there is another possible reason for this excess. It is possible that poor quality data from WISE bands W3 and W4 are causing excessive infrared emission for many of the DS candidates due to a WISE noise peak coinciding with the target objects, leading to an artificial increase in the infrared emission.

The ultimate objective of my project is to verify all these 302 potential Dyson Sphere across different survey databases. This verification process involves cross-referencing with multiple databases, ensuring the authenticity of photometric data in ALLWISE and 2MASS, and conducting a thorough literature review to explore previous research conducted on all the target candidates. Any discrepancies found for a candidate will result in its removal from the list of potential Dyson Sphere candidates. I used Aladin Lite for seeing target objects across the multi-wavelength observation, VizieR for conducting literature surveys and IRSA for look anomalies in photometric data.

Throughout my this investigation, I had to discard 136 potential Dyson Sphere candidates due to a variety of reasons. These included issues such as blending with nearby sources, low angular resolution of WISE, occurring due to the low angular resolution of WISE, exhibiting irregular structure in W3 and W4, indicating the presence of dust around the source, and being too faint to reliably classify.

After filtering out the contaminated sources, I am left with 166 verified potential Dyson Sphere candidates, which are listed in the Appendix B. To enhance the reliability of our candidates, I conducted additional cross-verification with SDSS, which provided access to photometric and spectroscopic data along with the class assigned to the sources. Our analysis showed that only 62 out of 166 candidates were observed through SDSS and have photometry data, and only one candidate had spectroscopic data available. It is worth noting that all observed candidates in SDSS are clearly classified as a star.

5.1 Future Scope

We plan to conduct detailed follow-up observations on the remaining 214 candidates, focusing on our best Dyson Sphere candidates. These top candidates will be selected based on their position in the observing sky relative to the telescope, their apparent magnitude, and the type of follow-up observation required. The optical and infrared spectroscopy can provide valuable information for further confirmation of Dyson Sphere candidates. Spectroscopy can reveal the chemical composition of the star and its surrounding environment, and identify any unusual features that could indicate the presence of a Dyson Sphere. The following details study about these sources can be done to enhance the reliability on our candidates.

1. The H-α line is the most prominent feature in the visible spectra of young stars (Joy, 1945). This line can be used to distinguish between a young star and a Dyson sphere candidate as H-α emission is often used as a signature of accretion in young stars. Accretion occurs when gas and dust in a protoplanetary disk are pulled onto a forming star. As the material falls onto the star, it heats up and emits light in various wavelengths, including H-α ($\lambda = 656.281$ nm). Therefore, the presence of H-α emission in a star's spectrum is often interpreted as evidence of ongoing accretion. This means that young stars are likely to exhibit strong H-α emission due to the accretion process. In contrast, Dyson spheres are hypothesized to surround main sequence stars, which may not exhibit significant H-α emission.

   Therefore, by analyzing the H-α emission in the vicinity of the DS candidates, we can potentially distinguish them from young stars. If a candidate exhibits strong H-α emission, it is more likely to be a young star with ongoing accretion, whereas if there is no H-α emission, it is more likely to be a mature star (i.e. main sequence star) with a Dyson sphere.

   However, it's important to note that this method alone may not be sufficient for definitive identification, as there are other factors that can affect H-alpha emission, such as stellar activity and variability. It should be used in conjunction with other methods, such as photometric and spectroscopic analysis, to increase the reliability of the results.

2. The presence of a Dyson sphere around a star is expected to

result in a scaling of the mid-infrared (MIR) and far-infrared (FIR) emissions by a factor 10^3 as described in section 2.3. However, the MIR and FIR data obtained from ALLWISE have large uncertainties, and therefore, it is necessary to conduct better MIR and FIR photometric observations to obtain more accurate measurements of the emissions and confirm the presence of the Dyson sphere.

3. JWST has the capability to observe in the mid-infrared and far-infrared spectral range, which is crucial for detecting the excess infrared radiation expected from a Dyson Sphere. So, a continuum spectrum obtained through the James Webb Space Telescope (JWST) could provide valuable information for verifying Dyson Sphere candidates and supporting the analysis process.

   Apart from this, the spectral from JWST could also be used to filter out young stars which are found in dusty regions. Dusty sources, such as protoplanetary disks or regions of active star formation, often exhibit non-continuum spectral features. One example of such a feature is the so-called Polycyclic Aromatic Hydrocarbon (PAH) emission feature, which arises from the presence of organic molecules in the dust. These molecules are excited by radiation from nearby stars, causing them to emit light at specific wavelengths in the infrared part of the spectrum.

   By analyzing the spectra of our DS candidates, we can look for the presence of such non-continuum features to help distinguish them from other sources, such as young stars. If we detect strong PAH emission in the spectra of a candidate, this would be a strong indication that it is associated with a dusty environment, and thus more likely to be a young star. On the other hand, if we do not see such features, it may be more likely that the object is a main sequence star or some other type of astronomical object.

Bibliography

Barentsen, G., Vink, J. S., Drew, J., Greimel, R., Wright, N., Drake, J., Martin, E., Valdivielso, L., and Corradi, R. (2011). T tauri candidates and accretion rates using iphas: method and application to ic 1396. *Monthly Notices of the Royal Astronomical Society*, 415(1):103–132.

Barentsen, G., Vink, J. S., Drew, J. E., and Sale, S. E. (2013). Bayesian inference of t tauri star properties using multi-wavelength survey photometry. *Monthly Notices of the Royal Astronomical Society*, 429(3):1981–2000.

Cocconi, G. and Morrison, P. (1959). Searching for interstellar communications. *Nature*, 184(4690):844–846.

Dick, S. (1998). *Life on Other Worlds: The 20th-Century Extraterrestrial Life Debate*. Cambridge University Press.

Dyson, F. J. (1960). Search for artificial stellar sources of infrared radiation. *Science*, 131(3414):1667–1668.

Gray, R. H. (2020). The extended kardashev scale. *The Astronomical Journal*, 159(5):228.

Jansky, K. G. (1933). Radio Waves from Outside the Solar System. *Nature*, 132(3323):66.

Joy, A. H. (1945). T Tauri Variable Stars. *Astrophysical Journal*, 102:168.

Kalari, V., Vink, J., Drew, J., Barentsen, G., Drake, J., Eislöffel, J., Martín, E., Parker, Q., Unruh, Y., Walton, N., et al. (2015). Classical t tauri stars with vphas+–i. h α and u-band accretion rates in the lagoon nebula m8. *Monthly Notices of the Royal Astronomical Society*, 453(1):1026–1046.

Kardashev, N. S. (1964). Transmission of Information by Extraterrestrial Civilizations. *Soviet Astronomy*, 8:217.

Krumholz, M. R. (2015). Notes on star formation. *arXiv preprint arXiv:1511.03457*.

Ritchie, H., Roser, M., and Rosado, P. (2022). Energy. *Our World in Data*. https://ourworldindata.org/energy.

Sagan, C. (1973). *The Cosmic Connection: An Extraterrestrial Perspective*. A Dell book. Anchor Press.

Salaris, M. and Cassisi, S. (2005). *Evolution of Stars and Stellar Populations*. Wiley.

Schwartz, R. N. and Townes, C. H. (1961). Interstellar and Interplanetary Communication by Optical Masers. *Nature*, 190(4772):205–208.

Shuch, H. P. (2011). *Project Ozma: The Birth of Observational SETI*, pages 13–18. Springer.

Suazo, M., Zackrisson, E., Wright, J. T., Korn, A. J., and Huston, M. (2022). Project Hephaistos – I. Upper limits on partial Dyson spheres in the Milky Way. *Monthly Notices of the Royal Astronomical Society*, 512(2):2988–3000.

Szegedi-Elek, E., Kun, M., Reipurth, B., Pál, A., Balázs, L., and Willman, M. (2013). A new hα emission-line survey in the orion nebula cluster. *The Astrophysical Journal Supplement Series*, 208(2):28.

Tarter, J. (2001). The search for extraterrestrial intelligence (seti). *Annual Review of Astronomy and Astrophysics*, 39(1):511–548.

Vioque, M., Oudmaijer, R., Schreiner, M., Mendigutía, I., Baines, D., Mowlavi, N., and Pérez-Martínez, R. (2020). Catalogue of new herbig ae/be and classical be stars-a machine learning approach to gaia dr2. *Astronomy & Astrophysics*, 638:A21.

Wijers, R. A. (2005). On the stellar luminosity of the universe. *arXiv preprint astro-ph/0506218*.

Wright, J. T. (2020). Dyson spheres. *arXiv preprint arXiv:2006.16734*.

Wright, J. T., Mullan, B., Sigurdsson, S., and Povich, M. S. (2014). The ĝ infrared search for extraterrestrial civilizations with large energy supplies. i. background and justification. *The Astrophysical Journal*, 792(1):26.

Appendices

APPENDIX A

ALL POTENTIAL DS CANDIDATES

This appendix contains the list of potential Dyson sphere candidates provided by Matias Suzao after filtering out false-positive candidates through CNN nebulae image classifiers. The list consists various parameters such as Gvar, RUWE, Astrometric Excess Noise (AEN), WISE ph_qual and WISE var_flag which have been considered to ensure the quality of 302 DS candidates. These parameters have been taken from the GAIA database. These parameters are explained below.

A.1 AEN

The term AEN, "astrometric_excess_ noise", refers to a measure of the excess noise in the astrometric observations of a celestial source. This parameter quantifies the discrepancy, represented as an angle, between the observed data of a source and the best-fit standard astrometric model. In other words, it indicates how much the observed data deviates from what is expected based on the astrometric model.

A.2 Remarks

This column provides the information literature surveys of DS candidates. The Remarks column contains different shortened keywords. The full descriptions of each shortened keyword are as follows:

- K&M: 1.7 million K and M dwarfs cross-matching (Medan+, 2021)
- TESS: Transiting Exoplanet Survey Satellite Input Catalog (TIC; Stassun et al. 2019)

- TESS C: A catalogue of cool dwarf targets for the TESS (Muirhead+, 2018) with effective temperature (T_{eff}) < 4000K and V-J > 2.7.
- NCJM: NCJM catalog of M dwarfs (Cook+, 2016)
- HPMS: High Proper Motion Stars (HPMS3) catalog (Knapp+, 2019) with proper motion (pm) > 150 mas/yr.

A.3 WISE Photometry Quality Index

The WISE ph_qual, WISE photometry quality index, is a code that indicates the quality of the WISE photometry for a given source, with a range from "A" (best quality) to "E" (worst quality). The code is based on the number of measurements available for each band (W1-W4) and the level of contamination from nearby sources. Here's a brief explanation of the different WISE ph_qual codes:

- "A": High-quality photometry, with at least 6 good measurements in each band.
- "B": Good-quality photometry, with at least 4 good measurements in each band.
- "C": Medium-quality photometry, with at least 2 good measurements in each band.
- "D": Poor-quality photometry, with only 1 good measurement in each band.
- "E": Lowest-quality photometry, with only 1 measurement in one or more bands and/or significant contamination from nearby sources.

It consists four values corresponding to a source in each band of WISE in the sequence of W1W2W3W4.

A.4 WISE Variable Flag

The WISE var_flag index is a binary flag indicating whether a source is detected as variable in WISE imaging observations in each band (W1-W4). The flag value is 1 if the source is variable and 0 if not. It comprises of four numbers in the order W1W2W3W4 that represent a source in each band of WISE.

	GAIA DR3 Source ID	ra	dec	Dist (pc)	AEN	para (mas)	p err (mas)	g mag	j mag	red frac (6’)	pm (mas per yr)	ruwe	Remarks	Nebu -lar Fea- tures	DS	Gvar	Mod	T_{DS}	γ	WISE ph_qual	WISE var_flag
1	2915906078111475840	86.463	-23.254	75.954	0.237	13.143	0.110	18.011	14.350	0.108	12.355	0.970	TESS,	No	Yes	0.923	261	100	0.1	b’AACC’	b’11nn’
2	3510237257322054912	194.421	-18.011	83.119	0.550	12.118	0.196	18.309	14.536	0.077	79.027	1.079	TESS, K&M	No	Yes	0.976	261	100	0.1	b’AACC’	b’11nn’
3	3978048187578510976	170.395	19.665	84.162	0.462	11.817	0.131	17.652	14.368	0.000	101.212	1.133	NCJM, TESS	No	Yes	1.083	255	100	0.1	b’AACC’	b’01nn’
4	5760183294402944896	132.025	-6.698	100.304	0.166	9.953	0.128	17.872	14.686	0.113	51.912	0.980	TESS C, K&M	No	Yes	0.940	250	100	0.1	b’AACC’	b’00nn’
5	3536922958580249472	165.030	-23.974	103.836	0.453	9.569	0.149	17.836	14.545	0.116	60.955	0.951	TESS C, K&M	No	Yes	1.121	247	100	0.1	b’AACC’	b’00nn’
6	628352207871960448	151.562	20.238	105.239	0.394	9.459	0.164	18.034	14.564	0.083	5.867	0.965	TESS	No	No	0.988	2636	125	0.1	b’AACC’	b’01nn’
7	6488635934221051136	353.882	-61.471	109.527	0.302	9.044	0.095	17.785	14.375	0.055	63.236	1.033	TESS	No	Yes	1.002	244	100	0.1	b’AACC’	b’00nn’
8	4394051130665487488	260.707	7.231	111.218	0.121	8.932	0.088	17.389	14.161	0.207	38.654	1.016	TESS. Blended	No	No	1.029	236	100	0.1	b’AABC’	b’00nn’
9	5685387641533656704	147.032	-15.974	113.933	0.414	8.694	0.146	17.944	14.651	0.107	34.013	0.982	TESS C, K&M	No	Yes	1.037	247	100	0.1	b’AACC’	b’21nn’
10	5569768603691556992	99.723	-41.046	114.037	0.149	8.732	0.045	16.776	13.854	0.173	98.037	1.048	TESS, K&M. Blended	No	No	0.986	223	100	0.1	b’AABB’	b’11nn’
11	1761730438755511552	314.431	14.755	114.542	0.504	8.704	0.150	17.971	14.605	0.095	56.628	1.036	K&M, TESS	No	Yes	1.044	248	100	0.1	b’AACC’	b’00nn’
12	286473012974810496	82.998	62.453	115.640	0.512	8.675	0.197	18.487	15.008	0.186	43.294	0.963	K&M, TESS. Blended	No	No	0.985	2641	125	0.1	b’AACC’	b’00nn’
13	6901426168753269248	310.046	-10.821	115.800	0.245	8.595	0.093	17.140	13.936	0.086	64.801	1.037	K&M, TESS. Blended	No	No	1.150	7385	175	0.1	b’AAAB’	b’111n’
14	6491167658527510144	342.976	-60.635	116.745	0.412	8.509	0.088	17.655	14.392	0.036	50.615	0.942	K&M, TESS. Blended	No	No	1.017	5008	150	0.1	b’AABB’	b’001n’

continued . . .

	GAIA DR3 Source ID	ra	dec	Dist (pc)	AEN	para (mas)	p err (mas)	g mag	j mag	red frac	pm (mas per yr)	ruwe	Remarks	Neb Fe	DS	Gvar	Mod	T_{DS}	γ	WISE ph_qual	WISE var_flag
15	4430833917781139840	234.222	7.695	118.357	0.293	8.424	0.103	17.456	14.303	0.077	127.387	1.060	TESS C, K&M, NJCM	No	Yes	0.966	234	100	0.1	b'AACC'	b'00nn'
16	1115438362942844672	103.623	75.343	120.375	0.743	8.179	0.136	18.198	14.673	0.093	8.548	1.006	TESS	No	Yes	0.953	249	100	0.1	b'AACC'	b'11nn'
17	5496034628081146112	92.337	-56.576	121.767	0.925	8.209	0.147	18.612	15.198	0.114	67.048	1.123	K&M, TESS. Blended	No	No	1.060	522	100	0.2	b'AABB'	b'11nn'
18	1614536893000145536	224.887	60.238	123.060	0.670	8.090	0.133	18.426	14.972	0.000	49.595	0.963	K&M, NJCM, TESS. s	No	Yes	1.072	253	100	0.1	b'AACC'	b'11nn'
19	1328197371906749696	251.098	37.156	123.652	0.574	8.032	0.111	17.957	14.620	0.075	90.834	0.945	TESS C, K&M.	No	Yes	0.986	244	100	0.1	b'BACC'	b'00nn'
20	757976927909863296	168.045	32.807	125.613	0.230	7.947	0.129	18.041	14.756	0.000	68.510	1.015	K&M, NJCM, TESS.	No	Yes	1.012	243	112.5	0.1	b'AACC'	b'11nn'
21	4630985578527718912	8.640	-81.665	126.130	0.000	7.889	0.034	16.243	13.470	0.257	57.687	0.990	K&M, TESS. Blended	No	No	0.828	206	100	0.1	b'AABB'	b'01nn'
22	1100972024033153792	101.288	65.194	126.210	0.537	7.900	0.143	17.960	14.728	0.082	28.076	1.073	NJCM, TESS	No	Yes	0.993	244	100	0.1	b'AACC'	b'00nn'
23	3488776577056140800	184.888	-24.666	126.673	0.392	7.847	0.139	17.851	14.523	0.083	18.497	0.888	TESS	No	Yes	1.121	241	100	0.1	b'AACC'	b'01nn'
24	6289125971652580224	207.276	-20.356	126.953	0.425	7.843	0.157	18.084	14.754	0.013	183.018	0.935	TESS C, K&M, HPMS	No	Yes	1.134	244	100	0.1	b'AACC'	b'11nn'
25	5039343402513263104	24.285	-23.292	127.050	0.657	7.836	0.143	17.910	14.631	0.000	65.357	0.924	K&M, TESS.	No	Yes	1.116	240	100	0.1	b'AACC'	b'11nn'
26	1526641731613608064	198.804	44.276	128.451	0.100	7.719	0.058	17.009	14.052	0.050	50.169	1.009	NCJM, K&M, TESS C. Blended	No	No	0.949	2606	112.5	0.15	b'AABB'	b'11n0'
27	3620635715173447040	207.110	-6.305	131.092	0.000	7.594	0.118	17.635	14.563	0.047	60.324	0.977	K&M, TESS C. Blended	No	No	1.084	233	100	0.1	b'AACC'	b'00nn'

continued . . .

	GAIA DR3 Source ID	ra	dec	Dist (pc)	AEN	para (mas)	p err (mas)	g mag	j mag	red frac	pm (mas per yr)	ruwe	Remarks	Neb Fe	DS	Gvar	Mod	T_{DS}	γ	WISE ph_qual	WISE var_flag
28	3261094210299919616	51.073	-2.783	131.110	0.386	7.525	0.133	17.737	14.498	0.032	10.644	0.943	TESS	No	Yes	1.211	2621	125	0.1	b'AABC'	b'11nn'
29	2092866786582167296	284.441	35.855	131.134	0.499	7.554	0.088	17.607	14.389	0.154	53.173	0.989	K&M, TESS.	No	Yes	1.029	235	100	0.1	b'AABC'	b'nnnn'
30	2787983737076819072	14.923	18.424	133.638	0.523	7.452	0.147	17.810	14.488	0.129	75.654	1.211	NCJM, TESS C, K&M.	No	Yes	1.083	236	100	0.1	b'AACC'	b'11nn'
31	6458044149186203520	314.676	-55.464	134.265	0.678	7.404	0.145	18.148	14.849	0.060	42.576	1.045	K&M, TESS	No	Yes	1.086	2628	125	0.1	b'AACC'	b'00nn'
32	1690729715910190976	187.347	73.921	135.057	0.155	7.348	0.108	18.204	14.973	0.000	49.577	0.989	K&M, TESS, Binary Star system	No	Yes	0.882	243	100	0.1	b'AACC'	b'11nn'
33	661992899995819392	131.800	21.601	136.518	0.094	7.296	0.076	16.947	14.083	0.061	35.767	1.015	NCJM, TESS,	No	Yes	0.872	219	100	0.1	b'AACC'	b'00nn'
34	1353970057604540160	256.943	40.809	137.581	0.721	7.287	0.149	18.759	15.350	0.065	91.214	1.023	K&M,	No	Yes	0.974	2639	125	0.1	b'AACC'	b'00nn'
35	6174337889720387072	211.288	-28.009	137.918	0.000	7.818	0.280	19.287	15.712	0.098	46.116	0.945	K&M, TESS. Blended	No	No	0.881	36566	200	0.15	b'BABC'	00nn
36	1315337479611688832	241.086	25.438	138.830	0.707	7.199	0.129	18.343	15.073	0.109	27.549	1.034	TESS	No	Yes	0.980	2632	125	0.1	b'AACC'	b'00nn'
37	6088807769255904896	202.057	-42.640	139.393	0.603	7.175	0.192	18.587	15.167	0.156	5.502	1.031	TESS	No	Yes	0.987	2635	125	0.1	b'AACC'	b'11nn'
38	883173678401486336	107.387	26.572	139.983	0.648	7.166	0.214	18.260	14.938	0.094	74.543	1.063	K&M, TESS	No	Yes	1.074	2629	125	0.1	b'AACC'	b'01nn'
39	2618501102056246400	329.629	-8.453	140.363	0.333	7.057	0.164	17.959	14.875	0.041	172.565	0.973	HPMS, NCJM, K&M	No	Yes	0.979	2622	125	0.1	b'AACC'	b'00nn'
40	939289281548249856	103.427	33.766	140.724	0.388	7.095	0.127	17.591	14.460	0.153	37.545	1.112	TESS	No	Yes	1.214	230	100	0.1	b'AACC'	b'01nn'
41	3483112241042201088	172.288	-29.273	141.259	0.171	7.046	0.087	17.160	14.186	0.096	56.467	1.060	TESS C, K&M	No	Yes	1.031	221	100	0.1	b'AACB'	b'11nn'
42	6503326058107971328	340.700	-59.319	141.804	0.615	7.044	0.154	18.571	15.149	0.130	92.424	1.019	K&M, TESS	No	Yes	0.991	2633	125	0.1	b'AACC'	b'22nn'

continued . . .

	GAIA DR3 Source ID	ra	dec	Dist (pc)	AEN	para (mas)	p err (mas)	g mag	j mag	red frac	pm (mas per yr)	ruwe	Remarks	Neb Fe	DS	Gvar	Mod	T_{DS}	γ	WISE ph_qual	WISE var_flag
43	6035861680171860992	243.477	-32.202	142.015	0.414	7.010	0.168	18.274	14.919	0.528	31.329	1.029	TESS. Faint	No	No	0.931	5014	150	0.1	b'AABC'	b'11nn'
44	2654924035339211904	343.591	0.681	142.055	0.513	6.975	0.162	17.793	14.432	0.000	20.761	1.025	TESS	No	Yes	1.184	232	100	0.1	b'AACC'	b'11nn'
45	2397293651903978112	342.335	-21.809	143.878	0.161	6.936	0.114	17.614	14.833	0.000	25.189	1.009	TESS	No	Yes	0.872	229	100	0.1	b'AACC'	b'11nn'
46	889362936730041728	104.452	32.011	144.105	0.324	6.860	0.133	18.045	14.810	0.118	113.692	0.911	K&M, TESS	No	Yes	1.115	2623	137.5	0.1	b'AABC'	b'00nn'
47	618553463324573568	142.254	14.776	144.274	0.000	6.858	0.164	18.035	14.802	0.000	122.833	1.012	NCJM, K&M, TESS C.	No	Yes	0.892	2621	112.5	0.15	b'AACC'	b'01nn'
48	2496905385291035264	40.007	-1.221	144.755	0.340	6.884	0.139	17.776	14.810	0.031	145.508	1.132	NCJM, K&M, TESS C.	No	Yes	0.895	233	100	0.1	b'AACC'	b'11nn'
49	1338448458113508480	256.626	35.635	145.044	0.435	6.855	0.106	17.820	14.707	0.086	51.243	1.047	NCJM, K&M, TESS.	No	Yes	1.004	235	100	0.1	b'AACC'	b'11nn'
50	1209419566002958208	234.549	18.283	151.530	0.000	6.616	0.176	18.301	15.364	0.035	194.754	0.973	NJCM, TESS C, K&M. Blended	No	No	0.944	2627	125	0.1	b'AABC'	b'00nn'
51	3665977169521275776	214.375	0.599	152.197	0.325	6.543	0.113	17.429	14.440	0.061	55.834	1.040	NCJM, TESS C, K&M.	No	Yes	0.868	224	100	0.1	b'AACC'	b'00nn'
52	1036767966673477120	135.326	57.534	152.777	0.599	6.504	0.169	18.381	15.241	0.021	9.671	1.016	NCJM, TESS.	No	Yes	1.016	2628	125	0.1	b'AACC'	b'11nn'
53	4814864398463549568	70.098	-42.557	153.112	0.531	6.481	0.111	17.888	14.568	0.030	44.031	0.977	K&M, Binary star system	No	Yes	1.027	232	100	0.1	b'BABC'	b'00nn'
54	1016422289979953664	136.149	50.962	153.226	0.678	6.490	0.179	18.483	15.205	0.048	54.973	1.050	NCJM, K&M.	No	Yes	1.057	2628	125	0.1	b'AACC'	b'11nn'
55	2310451960094696192	356.808	-37.590	153.754	0.000	6.433	0.101	17.140	14.267	0.133	25.596	0.997	TESS	No	Yes	0.867	218	100	0.1	b'AACB'	b'11nn'

continued . . .

	GAIA DR3 Source ID	ra	dec	Dist (pc)	AEN	para (mas)	p err (mas)	g mag	j mag	red frac	pm (mas per yr)	ruwe	Remarks	Neb Fe	DS	Gvar	Mod	T_{DS}	γ	WISE ph_qual	WISE var_flag
56	5170146837671740160	39.448	-14.173	153.940	0.000	6.472	0.115	17.879	14.838	0.033	61.673	0.984	K&M, TESS C	No	Yes	0.943	233	100	0.1	b'AACC'	b'00nn'
57	3629164111474614656	194.777	-7.095	154.622	0.000	6.419	0.140	18.000	14.969	0.067	53.037	0.980	K&M, TESS	No	Yes	0.953	2619	125	0.1	b'AABC'	b'00nn'
58	2387172475571686400	354.968	-23.063	154.925	0.396	6.373	0.124	17.465	14.396	0.056	26.181	0.996	TESS	No	Yes	1.029	224	100	0.1	b'AACC'	b'00nn'
59	6686966734993777792	300.245	-41.703	155.396	0.226	6.404	0.099	17.358	14.328	0.082	13.939	1.022	TESS	No	Yes	1.027	220	100	0.1	b'AACC'	b'11nn'
60	597270624767394816	132.358	9.356	155.645	0.000	6.400	0.130	17.813	14.861	0.062	82.697	0.970	NCJM, K&M. Open cluster star	No	Yes	0.903	2613	125	0.1	b'AACC'	b'00nn'
61	4889857310590694912	60.133	-28.120	156.162	0.000	6.382	0.099	17.833	14.884	0.065	21.119	0.997	TESS	No	Yes	0.977	228	100	0.1	b'AACC'	b'11nn'
62	3488393401547734912	181.768	-26.114	157.287	0.032	6.327	0.131	17.969	14.880	0.114	48.320	1.026	K&M, TESS	No	Yes	0.986	496	100	0.2	b'AACB'	b'11nn'
63	3451273339241871616	87.988	32.982	157.680	0.110	6.392	0.197	18.255	15.126	0.260	42.841	1.014	K&M	No	Yes	0.906	2625	137.5	0.1	b'AACC'	b'00nn'
64	911311005588551808	128.374	39.142	157.682	0.000	6.368	0.138	18.197	15.010	0.056	69.835	0.949	NCJM, K&M,	No	Yes	0.863	2622	125	0.1	b'AACC'	b'00nn'
65	3530813144262513536	191.058	-9.776	158.005	0.370	6.291	0.133	17.741	14.678	0.103	166.415	1.002	NCJM, HPMS, TESS C, K&M	No	Yes	1.021	227	100	0.1	b'AACC'	b'00nn'
66	952003729070420480	103.831	42.580	158.495	0.000	6.281	0.098	17.266	14.346	0.112	112.007	0.924	K&M, TESS C	No	Yes	0.990	218	100	0.1	b'AACB'	b'01nn'
67	4461290080634930432	250.848	13.981	158.582	0.356	6.312	0.145	18.389	15.104	0.071	18.821	0.982	NCJM, TESS. Irregu	No	No	0.938	2626	125	0.1	b'AACC'	b'00nn'
68	2539799842150995968	16.748	3.632	159.307	0.436	6.288	0.141	17.874	14.977	0.000	80.312	0.938	NCJM, K&M, TESS C	No	Yes	1.021	2614	125	0.1	b'AACC'	b'11nn'
69	3609133689676051456	199.863	-13.722	159.309	0.000	6.284	0.149	18.031	15.013	0.077	74.493	1.024	K&M, TESS C. Blended	No	No	0.982	5004	125	0.15	b'AABB'	b'00nn'

continued ...

	GAIA DR3 Source ID	ra	dec	Dist (pc)	AEN	para (mas)	p err (mas)	g mag	j mag	red frac	pm (mas per yr)	ruwe	Remarks	Neb Fe	DS	Gvar	Mod	T_{DS}	γ	WISE ph_qual	WISE var_flag
70	482440516581202688	72.711	66.150	159.468	0.087	6.269	0.122	18.277	15.233	0.392	86.798	1.019	K&M, TESS C	No	Yes	0.932	2622	125	0.1	b'AACC'	b'11nn'
71	1750229409690485760	313.423	8.587	159.792	0.416	6.281	0.188	18.405	15.183	0.140	25.134	0.945	QSO, TESS. Blended	No	No	0.930	36280	200	0.1	b'AABC'	b'00nn'
72	3043112048663066112	118.634	-7.143	159.802	0.304	6.233	0.117	17.654	14.684	0.103	16.429	0.932	TESS	No	Yes	1.106	225	100	0.1	b'AACC'	b'10nn'
73	1023025063462941824	141.595	53.824	160.872	0.000	6.211	0.138	18.367	15.294	0.027	51.315	0.958	NCJM, K&M, TESS	No	Yes	0.878	2887	125	0.2	b'AABB'	b'00nn'
74	4128901290300825984	254.947	-19.426	162.003	0.592	6.127	0.160	18.087	14.630	0.517	32.996	1.072	TESS	No	Yes	1.062	2617	125	0.1	b'AACC'	b'00nn'
75	4649665864475436160	79.346	-73.413	162.147	1.028	6.220	0.189	19.002	15.710	0.464	52.229	1.016	K&M, TESS	No	Yes	0.879	5023	150	0.1	b'AABC'	b'00nn'
76	2536856105926470912	13.684	0.073	162.813	0.000	6.104	0.115	17.650	14.585	0.088	76.962	1.013	NCJM, K&M, TESS C	No	Yes	0.871	2609	125	0.1	b'AACC'	b'11nn'
77	826905075632859648	148.068	50.235	165.153	0.419	5.997	0.134	18.262	15.079	0.079	58.151	0.936	NCJM, K&M, TESS. Blended	No	No	1.009	2621	125	0.1	b'AACC'	b'00nn'
78	1369633803332569088	236.577	32.445	165.820	0.639	6.013	0.168	18.807	15.467	0.070	59.031	1.002	NCJM, TESS	No	Yes	1.018	2632	125	0.1	b'AACC'	b'00nn'
79	6885510703580632576	318.162	-13.627	166.119	0.118	5.988	0.152	17.944	14.909	0.069	30.062	1.018	TESS	No	Yes	0.982	2616	125	0.1	b'AACC'	b'00nn'
80	5481309418607141888	92.585	-61.699	166.379	0.000	6.033	0.114	18.097	15.032	0.147	82.013	0.964	K&M, TESS	No	Yes	0.831	233	100	0.1	b'AACC'	b'11nn'
81	834831828618687616	156.748	49.308	166.999	0.000	5.936	0.092	17.491	14.632	0.034	88.970	1.006	K&M, TESS	No	Yes	0.950	220	100	0.1	b'AACC'	b'00nn'
82	1850962129541995648	323.232	32.297	167.374	0.000	5.940	0.095	17.811	14.755	0.190	15.014	0.998	TESS	No	Yes	1.049	225	100	0.1	b'AACC'	b'00nn'
83	1447646077468827776	198.878	25.591	167.583	0.218	5.951	0.183	18.529	15.230	0.034	86.414	0.959	NCJM, K&M, TESS.	No	Yes	1.005	2626	125	0.1	b'AACC'	b'00nn'
84	3854090071297359616	144.976	7.008	168.363	0.000	5.894	0.103	17.402	14.417	0.019	15.504	0.959	TESS	No	Yes	0.923	218	100	0.1	b'AACB'	b'11nn'

continued . . .

	GAIA DR3 Source ID	ra	dec	Dist (pc)	AEN	para (mas)	p err (mas)	g mag	j mag	red frac	pm (mas per yr)	ruwe	Remarks	Neb Fe	DS	Gvar	Mod	T_{DS}	γ	WISE ph_qual	WISE var_flag
85	2996292365351686144	86.498	-14.150	168.634	0.319	5.892	0.119	17.932	14.897	0.171	47.226	1.036	K&M, TESS	No	Yes	0.923	2616	125	0.1	b'AABC'	b'00nn'
86	3636165908894524544	199.359	-4.385	169.208	0.000	5.869	0.107	17.706	14.618	0.067	66.765	0.989	K&M, TESS	No	Yes	0.871	224	100	0.1	b'AACC'	b'00nn'
87	477541264565874816	73.711	61.463	169.636	0.307	5.829	0.101	17.674	14.580	0.535	79.977	0.930	K&M, TESS C	No	Yes	0.992	224	100	0.1	b'AACC'	b'00nn'
88	2344470574980336256	13.788	-25.750	170.990	0.417	5.814	0.145	17.660	14.650	0.083	31.409	1.015	TESS	No	Yes	1.156	222	100	0.1	b'AACC'	b'11nn'
89	6405584490920011648	331.399	-63.454	171.004	0.150	5.807	0.098	17.845	14.848	0.057	56.463	1.039	K&M, TESS	No	Yes	0.912	2612	125	0.1	b'AACC'	b'11nn'
90	3498693553461662208	192.333	-23.819	171.900	0.583	5.805	0.167	18.203	15.144	0.125	26.387	1.014	TESS	No	Yes	0.996	5004	150	0.1	b'AABC'	b'11nn'
91	1663135032069421056	202.039	60.202	172.047	0.434	5.808	0.113	18.001	14.989	0.037	85.056	1.080	K&M, TESS	No	Yes	1.022	231	100	0.1	b'AACC'	b'11nn'
92	647720891173924480	144.821	27.290	172.487	0.510	5.862	0.173	17.999	14.925	0.023	50.544	1.005	NCJM, K&M, TESS	No	Yes	0.877	2615	125	0.1	b'AACC'	b'00nn'
93	4619397649388055936	48.286	-80.995	172.730	0.311	5.726	0.091	18.077	15.029	0.086	98.944	1.029	K&M, TESS	No	Yes	1.101	231	100	0.1	b'AACC'	b'11nn'
94	3646420641529967744	216.011	-2.513	173.147	0.000	5.767	0.115	17.502	14.678	0.064	23.588	0.975	NCJM, TESS	No	Yes	0.940	220	100	0.1	b'AACC'	b'00nn'
95	4784624938185655680	71.960	-50.214	173.229	0.000	5.746	0.102	18.288	15.181	0.091	37.047	0.972	TESS	No	Yes	0.877	234	100	0.1	b'AACC'	b'11nn'
96	6806054972540387328	313.447	-23.538	174.853	0.408	5.650	0.163	18.010	14.909	0.097	62.774	1.004	K&M, TESS. Faint	No	No	1.134	2615	125	0.1	b'AACC'	b'01nn'
97	1150574390879641472	105.397	86.256	175.013	0.508	5.664	0.101	18.050	14.806	0.071	37.986	1.018	TESS	No	Yes	1.088	230	100	0.1	b'AACC'	b'00nn'
98	1103045771685331328	106.024	67.983	176.265	0.715	5.657	0.175	18.666	15.503	0.060	89.934	1.045	K&M, TESS	No	Yes	0.986	505	100	0.2	b'AACC'	b'00nn'
99	3595041077343698944	178.954	-7.864	178.302	0.000	5.534	0.125	18.018	14.930	0.071	23.302	0.940	TESS	No	Yes	0.968	2612	125	0.1	b'AACC'	b'00nn'
100	2789153445649630464	11.761	19.032	178.828	0.346	5.550	0.146	18.026	15.033	0.194	56.795	0.901	NCJM, K&M, TESS	No	Yes	1.063	2616	125	0.1	b'AACC'	b'00nn'

continued . . .

	GAIA DR3 Source ID	ra	dec	Dist (pc)	AEN	para (mas)	p err (mas)	g mag	j mag	red frac	pm (mas per yr)	ruwe	Remarks	Neb Fe	DS	Gvar	Mod	T_{DS}	γ	WISE ph_qual	WISE var_flag
101	4876715604017587072	74.395	-29.687	179.089	0.638	5.484	0.145	18.567	15.273	0.018	51.889	0.996	K&M, TESS.	No	Yes	1.020	2626	125	0.1	b'AABC'	b'00nn'
102	4644937556449853696	38.844	-71.890	179.773	0.381	5.523	0.102	18.145	15.047	0.042	47.813	0.981	K&M, TESS	No	Yes	0.994	231	100	0.1	b'AACC'	b'11nn'
103	5631833320661544448	143.390	-32.108	180.244	0.167	5.515	0.064	17.175	14.304	0.192	40.739	1.038	K&M, TESS	No	Yes	1.027	211	100	0.1	b'AACC'	b'00nn'
104	1049350021827111808	147.766	57.727	180.860	0.289	5.477	0.119	18.181	15.081	0.026	52.145	0.904	NCJM, K&M, TESS	No	Yes	0.908	231	100	0.1	b'AACC'	b'11nn'
105	6575136021511219072	331.744	-36.788	181.872	0.059	5.460	0.070	16.958	14.108	0.033	82.280	1.012	K&M. Blended	No	No	0.927	205	100	0.1	b'AABB'	b'01nn'
106	1894169672338918144	333.758	28.883	183.709	0.593	5.429	0.160	18.295	15.163	0.157	15.993	1.038	TESS. Blended	No	No	0.917	2620	125	0.1	b'AACC'	b'01nn'
107	5798835496119725568	225.306	-70.400	184.515	0.000	5.371	0.057	16.895	14.052	0.317	27.543	0.964	TESS. Blended	No	No	0.951	2852	125	0.15	b'AAAA'	b'2100'
108	1098727779065302784	118.481	71.356	184.827	0.867	5.450	0.228	19.048	15.632	0.115	59.628	1.101	K&M, TESS. Blended	No	No	0.958	36814	200	0.2	b'AAAB'	b'000n'
109	4584771764787526656	275.646	25.389	185.202	0.000	5.387	0.090	17.823	14.965	0.245	51.255	0.995	K&M, TESS. Blended	No	No	0.990	2608	125	0.1	b'AABC'	b'nnnn'
110	2353610295450275968	19.781	-20.156	185.283	0.595	5.368	0.169	18.397	15.261	0.054	44.404	1.044	K&M, TESS	No	Yes	0.943	2619	125	0.1	b'AACC'	b'00nn'
111	4426899659020024192	239.052	6.096	185.514	0.000	5.351	0.047	15.997	13.345	0.078	11.031	1.040	TESS	No	Yes	0.801	187	100	0.1	b'AABB'	b'00nn'
112	6266957794311581056	237.094	-13.236	186.482	0.084	5.330	0.083	17.151	14.186	0.257	82.901	1.008	K&M, TESS.	No	Yes	1.029	210	100	0.1	b'AACC'	b'00nn'
113	2798379241559922688	0.829	20.175	186.585	0.000	5.351	0.127	17.832	14.804	0.077	74.523	0.985	NCJM, K&M	No	Yes	0.915	2606	125	0.1	b'AACC'	b'00nn'
114	1559280317671115776	206.097	52.024	187.092	0.681	5.355	0.154	18.715	15.528	0.028	10.748	1.077	TESS. Blended	No	No	0.962	5009	150	0.1	b'AABC'	b'00nn'

continued . . .

	GAIA DR3 Source ID	ra	dec	Dist (pc)	AEN	para (mas)	p err (mas)	g mag	j mag	red frac	pm (mas per yr)	ruwe	Remarks	Neb Fe	DS	Gvar	Mod	T_{DS}	γ	WISE ph_qual	WISE var_flag
115	4571794808858923776	256.981	23.897	187.420	0.000	5.301	0.105	18.099	15.026	0.176	10.973	0.974	TESS. Blended	No	No	1.181	2612	125	0.1	b'AACC'	b'nnnn'
116	3683792006674301056	190.210	-0.896	189.906	0.106	5.264	0.127	17.895	15.051	0.053	80.751	1.028	K&M, TESS.	No	Yes	0.852	2608	125	0.1	b'AACC'	b'01nn'
117	1884132853460920192	341.569	27.885	189.971	0.000	5.238	0.094	17.238	14.279	0.087	24.839	0.962	NCJM, TESS	No	No	0.862	211	100	0.1	b'AACC'	b'01nn'
118	603417375802848768	128.986	13.729	190.800	0.538	5.189	0.181	18.257	15.092	0.093	57.757	0.982	UV, QSO, K&M, TESS	No	No	1.004	68064	325	0.2	b'AAAC'	110n
119	3772418867277249280	152.884	-7.759	190.823	0.162	5.192	0.093	16.954	14.174	0.087	53.455	1.112	K&M, TESS. Blended	No	No	1.007	204	100	0.1	b'AACC'	b'nnnn'
120	2907012845810852096	81.424	-28.043	191.628	0.000	5.220	0.164	18.696	15.486	0.088	24.218	1.015	TESS.	No	Yes	0.972	5007	137.5	0.1	b'AABC'	b'11nn'
121	4731386069772654720	55.511	-56.085	191.693	0.565	5.214	0.132	18.569	15.463	0.093	72.476	1.050	K&M, TESS	No	Yes	0.992	2622	125	0.1	b'AACC'	b'00nn'
122	1030096778655069312	133.681	54.935	192.945	0.000	5.158	0.138	18.260	15.264	0.063	30.240	1.021	NCJM, TESS. Blended.	No	Yes	0.933	7647	162.5	0.2	b'AAAB'	b'000n'
123	1885602483892413440	346.598	29.430	193.661	0.000	5.126	0.114	17.706	14.773	0.066	85.287	0.945	NCJM, K&M, TESS	No	Yes	0.929	218	100	0.1	b'AACC'	b'00nn'
124	3262914868412180096	53.688	-1.752	194.154	0.233	5.165	0.137	18.026	15.159	0.053	44.124	1.020	K&M, TESS. Irregu	No	No	0.989	36263	200	0.1	b'AABC'	00nn
125	4088762514509139968	287.121	-16.290	195.079	0.100	5.070	0.081	17.030	14.271	0.258	140.726	1.034	K&M, TESS. Faint	No	No	0.974	2589	125	0.1	b'AACC'	b'00nn'
126	1651751444590308608	257.989	71.647	195.215	0.221	5.079	0.115	18.556	15.343	0.120	14.354	0.984	TESS. Blended	No	No	0.897	234	100	0.1	b'AACC'	b'22nn'
127	4291156633546209408	292.880	4.529	195.235	0.000	5.088	0.117	17.437	14.517	0.562	59.935	1.036	K&M, TESS. Faint	No	No	0.920	212	100	0.1	b'AACC'	b'11nn'

continued . . .

	GAIA DR3 Source ID	ra	dec	Dist (pc)	AEN	para (mas)	p err (mas)	g mag	j mag	red frac	pm (mas per yr)	ruwe	Remarks	Neb Fe	DS	Gvar	Mod	T_{DS}	γ	WISE ph_qual	WISE var_flag
128	2901405993640618624	85.298	-31.908	195.609	0.000	5.076	0.089	17.974	14.927	0.038	41.787	0.953	K&M, TESS. Blended	No	No	0.993	2609	125	0.1	b'AABB'	b'00nn'
129	1876027833559029632	340.893	23.816	196.086	0.260	5.113	0.144	18.163	15.105	0.049	25.878	1.042	NCJM, TESS	No	Yes	0.872	2612	112.5	0.1	b'AACC'	b'11nn'
130	1622841813561817984	238.558	57.996	196.799	0.453	5.065	0.111	18.167	15.166	0.041	44.996	1.088	NCJM, K&M, TESS	No	Yes	0.889	227	100	0.1	b'AACC'	b'11nn'
131	1726532322771758208	186.356	84.894	197.891	0.000	5.033	0.123	18.494	15.556	0.222	73.835	0.926	K&M, TESS. Blended	No	No	1.007	2619	125	0.1	b'AACC'	b'01nn'
132	1358571238888935552	256.963	44.814	199.439	0.000	4.990	0.082	17.888	14.955	0.096	17.353	0.990	TESS. Blended	No	No	0.862	221	100	0.1	b'AACC'	b'00nn'
133	551881753981232896	79.124	76.834	200.188	0.534	5.018	0.154	18.494	15.403	0.152	14.992	1.033	TESS. Faint	No	No	1.033	2618	125	0.1	b'AACC'	b'11nn'
134	2555452390900570752	9.063	5.962	201.819	0.000	4.911	0.104	17.512	14.680	0.053	73.305	0.935	NCJM, K&M, TESS	No	Yes	0.884	2598	125	0.1	b'AACC'	b'00nn'
135	4354273067714452352	248.096	-4.367	203.112	0.423	4.971	0.184	18.435	15.266	0.383	23.023	1.029	TESS. Faint	No	No	0.959	36270	200	0.1	b'AABC'	11nn
136	2440574312223232000	355.576	-6.039	203.896	0.000	4.925	0.137	17.999	15.142	0.156	51.485	0.965	NCJM, K&M, TESS	No	Yes	0.962	4993	137.5	0.1	b'AACC'	b'00nn'
137	6007147938313420544	229.642	-37.912	204.501	0.000	4.832	0.120	17.768	14.803	0.160	13.742	0.878	TESS	No	Yes	0.894	216	100	0.1	b'AACC'	b'00nn'
138	6489518051784208000	352.204	-58.686	204.944	0.265	4.853	0.086	17.692	14.799	0.036	52.326	1.070	NCJM, TESS	No	Yes	0.910	2601	125	0.1	b'AABC'	b'11nn'
139	222438624003605888	53.195	36.221	205.763	0.000	4.846	0.099	16.990	14.380	0.172	63.599	0.983	K&M, TESS.	No	Yes	0.826	200	100	0.1	b'AACC'	b'11nn'
140	6635616067348164224	275.678	-59.353	206.105	0.000	4.847	0.130	18.229	15.278	0.140	43.104	0.998	K&M, TESS	No	Yes	1.044	2610	125	0.1	b'AACC'	b'00nn'

continued . . .

	GAIA DR3 Source ID	ra	dec	Dist (pc)	AEN	para (mas)	p err (mas)	g mag	j mag	red frac	pm (mas per yr)	ruwe	Remarks	Neb Fe	DS	Gvar	Mod	T_{DS}	γ	WISE ph_qual	WISE var_flag
141	6346053430995645568	290.521	-84.803	207.185	0.579	4.803	0.131	18.306	15.275	0.139	108.576	1.014	K&M, TESS. Faint	No	No	0.910	2612	112.5	0.1	b'AACC'	b'00nn'
142	330098133966211840	30.638	35.925	207.212	0.000	4.887	0.151	18.440	15.426	0.120	7.672	0.983	TESS. Blended	No	No	0.848	63297	275	0.1	b'AABC'	01nn
143	1333395858587009536	258.488	31.375	208.296	0.352	4.760	0.113	18.423	15.396	0.092	21.135	0.973	TESS. Blended	No	No	0.944	7386	162.5	0.1	b'AABC'	b'00nn'
144	5465707902660372480	153.290	-28.239	208.854	0.000	4.752	0.098	17.552	14.700	0.088	45.942	0.975	K&M, TESS. Blended	No	No	0.998	212	100	0.1	b'AACC'	b'00nn'
145	595786357085040640	129.250	7.085	209.235	0.061	4.753	0.095	17.419	14.603	0.076	32.267	1.015	NCJM, TESS	No	Yes	0.893	208	100	0.1	b'AACC'	b'00nn'
146	763681404688064512	168.319	36.935	210.434	0.000	4.705	0.057	16.456	13.734	0.063	14.722	1.022	TESS. Blended	No	No	0.943	2575	125	0.1	b'AABB'	b'00nn'
147	2958907320740440960	76.343	-26.718	210.575	0.422	4.809	0.131	18.467	15.462	0.155	27.083	1.006	TESS	No	Yes	0.980	2613	125	0.1	b'AACC'	b'11nn'
148	6299151559192363776	217.050	-14.751	211.345	0.000	4.715	0.145	17.957	15.124	0.049	60.477	0.947	K&M, TESS	No	Yes	1.041	2605	125	0.1	b'AABC'	b'00nn'
149	5118730826393708288	35.981	-25.798	211.444	0.091	4.691	0.099	17.567	14.569	0.048	27.954	0.972	TESS	No	Yes	1.088	214	100	0.1	b'AACC'	b'11nn'
150	4843191593270342656	59.016	-40.530	211.900	0.000	4.681	0.077	17.713	14.928	0.048	32.280	1.064	TESS.	No	Yes	0.941	63287	275	0.1	b'AAAB'	b'00nn'
151	2712741648126780416	341.761	7.519	213.855	0.000	4.665	0.107	17.470	14.664	0.036	56.387	0.983	NCJM, TESS, K&M. Blended	No	No	1.070	2594	125	0.1	b'AACB'	b'00nn'
152	4931144414593677312	24.047	-46.211	215.016	0.000	4.631	0.125	18.181	15.161	0.032	38.692	0.992	TESS. Blended	No	No	0.957	2607	125	0.1	b'AACC'	b'00nn'
153	256229987878276352	74.318	49.078	215.654	0.143	4.607	0.121	17.923	14.940	0.628	15.996	1.026	TESS. Faint	No	No	1.043	2604	125	0.1	b'AACC'	b'nnnn'
154	3543734050861649408	175.360	-18.591	216.622	0.240	4.599	0.124	17.788	14.968	0.065	9.457	1.069	TESS	No	Yes	1.017	2601	125	0.1	b'AACC'	b'00nn'
155	4226700375674235136	311.829	-1.986	217.174	0.156	4.560	0.061	16.488	13.857	0.079	72.508	1.103	K&M, TESS	No	Yes	0.828	188	100	0.1	b'AACC'	b'00nn'

continued . . .

	GAIA DR3 Source ID	ra	dec	Dist (pc)	AEN	para (mas)	p err (mas)	g mag	j mag	red frac	pm (mas per yr)	ruwe	Remarks	Neb Fe	DS	Gvar	Mod	T_{DS}	γ	WISE ph_qual	WISE var_flag
156	5065248343140177536	42.947	-29.933	217.545	0.313	4.589	0.113	17.913	14.951	0.000	33.807	1.039	TESS	No	Yes	0.919	218	100	0.1	b'AACC'	b'11nn'
157	970166080613583232	92.862	49.824	217.829	0.000	4.571	0.078	17.203	14.516	0.139	67.288	0.971	K&M, TESS	No	Yes	0.838	204	100	0.1	b'AACC'	b'00nn'
158	5441348085110168960	158.933	-38.312	218.203	0.000	4.538	0.065	17.150	14.274	0.108	62.157	0.929	K&M, TESS	No	Yes	0.888	202	100	0.1	b'AACC'	b'00nn'
159	548788759052488448	40.866	75.978	218.567	0.000	4.573	0.106	18.145	15.257	0.377	62.770	0.975	K&M, TESS. Faint & Irregu	No	No	0.964	485	100	0.2	b'AACC'	b'00nn'
160	5094455018402626560	60.175	-19.579	219.454	0.173	4.497	0.107	17.855	14.914	0.075	24.075	1.013	TESS. Blended	No	No	0.941	2601	112.5	0.1	b'AACC'	b'00nn'
161	929078190075974528	122.541	45.340	220.276	0.118	4.510	0.089	17.274	14.527	0.063	15.065	1.033	TESS. Blended	No	No	0.855	204	100	0.1	b'AACC'	b'00nn'
162	823662302309125504	151.784	49.088	220.890	0.000	4.494	0.128	18.203	15.193	0.049	108.252	1.034	NCJM, K&M, TESS	No	Yes	0.892	2607	112.5	0.1	b'AACC'	b'00nn'
163	1106405707419734528	101.744	69.649	221.016	0.219	4.491	0.085	17.447	14.837	0.094	29.148	1.068	TESS	No	Yes	0.892	4977	162.5	0.1	b'AABC'	b'11nn'
164	5086043990671838720	51.059	-24.845	221.568	0.519	4.491	0.146	18.153	15.059	0.125	35.706	1.138	TESS	No	Yes	0.906	219	100	0.1	b'AACC'	b'11nn'
165	6817461546684629888	324.747	-22.188	221.902	0.097	4.488	0.075	16.888	14.360	0.069	75.630	1.033	K&M, TESS	No	Yes	0.835	196	100	0.1	b'AACC'	b'11nn'
166	3634795878750939776	199.077	-5.804	221.961	0.172	4.503	0.142	17.849	14.936	0.143	58.313	1.033	TESS, K&M	No	Yes	0.960	216	100	0.1	b'AACC'	b'11nn'
167	2113794336847287040	270.844	42.592	223.214	0.123	4.472	0.100	18.057	15.171	0.088	19.966	1.020	NCJM, TESS	No	Yes	0.999	220	100	0.1	b'AACC'	b'11nn'
168	6854663217672327040	310.425	-23.354	223.274	0.138	4.438	0.099	17.170	14.312	0.107	26.829	1.032	TESS. Blended	No	No	0.842	202	100	0.1	b'AACC'	b'20nn'
169	2152693481986456960	270.571	59.961	223.447	0.409	4.438	0.113	18.329	15.230	0.074	24.799	1.008	TESS	No	Yes	1.047	2609	125	0.1	b'AABB'	b'11nn'
170	4718904246271596800	28.189	-57.037	224.449	0.000	4.428	0.051	16.958	14.270	0.086	72.567	1.004	K&M, TESS. Blended	No	No	0.932	198	100	0.1	b'AABB'	b'22nn'

continued . . .

	GAIA DR3 Source ID	ra	dec	Dist (pc)	AEN	para (mas)	p err (mas)	g mag	j mag	red frac	pm (mas per yr)	ruwe	Remarks	Neb Fe	DS	Gvar	Mod	T_{DS}	γ	WISE ph_qual	WISE var_flag
171	831383145976762496	164.128	47.326	224.534	0.000	4.440	0.103	17.740	15.082	0.111	33.461	0.972	TESS. Blended	No	No	0.977	478	100	0.2	b'AACB'	b'11nn'
172	1736572861093767296	315.233	6.316	225.118	0.000	4.381	0.116	17.830	14.847	0.116	9.758	0.993	TESS. Blended	No	No	0.902	215	100	0.1	b'AACC'	b'00nn'
173	1477380273498107264	214.556	31.407	225.139	0.000	4.378	0.106	17.740	14.840	0.000	9.007	0.979	TESS. Blended	No	No	0.947	2600	125	0.1	b'AABB'	b'11nn'
174	4737777118547954176	51.232	-48.428	229.985	0.000	4.345	0.105	18.258	15.401	0.054	10.132	0.930	UV, TESS. Irregu.	No	No	0.847	72301	300	0.1	b'AABC'	22nn
175	1443772124343102848	204.390	23.395	230.589	0.517	4.315	0.124	17.927	15.170	0.032	7.865	1.051	NCJM, TESS. Blended	No	No	1.051	2601	125	0.1	b'AACC'	b'11nn'
176	4032337162611310208	175.989	36.608	231.992	0.400	4.270	0.120	17.653	14.775	0.000	106.698	1.217	NCJM, K&M, TESS. Blended	No	No	0.949	209	100	0.1	b'AACC'	b'11nn'
177	2154062850702747904	280.844	57.205	231.994	0.420	4.310	0.116	18.310	15.329	0.087	26.567	1.031	TESS	No	Yes	0.906	223	100	0.1	b'AACC'	b'11nn'
178	5458954908402727936	153.397	-33.713	232.039	0.000	4.255	0.108	17.827	14.767	0.174	39.183	0.987	TESS.	No	Yes	0.925	214	100	0.1	b'AACC'	b'00nn'
179	6755031658716353024	298.999	-26.020	233.059	0.000	4.275	0.122	17.665	14.993	0.117	23.437	0.968	TESS	No	Yes	0.862	2594	125	0.1	b'AACC'	b'11nn'
180	3048572670087473536	110.534	-8.387	233.598	0.000	4.241	0.083	17.326	14.501	0.296	11.714	1.054	TESS. Faint	No	No	0.945	203	100	0.1	b'AACB'	b'00nn'
181	1511266779486191104	210.917	49.394	233.955	0.256	4.236	0.061	17.261	14.463	0.000	44.305	1.077	K&M, TESS. Blended	No	No	0.874	202	100	0.1	b'AACC'	b'00nn'
182	2365292026675460352	3.634	-19.493	234.597	0.000	4.221	0.083	16.969	14.166	0.037	31.769	1.006	NCJM, TESS	No	Yes	0.838	195	100	0.1	b'AACC'	b'00nn'
183	3576241906705727104	184.435	-13.114	234.735	0.147	4.226	0.084	16.893	14.273	0.118	19.924	1.024	TESS. Irregu	No	No	1.058	195	100	0.1	b'AACB'	b'00nn'
184	2399548166136526336	345.388	-19.260	234.952	0.000	4.191	0.117	17.578	14.763	0.073	32.750	1.005	TESS. Blended	No	No	0.868	4978	137.5	0.1	b'AABC'	b'01nn'

continued . . .

	GAIA DR3 Source ID	ra	dec	Dist (pc)	AEN	para (mas)	p err (mas)	g mag	j mag	red frac	pm (mas per yr)	ruwe	Remarks	Neb Fe	DS	Gvar	Mod	T_{DS}	γ	WISE ph_qual	WISE var_flag
185	915612711689028352	126.028	42.136	235.036	0.000	4.221	0.095	17.071	14.376	0.073	65.117	0.926	K&M, TESS.	No	Yes	0.953	198	100	0.1	b'AACC'	b'21nn'
186	6471043885615813504	308.916	-53.823	235.092	0.000	4.248	0.101	17.413	14.708	0.105	53.044	0.978	K&M, TESS. Blended	No	No	0.852	2589	125	0.1	b'AABB'	b'11nn'
187	6294757704570139264	208.861	-16.576	235.184	0.279	4.236	0.104	17.262	14.549	0.143	34.485	1.212	TESS	No	Yes	1.087	201	100	0.1	b'AACC'	b'00nn'
188	1295985460782929024	223.349	37.803	235.222	0.473	4.180	0.133	18.501	15.390	0.114	55.370	1.008	K&M, TESS. Blended	No	No	1.075	2609	125	0.1	b'AACC'	b'00nn'
189	6188117377462638336	203.281	-28.727	235.966	0.000	4.292	0.136	17.750	15.032	0.106	18.695	0.943	TESS. Blended	No	No	1.021	474	100	0.2	b'AACB'	b'00nn'
190	3473317958963571840	184.297	-29.363	236.078	0.000	4.233	0.122	17.407	14.532	0.134	7.809	0.984	TESS	No	Yes	0.858	202	100	0.1	b'AACC'	b'33nn'
191	3190924756901443328	64.499	-11.189	236.138	0.000	4.213	0.119	17.590	14.651	0.070	18.925	0.988	TESS	No	Yes	1.005	205	100	0.1	b'AACC'	b'11nn'
192	676429247151235328	124.994	21.936	236.425	0.509	4.181	0.128	17.878	14.775	0.050	39.305	1.048	NCJM, TESS	No	No	0.878	2599	125	0.1	b'AACC'	b'00nn'
193	1586970285360406784	225.041	45.370	237.654	0.676	4.147	0.096	17.652	14.658	0.023	30.605	1.263	UV source. TESS	No	No	1.572	36242	200	0.1	b'AAAB'	100n
194	1238005493935425024	221.782	20.041	237.687	0.397	4.134	0.126	17.719	14.819	0.000	33.528	0.987	NCJM, TESS. Blended	No	No	1.147	210	100	0.1	b'AACC'	b'00nn'
195	6818973272093697280	331.425	-22.564	238.803	0.000	4.198	0.127	17.920	15.059	0.000	7.243	0.971	TESS.	No	Yes	0.961	2601	125	0.1	b'AACC'	b'00nn'
196	4689531029378339840	5.624	-72.634	239.147	0.000	4.153	0.078	17.693	14.938	0.277	28.348	1.016	TESS	No	Yes	0.918	209	100	0.1	b'AACC'	b'01nn'
197	2435392417000825984	355.478	-10.457	239.235	0.000	4.138	0.136	17.957	14.965	0.091	29.303	0.979	NCJM, TESS.	No	Yes	0.889	2600	125	0.1	b'AACC'	b'00nn'
198	4743348623139858816	35.401	-53.798	239.257	0.000	4.148	0.051	16.938	14.314	0.028	32.862	1.006	TESS. Blended	No	No	0.853	195	100	0.1	b'AABB'	b'11nn'
199	6402749267044915840	327.223	-63.652	241.404	0.112	4.110	0.052	16.799	14.069	0.075	46.922	1.016	K&M, TESS	No	Yes	0.867	191	100	0.1	b'AACC'	b'11nn'
200	1005962056045974912	90.703	61.382	241.702	0.000	4.088	0.082	17.305	14.516	0.185	9.111	0.977	TESS	No	Yes	0.881	202	100	0.1	b'AACC'	b'00nn'

continued . . .

	GAIA DR3 Source ID	ra	dec	Dist (pc)	AEN	para (mas)	p err (mas)	g mag	j mag	red frac	pm (mas per yr)	ruwe	Remarks	Neb Fe	DS	Gvar	Mod	T_{DS}	γ	WISE ph_qual	WISE var_flag
201	1489795963094761472	220.973	41.737	242.837	0.000	4.111	0.118	18.385	15.393	0.088	34.850	0.968	NCJM, TESS. Blended	No	No	0.922	4991	162.5	0.1	b'AABC'	b'11nn'
202	4903570969367489152	13.096	-59.825	243.185	0.496	4.093	0.122	18.215	15.412	0.061	67.899	1.063	K&M, TESS. Irregu. Blended	No	No	0.978	45533	225	0.15	b'AAAB'	b'nnnn'
203	6459261686515092736	325.157	-56.391	243.212	0.000	4.131	0.137	18.414	15.465	0.086	17.173	0.901	TESS. Blended	No	No	0.951	7378	175	0.1	b'AABC'	b'11nn'
204	101027079730076544	34.710	23.676	243.475	0.000	4.052	0.128	17.765	14.864	0.085	25.080	0.959	TESS	No	Yes	1.101	4980	150	0.1	b'AACC'	b'00nn'
205	4674754658232078848	66.974	-66.177	243.654	0.349	4.066	0.099	18.321	15.486	0.089	14.455	0.993	TESS	No	Yes	0.957	2606	125	0.1	b'AACC'	b'00nn'
206	3160764770700057216	104.694	12.028	245.466	0.000	4.010	0.114	17.518	14.603	0.129	18.124	0.967	TESS. Irregu.	No	No	1.069	7357	175	0.1	b'AABC'	b'01nn'
207	3064546164554840960	122.831	-5.704	246.441	0.589	4.214	0.293	19.064	15.972	0.083	28.479	0.984	TESS. Irregu. Blended	No	No	0.958	36539	200	0.15	b'AABC'	00nn
208	2423801369716357888	6.279	-12.362	247.289	0.217	4.006	0.085	17.008	14.333	0.000	25.709	1.100	TESS. Ir-regu.Blended	No	No	0.992	195	100	0.1	b'AACC'	b'00nn'
209	4714834812001755648	31.501	-59.289	247.801	0.156	3.992	0.089	17.850	14.828	0.111	61.822	1.097	K&M, TESS.	No	Yes	1.039	2595	125	0.1	b'AABB'	b'00nn'
210	3633556041951797120	204.694	-4.271	247.822	0.000	3.989	0.118	17.928	15.204	0.088	59.879	0.992	K&M, TESS	No	No	0.861	2598	125	0.1	b'AACC'	b'00nn'
211	3831516238585092096	152.951	-0.631	248.749	0.109	3.956	0.121	17.512	14.801	0.152	44.716	0.945	K&M, TESS. Blended	No	No	0.945	7359	162.5	0.1	b'AABC'	b'nnnn'
212	6403688932874231168	324.535	-62.227	249.080	0.301	3.997	0.103	17.924	15.045	0.036	39.840	1.074	TESS. Faint	No	No	0.847	2597	125	0.1	b'AACB'	b'01nn'
213	3176818022716814720	64.244	-13.865	249.287	0.152	3.990	0.071	17.047	14.268	0.035	54.700	1.056	TESS, K&M	No	Yes	1.001	195	100	0.1	b'AACB'	b'11nn'
214	6412717744403679744	331.949	-56.250	250.235	0.000	3.960	0.059	16.829	14.305	0.060	24.511	0.978	TESS	No	Yes	0.835	192	100	0.1	b'AACB'	b'00nn'

continued . . .

	GAIA DR3 Source ID	ra	dec	Dist (pc)	AEN	para (mas)	p err (mas)	g mag	j mag	red frac	pm (mas per yr)	ruwe	Remarks	Neb Fe	DS	Gvar	Mod	T_{DS}	γ	WISE ph_qual	WISE var_flag
215	1117427693010918400	135.084	68.930	250.689	0.000	3.912	0.101	17.740	14.827	0.000	25.570	1.007	TESS	No	Yes	1.430	205	100	0.1	b'AACC'	b'00nn'
216	4898684774054542208	68.892	-21.411	251.546	0.206	3.922	0.079	17.376	14.712	0.098	7.739	1.058	TESS	No	Yes	0.898	201	100	0.1	b'AACC'	b'00nn'
217	2689569479227015808	318.044	-0.158	252.528	0.000	3.922	0.073	16.867	14.079	0.116	52.741	0.973	K&M, TESS. Blended	No	No	0.958	190	100	0.1	b'AACC'	b'11nn'
218	5057336772862673152	52.250	-28.840	253.165	0.000	3.905	0.106	18.009	15.146	0.043	17.741	1.034	TESS	No	Yes	0.893	215	100	0.1	b'AACC'	b'00nn'
219	6754939982636033024	297.795	-26.419	253.732	0.000	3.899	0.103	17.539	14.671	0.161	35.354	0.933	TESS. Irregu	No	No	0.957	2588	125	0.1	b'AABC'	b'00nn'
220	1566609769556349824	197.882	58.258	253.882	0.000	3.877	0.073	17.490	14.633	0.048	7.909	0.994	TESS	No	Yes	1.016	202	100	0.1	b'AACC'	b'01nn'
221	4823360079996664064	75.844	-38.516	254.022	0.000	3.914	0.087	17.972	15.065	0.088	0.731	1.013	TESS. Blended	No	No	0.908	473	112.5	0.15	b'AABB'	b'00nn'
222	2958925393962238208	76.152	-26.497	254.280	0.110	3.891	0.107	18.190	15.304	0.093	16.491	1.007	TESS. Irregu	No	No	0.847	2603	125	0.1	b'AACC'	b'01nn'
223	721252964664551424	158.890	21.652	254.546	0.000	3.902	0.104	17.751	15.042	0.036	25.125	0.933	TESS. Faint	No	No	0.875	2591	125	0.1	b'AACC'	b'00nn'
224	797656142189135744	143.088	34.975	254.864	0.235	3.856	0.095	16.904	14.148	0.029	47.825	1.111	TESS, K&M. Blended	No	No	0.962	117320	425	0.1	b'AAAC'	110n
225	4865354208632893056	65.478	-38.626	255.523	0.154	3.866	0.101	18.018	15.039	0.035	9.183	1.011	TESS. Blended	No	No	1.072	2599	125	0.1	b'AABC'	b'11nn'
226	5083549374883972992	57.554	-25.108	256.147	0.000	3.860	0.074	17.403	14.660	0.063	24.948	1.018	TESS.	No	Yes	0.901	199	100	0.1	b'AACC'	b'21nn'
227	5623480090308822400	139.769	-35.868	256.554	0.206	3.859	0.063	17.275	14.576	0.252	7.800	1.048	TESS	Yes WI	No	0.930	198	100	0.1	b'AACC'	b'11nn'
228	4594031508116001280	263.253	25.860	256.984	0.000	3.852	0.057	17.126	14.380	0.127	58.891	0.947	K&M, TESS. Blended	No	No	0.913	195	100	0.1	b'AACC'	b'00nn'
229	5138097894788103424	31.127	-18.926	257.139	0.000	3.854	0.104	17.675	14.934	0.071	41.580	0.970	K&M, TESS	No	Yes	0.897	204	100	0.1	b'AACC'	b'00nn'
230	5055743271276879488	53.541	-30.814	257.998	0.000	3.852	0.104	17.983	15.154	0.103	8.450	1.002	TESS. Blended	No	No	0.930	211	100	0.1	b'AACC'	b'01nn'

continued . . .

	GAIA DR3 Source ID	ra	dec	Dist (pc)	AEN	para (mas)	p err (mas)	g mag	j mag	red frac	pm (mas per yr)	ruwe	Remarks	Neb Fe	DS	Gvar	Mod	T_{DS}	γ	WISE ph_qual	WISE var_flag
231	1082166694409052288	118.331	57.121	258.204	0.000	3.829	0.112	17.766	14.997	0.100	41.675	0.995	K&M, TESS	No	Yes	0.857	2591	125	0.1	b'AACC'	b'11nn'
232	5468611605493851264	156.212	-27.707	258.610	0.000	3.868	0.123	17.991	15.278	0.167	28.624	0.980	TESS.	No	Yes	0.939	2598	125	0.1	b'AACC'	b'00nn'
233	3384021878028948096	98.171	25.687	260.327	0.000	3.841	0.084	17.185	14.508	0.264	38.177	0.969	TESS. Irregu	No	No	0.809	2580	125	0.1	b'AABC'	b'00nn'
234	2667886899474087680	326.464	-6.459	260.751	0.337	3.786	0.123	17.527	14.646	0.118	18.743	0.951	TESS	No	Yes	0.906	203	100	0.1	b'AACC'	b'00nn'
235	1922953478004114816	359.286	44.125	262.312	0.224	3.801	0.121	17.857	14.926	0.156	31.587	1.045	TESS	No	Yes	0.852	205	100	0.1	b'AACC'	b'00nn'
236	1638984740202462080	267.297	71.071	262.508	0.431	3.797	0.088	17.814	14.943	0.096	20.241	1.125	TESS. Blended	No	No	1.122	2590	125	0.1	b'AABB'	b'11nn'
237	3094722295538135296	123.592	4.721	262.902	0.000	3.773	0.085	17.138	14.476	0.099	22.023	0.930	TESS. Blended	No	No	0.831	193	100	0.1	b'AACC'	b'10nn'
238	6592971302704572288	326.779	-31.137	263.809	0.000	3.760	0.079	17.091	14.407	0.029	12.922	0.941	TESS.	No	Yes	0.932	193	100	0.1	b'AACB'	b'00nn'
239	1875560270535342592	336.203	23.260	265.185	0.253	3.747	0.107	17.583	14.815	0.076	22.791	1.044	NCJM, TESS	No	Yes	0.876	203	100	0.1	b'AACC'	b'11nn'
240	4882795589785778432	63.080	-32.792	265.358	0.182	3.793	0.159	18.800	15.690	0.030	13.349	0.957	TESS. Blended	No	No	0.964	36529	200	0.1	b'AABC'	00nn
241	3256018280511121024	64.902	1.803	265.828	0.000	3.727	0.094	17.351	14.626	0.096	8.149	1.002	TESS. Faint	No	No	0.866	198	100	0.1	b'AACC'	b'00nn'
242	3383511807713437696	98.073	24.480	266.080	0.000	4.024	0.431	19.826	16.547	0.226	22.064	0.995	TESS. Blended	Faint	No	0.911	37868	200	0.4	b'ABBC'	0nnn
243	133263046965499392	38.598	31.670	266.549	0.127	3.709	0.073	16.939	14.328	0.112	13.769	1.018	TESS, LAM-OST	No	Yes	0.865	188	100	0.1	b'AACC'	b'00nn'
244	6526627600017876864	351.272	-47.934	266.621	0.282	3.716	0.095	17.739	15.036	0.111	37.869	1.056	TESS. Blended	No	No	0.991	2589	125	0.1	b'AACC'	b'nnnn'
245	4727877047133922176	43.814	-57.411	267.422	0.000	3.704	0.089	17.920	15.131	0.024	20.703	0.982	TESS. Blended	No	No	0.898	7363	175	0.1	b'AABB'	b'00nn'
246	858610318053921920	176.861	59.892	268.280	0.436	3.646	0.082	17.413	14.640	0.073	23.045	1.085	TESS.	No	Yes	1.006	198	100	0.1	b'AACC'	b'11nn'

continued . . .

	GAIA DR3 Source ID	ra	dec	Dist (pc)	AEN	para (mas)	p err (mas)	g mag	j mag	red frac	pm (mas per yr)	ruwe	Remarks	Neb Fe	DS	Gvar	Mod	T_{DS}	γ	WISE ph_qual	WISE var_flag
247	6668113546550866816	305.132	-48.657	268.519	0.168	3.685	0.088	17.130	14.467	0.072	6.525	1.076	TESS. Irregu	No	No	0.967	194	100	0.1	b'AACB'	b'11nn'
248	727690403382030848	156.473	25.838	268.866	0.000	3.713	0.109	17.719	14.977	0.000	50.757	1.006	K&M, TESS. Irregu	No	No	0.786	2589	125	0.1	b'AACC'	b'00nn'
249	1623882363879075200	245.566	58.807	269.360	0.244	3.669	0.109	18.446	15.422	0.093	10.242	0.988	TESS	No	Yes	0.890	218	100	0.1	b'AACC'	b'00nn'
250	3080917549095781376	118.139	-3.103	269.615	0.000	3.676	0.099	17.597	14.753	0.139	7.431	1.051	TESS. Faint	No	No	0.803	2587	125	0.1	b'AACC'	b'nnnn'
251	1912121231182574208	351.232	34.261	269.639	0.000	3.692	0.081	17.327	14.622	0.138	60.450	0.989	K&M, TESS. Blended	No	No	0.937	2583	125	0.1	b'AABB'	b'11nn'
252	3297949054086097408	61.762	7.180	269.787	0.000	3.689	0.106	17.124	14.504	0.118	29.464	0.960	TESS. Faint	No	No	0.871	193	100	0.1	b'AACC'	b'nnnn'
253	5477382684625909248	97.928	-63.093	270.692	0.000	3.704	0.118	18.391	15.429	0.155	21.595	1.005	TESS. Irregu	No	No	0.900	218	100	0.1	b'AACC'	b'nnnn'
254	2480882305418201856	23.396	-4.029	270.901	0.418	3.688	0.122	17.534	14.711	0.025	62.976	1.132	K&M, TESS	No	Yes	0.953	199	100	0.1	b'AACC'	b'11nn'
255	1729065253964773760	239.688	88.849	271.901	0.000	3.650	0.064	17.553	14.821	0.200	6.004	0.913	TESS. Blended	No	No	0.838	2586	137.5	0.1	b'AABB'	b'01nn'
256	2437221214075471744	354.011	-9.333	272.107	0.210	3.681	0.112	17.312	14.765	0.000	28.321	1.014	TESS	No	Yes	0.875	2582	125	0.1	b'AACB'	b'00nn'
257	1390217593013664512	234.411	41.442	272.428	0.459	3.624	0.119	18.204	15.302	0.089	22.269	1.034	TESS.	No	Yes	0.998	215	100	0.1	b'AACC'	b'01nn'
258	4855620507070226304	58.684	-38.977	272.599	0.278	3.642	0.095	17.997	14.993	0.077	33.445	1.036	TESS. Irregu	No	No	0.982	210	100	0.1	b'AACC'	b'11nn'
259	2302726649664192640	285.549	84.567	272.776	0.263	3.624	0.087	17.765	14.881	0.143	30.387	1.027	TESS. Irregu	No	No	0.852	203	100	0.1	b'AACC'	b'11nn'
260	4400845665847062272	235.343	-4.515	273.067	0.201	3.624	0.089	17.064	14.274	0.236	11.971	1.131	TESS. Blended	No	No	0.892	2575	125	0.1	b'AABB'	b'00nn'
261	3818640132790416000	169.681	8.036	273.922	0.266	3.614	0.108	17.618	14.804	0.086	41.330	1.102	NCJM, K&M, TESS. Blended	No	No	0.885	4971	150	0.1	b'AABC'	b'11nn'

continued . . .

	GAIA DR3 Source ID	ra	dec	Dist (pc)	AEN	para (mas)	p err (mas)	g mag	j mag	red frac	pm (mas per yr)	ruwe	Remarks	Neb Fe	DS	Gvar	Mod	T_{DS}	γ	WISE ph_qual	WISE var_flag
262	6701056903488196480	304.602	-30.917	274.245	0.076	3.613	0.089	17.373	14.645	0.096	22.560	1.027	TESS. Faint & Irregu ,	No	No	0.963	2583	125	0.1	b'AABB'	b'00nn'
263	4851401543515220736	49.477	-41.304	274.254	0.000	3.593	0.095	18.008	15.018	0.093	17.698	0.988	TESS.	No	Yes	0.849	2595	137.5	0.1	b'AABB'	b'11nn'
264	4851380137398151808	49.097	-41.541	274.607	0.000	3.597	0.079	17.702	14.884	0.167	37.681	0.958	TESS. Blended	No	No	0.917	202	100	0.1	b'AACC'	b'22nn'
265	3694287467929202048	185.319	-2.153	274.714	0.000	3.600	0.109	17.456	14.687	0.000	21.227	0.968	TESS. Blended	No	No	0.969	4968	162.5	0.1	b'AABB'	b'00nn'
266	6783520279866548480	322.007	-31.786	274.906	0.000	3.597	0.093	16.902	14.217	0.029	32.911	0.976	TESS.	No	Yes	0.833	187	100	0.1	b'AACB'	b'11nn'
267	2623244940679403008	337.892	-5.523	275.686	0.000	3.634	0.119	17.629	14.842	0.019	16.849	0.983	TESS. Blended	No	No	0.865	2586	137.5	0.1	b'AACC'	b'00nn'
268	4932875462509521280	13.405	-48.492	275.717	0.000	3.597	0.076	17.474	14.720	0.030	82.362	0.972	K&M, TESS.	No	Yes	0.986	198	100	0.1	b'AACC'	b'11nn'
269	3929437305341869056	194.689	12.620	275.741	0.000	3.548	0.083	16.998	14.249	0.000	41.018	0.989	K&M, TESS.	No	Yes	0.921	190	100	0.1	b'AACC'	b'11nn'
270	228005004699478016	66.206	40.527	275.915	0.000	3.602	0.119	17.712	14.848	0.504	14.193	1.006	TESS. Faint	No	No	1.016	2588	125	0.1	b'AACC'	b'11nn'
271	2597994110686486400	338.992	-13.500	276.711	0.000	3.613	0.102	17.286	14.650	0.063	8.927	0.936	TESS. Blended	No	No	0.801	2580	125	0.1	b'AACB'	b'00nn'
272	1066493366609312256	150.480	66.754	277.809	0.243	3.569	0.070	17.181	14.602	0.043	26.508	1.140	TESS. Blended	No	No	0.978	192	100	0.1	b'AACB'	b'00nn'
273	3819217208891753472	146.655	-8.654	278.020	0.135	3.575	0.105	17.756	14.970	0.113	16.688	1.040	TESS. Blended	No	No	0.898	2589	125	0.1	b'AABC'	b'00nn'
274	2478471596110203008	20.161	-7.177	278.444	0.000	3.524	0.087	17.137	14.349	0.138	51.926	1.022	NCJM, K&M, TESS	No	Yes	1.123	2575	125	0.1	b'AABB'	b'11nn'
275	3355250819828269568	98.817	12.873	280.188	0.000	3.582	0.260	18.751	15.584	0.407	27.749	0.887	Herbig Ae/Be	No	No	1.030	36786	200	0.2	b'AABC'	b'00nn'

continued . . .

	GAIA DR3 Source ID	ra	dec	Dist (pc)	AEN	para (mas)	p err (mas)	g mag	j mag	red frac	pm (mas per yr)	ruwe	Remarks	Neb Fe	DS	Gvar	Mod	T_{DS}	γ	WISE ph_qual	WISE var_flag
276	714714207670830336	138.988	35.676	281.396	0.247	3.506	0.083	16.716	14.312	0.111	18.425	1.190	TESS, LAM-OST. Blended	No	No	0.847	2565	125	0.1	b'AABB'	b'00nn'
277	6760241209234737920	283.618	-31.364	281.567	0.988	3.771	0.419	19.570	16.247	0.363	48.798	1.018	K&M, TESS. Irregu	No	No	0.952	37073	200	0.25	b'AABC'	b'11nnn'
278	1131031396329260288	152.541	77.713	282.665	0.000	3.514	0.093	17.875	15.089	0.077	15.386	1.002	TESS. Blended.	No	No	0.944	2590	125	0.1	b'AABC'	b'00nn'
279	3340157961149521152	86.489	12.017	282.982	0.000	3.524	0.105	17.623	14.950	0.393	95.277	0.997	K&M, TESS. Faint	No	No	0.820	2587	125	0.1	b'AACC'	b'00nn'
280	2966133315455819648	86.805	-20.128	283.725	0.000	3.454	0.068	17.149	14.358	0.099	18.139	0.987	TESS	No	Yes	0.878	190	100	0.1	b'AACC'	b'00nn'
281	5112579608592599680	55.008	-14.308	284.664	0.000	3.469	0.059	16.860	14.259	0.032	25.304	0.947	TESS.	No	Yes	0.864	85782	325	0.1	b'ABCC'	b'0nnn'
282	1654323820762575872	240.591	72.466	285.078	0.000	3.465	0.073	17.829	15.140	0.127	27.630	0.978	TESS. Blended	No	No	0.870	204	100	0.1	b'AACC'	b'11nn'
283	1665884498333848320	204.501	64.461	285.500	0.000	3.491	0.109	18.263	15.363	0.028	58.764	0.967	NCJM, TESS, K&M. Blended	No	No	0.826	2598	125	0.1	b'AACC'	b'00nn'
284	6223781965550159232	218.203	-26.020	286.831	0.000	3.394	0.231	18.581	15.304	0.167	48.226	0.947	TESS, K&M. Blended	No	No	1.080	40759	215	0.1	b'AABC'	b'11nn'
285	1050495536848847360	145.782	59.436	286.832	0.260	3.439	0.076	17.229	14.632	0.026	21.279	1.097	TESS.	No	Yes	0.822	192	100	0.1	b'AACC'	b'00nn'
286	4573357386681921024	255.295	26.571	287.815	0.000	3.449	0.089	17.816	15.088	0.089	16.235	1.007	TESS. Blended	No	No	0.814	2589	125	0.1	b'AABC'	b'00nn'
287	397088899250816128	23.501	45.225	288.245	0.000	3.417	0.095	17.186	14.426	0.118	10.352	0.972	TESS. Irregu	No	No	0.995	190	100	0.1	b'AABB'	b'11nn'
288	5083177117181902208	59.763	-24.952	288.938	0.000	3.474	0.126	18.341	15.308	0.042	19.634	1.000	TESS. Irregu	No	No	0.963	45264	225	0.1	b'AABC'	b'000n'
289	2159638130570202880	278.512	61.584	290.555	0.311	3.359	0.100	18.021	15.183	0.102	22.791	1.017	TESS	No	Yes	0.917	205	100	0.1	b'AACB'	b'11nn'

continued . . .

	GAIA DR3 Source ID	ra	dec	Dist (pc)	AEN	para (mas)	p err (mas)	g mag	j mag	red frac	pm (mas per yr)	ruwe	Remarks	Neb Fe	DS	Gvar	Mod	T_{DS}	γ	WISE ph_qual	WISE var_flag
290	1946037385330429824	326.486	32.173	290.564	0.157	3.383	0.097	17.750	14.970	0.148	8.102	0.981	TESS. Faint	No	No	0.920	2587	125	0.1	b'AACC'	b'00nn'
291	2903767607178651776	85.357	-30.960	290.673	0.089	3.441	0.113	18.185	15.440	0.045	23.408	1.031	TESS	No	Yes	0.937	473	100	0.2	b'AACB'	b'11nn'
292	5136900805798685952	30.749	-19.934	292.346	0.225	3.391	0.098	17.409	14.745	0.032	23.817	1.050	TESS. Irregu	No	No	1.035	195	100	0.1	b'AACC'	b'11nn'
293	4824747599248448640	75.156	-35.354	292.959	0.000	3.396	0.093	18.029	15.393	0.067	41.129	0.981	K&M, TESS. Blended	No	No	0.909	2592	125	0.1	b'AABC'	b'00nn'
294	5119054319034868224	38.881	-25.026	293.370	0.000	3.381	0.159	17.826	15.162	0.042	17.518	1.006	TESS. Blended	No	No	0.928	45252	225	0.1	b'AAAB'	b'000n'
295	1344591738816056832	267.754	40.595	294.423	0.255	3.382	0.091	17.864	15.172	0.062	43.895	1.049	K&M, TESS. Blended	No	No	0.945	2589	125	0.1	b'AABC'	b'00nn'
296	6826811145027574144	330.585	-16.358	295.565	0.236	3.350	0.111	17.184	14.615	0.019	30.941	1.072	TESS. Blended	No	No	0.936	2576	125	0.1	b'AABC'	b'00nn'
297	4824534087834366080	74.719	-36.568	295.917	0.066	3.342	0.060	17.177	14.533	0.119	21.210	1.030	TESS. Blended	No	No	0.903	188	100	0.1	b'AACC'	b'00nn'
298	1020168880146788736	145.222	52.265	296.473	0.000	3.317	0.081	17.329	14.683	0.023	25.186	0.964	TESS.	No	Yes	0.827	191	100	0.1	b'AACC'	b'11nn'
299	3713867742794348928	206.518	4.236	298.965	0.000	3.296	0.087	17.418	14.739	0.095	17.953	1.020	TESS. Blended	No	No	1.059	194	100	0.1	b'AACC'	b'21nn'
300	823019947000506880	152.824	49.272	299.164	0.123	3.322	0.104	17.850	15.076	0.049	6.457	1.040	TESS. Blended	No	No	0.970	2587	125	0.1	b'AACC'	b'00nn'
301	4700193234130583808	37.084	-63.909	300.111	0.835	3.417	0.190	19.146	16.107	0.045	23.645	1.079	TESS. Irregu	No	No	0.950	36530	200	0.15	b'AABC'	b'00nn'
302	6006311102587627648	232.844	-38.745	305.217	0.144	3.294	0.161	18.244	15.490	0.300	49.421	1.007	K&M, TESS. Faint	No	No	0.902	36513	200	0.15	b'AABC'	b'000n'

APPENDIX B

Final DS candidates

The final list of DS candidates is shown in the below table. It consists of 166 candidates.

	GAIA DR3 Source ID	ra	dec	Dist (pc)	AEN	para (mas)	p err (mas)	g mag	j mag	red frac (6')	pm (mas per yr)	ruwe	Remarks	Nebular Features	DS	Gvar	Mod	T_{DS}	γ	WISE ph_qual	WISE var_flag
1	2915906078111475840	86.463	-23.254	75.954	0.237	13.143	0.110	18.011	14.350	0.108	12.355	0.970	TESS,	No	Yes	0.923	261	100	0.1	b'AACC'	b'11nn'
2	3510237257322054912	194.421	-18.011	83.119	0.550	12.118	0.196	18.309	14.536	0.077	79.027	1.079	TESS, K&M	No	Yes	0.976	261	100	0.1	b'AACC'	b'11nn'
3	3978048187578510976	170.395	19.665	84.162	0.462	11.817	0.131	17.652	14.368	0.000	101.212	1.133	NCJM, TESS C	No	Yes	1.083	255	100	0.1	b'AACC'	b'01nn'
4	5760183294402944896	132.025	-6.698	100.304	0.166	9.953	0.128	17.872	14.686	0.113	51.912	0.980	TESS C, K&M	No	Yes	0.940	250	100	0.1	b'AACC'	b'00nn'
5	3536922958580249472	165.030	-23.974	103.836	0.453	9.569	0.149	17.836	14.545	0.116	60.955	0.951	TESS C, K&M	No	Yes	1.121	247	100	0.1	b'AACC'	b'00nn'
6	6488635934221051136	353.882	-61.471	109.527	0.302	9.044	0.095	17.785	14.375	0.055	63.236	1.033	TESS	No	Yes	1.002	244	100	0.1	b'AACC'	b'00nn'
7	5685387641533656704	147.032	-15.974	113.933	0.414	8.694	0.146	17.944	14.651	0.107	34.013	0.982	TESS C, K&M	No	Yes	1.037	247	100	0.1	b'AACC'	b'21nn'
8	1761730438755511552	314.431	14.755	114.542	0.504	8.704	0.150	17.971	14.605	0.095	56.628	1.036	K&M, TESS	No	Yes	1.044	248	100	0.1	b'AACC'	b'00nn'
9	4430833917781139840	234.222	7.695	118.357	0.293	8.424	0.103	17.456	14.303	0.077	127.387	1.060	TESS C, K&M, NJCM	No	Yes	0.966	234	100	0.1	b'AACC'	b'00nn'
10	1115438362942844672	103.623	75.343	120.375	0.743	8.179	0.136	18.198	14.673	0.093	8.548	1.006	TESS	No	Yes	0.953	249	100	0.1	b'AACC'	b'11nn'
11	1614536893000145536	224.887	60.238	123.060	0.670	8.090	0.133	18.426	14.972	0.000	49.595	0.963	K&M, NJCM, TESS	No	Yes	1.072	253	100	0.1	b'AACC'	b'11nn'
12	1328197371906749696	251.098	37.156	123.652	0.574	8.032	0.111	17.957	14.620	0.075	90.834	0.945	TESS C, K&M.	No	Yes	0.986	244	100	0.1	b'BACC'	b'00nn'
13	757976927909863296	168.045	32.807	125.613	0.230	7.947	0.129	18.041	14.756	0.000	68.510	1.015	K&M, NJCM, TESS	No	Yes	1.012	243	112.5	0.1	b'AACC'	b'11nn'
14	1100972024033153792	101.288	65.194	126.210	0.537	7.900	0.143	17.960	14.728	0.082	28.076	1.073	NJCM, TESS	No	Yes	0.993	244	100	0.1	b'AACC'	b'00nn'
15	3488776577056140800	184.888	-24.666	126.673	0.392	7.847	0.139	17.851	14.523	0.083	18.497	0.888	TESS	No	Yes	1.121	241	100	0.1	b'AACC'	b'01nn'

continued . . .

	GAIA DR3 Source ID	ra	dec	Dist (pc)	AEN	para (mas)	p err (mas)	g mag	j mag	red frac	pm (mas per yr)	ruwe	Remarks	Nebu Features	DS	Gvar	Mod	T_{DS}	γ	WISE ph_qual	WISE var_flag
16	6289125971652580224	207.276	-20.356	126.953	0.425	7.843	0.157	18.084	14.754	0.013	183.018	0.935	TESS C, K&M, HPMS	No	Yes	1.134	244	100	0.1	b'AACC'	b'11nn'
17	5039343402513263104	24.285	-23.292	127.050	0.657	7.836	0.143	17.910	14.631	0.000	65.357	0.924	K&M, TESS	No	Yes	1.116	240	100	0.1	b'AACC'	b'11nn'
18	3261094210299919616	51.073	-2.783	131.110	0.386	7.525	0.133	17.737	14.498	0.032	10.644	0.943	TESS	No	Yes	1.211	2621	125	0.1	b'AABC'	b'11nn'
19	2092866786582167296	284.441	35.855	131.134	0.499	7.554	0.088	17.607	14.389	0.154	53.173	0.989	K&M, TESS	No	Yes	1.029	235	100	0.1	b'AABC'	b'nnnn'
20	2787983737076819072	14.923	18.424	133.638	0.523	7.452	0.147	17.810	14.488	0.129	75.654	1.211	NCJM, TESS C, K&M.	No	Yes	1.083	236	100	0.1	b'AACC'	b'11nn'
21	6458044149186203520	314.676	-55.464	134.265	0.678	7.404	0.145	18.148	14.849	0.060	42.576	1.045	K&M, TESS	No	Yes	1.086	2628	125	0.1	b'AACC'	b'00nn'
22	1690729715910190976	187.347	73.921	135.057	0.155	7.348	0.108	18.204	14.973	0.000	49.577	0.989	K&M, TESS, Binary Star system	No	Yes	0.882	243	100	0.1	b'AACC'	b'11nn'
23	661992899995819392	131.800	21.601	136.518	0.094	7.296	0.076	16.947	14.083	0.061	35.767	1.015	NCJM, TESS,	No	Yes	0.872	219	100	0.1	b'AACC'	b'00nn'
24	1353970057604540160	256.943	40.809	137.581	0.721	7.287	0.149	18.759	15.350	0.065	91.214	1.023	K&M,	No	Yes	0.974	2639	125	0.1	b'AACC'	b'00nn'
25	1315337479611688832	241.086	25.438	138.830	0.707	7.199	0.129	18.343	15.073	0.109	27.549	1.034	TESS	No	Yes	0.980	2632	125	0.1	b'AACC'	b'00nn'
26	6088807769255904896	202.057	-42.640	139.393	0.603	7.175	0.192	18.587	15.167	0.156	5.502	1.031	TESS	No	Yes	0.987	2635	125	0.1	b'AACC'	b'11nn'
27	883173678401486336	107.387	26.572	139.983	0.648	7.166	0.214	18.260	14.938	0.094	74.543	1.063	K&M, TESS	No	Yes	1.074	2629	125	0.1	b'AACC'	b'01nn'
28	2618501102056246400	329.629	-8.453	140.363	0.333	7.057	0.164	17.959	14.875	0.041	172.565	0.973	HPMS, NCJM, K&M	No	Yes	0.979	2622	125	0.1	b'AACC'	b'00nn'
29	939289281548249856	103.427	33.766	140.724	0.388	7.095	0.127	17.591	14.460	0.153	37.545	1.112	TESS	No	Yes	1.214	230	100	0.1	b'AACC'	b'01nn'
30	3483112241042201088	172.288	-29.273	141.259	0.171	7.046	0.087	17.160	14.186	0.096	56.467	1.060	TESS C, K&M	No	Yes	1.031	221	100	0.1	b'AACB'	b'11nn'

continued . . .

	GAIA DR3 Source ID	ra	dec	Dist (pc)	AEN	para (mas)	p err (mas)	g mag	j mag	red frac	pm (mas per yr)	ruwe	Remarks	Nebu Fea-tures	DS	Gvar	Mod	T_{DS}	γ	WISE ph_qual	WISE var_flag
31	6503326058107971328	340.700	-59.319	141.804	0.615	7.044	0.154	18.571	15.149	0.130	92.424	1.019	K&M, TESS	No	Yes	0.991	2633	125	0.1	b'AACC'	b'22nn'
32	2654924035339211904	343.591	0.681	142.055	0.513	6.975	0.162	17.793	14.432	0.000	20.761	1.025	TESS	No	Yes	1.184	232	100	0.1	b'AACC'	b'11nn'
33	2397293651903978112	342.335	-21.809	143.878	0.161	6.936	0.114	17.614	14.833	0.000	25.189	1.009	TESS	No	Yes	0.872	229	100	0.1	b'AACC'	b'11nn'
34	889362936730041728	104.452	32.011	144.105	0.324	6.860	0.133	18.045	14.810	0.118	113.692	0.911	K&M, TESS	No	Yes	1.115	2623	137.5	0.1	b'AABC'	b'00nn'
35	618553463324573568	142.254	14.776	144.274	0.000	6.858	0.164	18.035	14.802	0.000	122.833	1.012	NCJM, K&M, TESS	No	Yes	0.892	2621	112.5	0.15	b'AACC'	b'01nn'
36	2496905385291035264	40.007	-1.221	144.755	0.340	6.884	0.139	17.776	14.810	0.031	145.508	1.132	NCJM, K&M, TESS	No	Yes	0.895	233	100	0.1	b'AACC'	b'11nn'
37	1338448458113508480	256.626	35.635	145.044	0.435	6.855	0.106	17.820	14.707	0.086	51.243	1.047	NCJM, K&M, TESS	No	Yes	1.004	235	100	0.1	b'AACC'	b'11nn'
38	3665977169521275776	214.375	0.599	152.197	0.325	6.543	0.113	17.429	14.440	0.061	55.834	1.040	NCJM, TESS C, K&M.	No	Yes	0.868	224	100	0.1	b'AACC'	b'00nn'
39	1036767966673477120	135.326	57.534	152.777	0.599	6.504	0.169	18.381	15.241	0.021	9.671	1.016	NCJM, TESS	No	Yes	1.016	2628	125	0.1	b'AACC'	b'11nn'
40	4814864398463549568	70.098	-42.557	153.112	0.531	6.481	0.111	17.888	14.568	0.030	44.031	0.977	K&M, Binary star system	No	Yes	1.027	232	100	0.1	b'BABC'	b'00nn'
41	1016422289979953664	136.149	50.962	153.226	0.678	6.490	0.179	18.483	15.205	0.048	54.973	1.050	NCJM, K&M.	No	Yes	1.057	2628	125	0.1	b'AACC'	b'11nn'
42	2310451960094696192	356.808	-37.590	153.754	0.000	6.433	0.101	17.140	14.267	0.133	25.596	0.997	TESS	No	Yes	0.867	218	100	0.1	b'AACB'	b'11nn'
43	5170146837671740160	39.448	-14.173	153.940	0.000	6.472	0.115	17.879	14.838	0.033	61.673	0.984	K&M, TESS C	No	Yes	0.943	233	100	0.1	b'AACC'	b'00nn'
44	3629164111474614656	194.777	-7.095	154.622	0.000	6.419	0.140	18.000	14.969	0.067	53.037	0.980	K&M, TESS	No	Yes	0.953	2619	125	0.1	b'AABC'	b'00nn'

continued . . .

	GAIA DR3 Source ID	ra	dec	Dist (pc)	AEN	para (mas)	p err (mas)	g mag	j mag	red frac	pm (mas per yr)	ruwe	Remarks	Nebu Fea-tures	DS	Gvar	Mod	T_{DS}	γ	WISE ph_qual	WISE var_flag
45	2387172475571686400	354.968	-23.063	154.925	0.396	6.373	0.124	17.465	14.396	0.056	26.181	0.996	TESS	No	Yes	1.029	224	100	0.1	b'AACC'	b'00nn'
46	6686966734993777792	300.245	-41.703	155.396	0.226	6.404	0.099	17.358	14.328	0.082	13.939	1.022	TESS	No	Yes	1.027	220	100	0.1	b'AACC'	b'11nn'
47	597270624767394816	132.358	9.356	155.645	0.000	6.400	0.130	17.813	14.861	0.062	82.697	0.970	NCJM, K&M. Open cluster star	No	Yes	0.903	2613	125	0.1	b'AACC'	b'00nn'
48	4889857310590694912	60.133	-28.120	156.162	0.000	6.382	0.099	17.833	14.884	0.065	21.119	0.997	TESS	No	Yes	0.977	228	100	0.1	b'AACC'	b'11nn'
49	3488393401547734912	181.768	-26.114	157.287	0.032	6.327	0.131	17.969	14.880	0.114	48.320	1.026	K&M, TESS	No	Yes	0.986	496	100	0.2	b'AACB'	b'11nn'
50	3451273339241871616	87.988	32.982	157.680	0.110	6.392	0.197	18.255	15.126	0.260	42.841	1.014	K&M	No	Yes	0.906	2625	137.5	0.1	b'AACC'	b'00nn'
51	911311005588551808	128.374	39.142	157.682	0.000	6.368	0.138	18.197	15.010	0.056	69.835	0.949	NCJM, K&M,	No	Yes	0.863	2622	125	0.1	b'AACC'	b'00nn'
52	3530813144262513536	191.058	-9.776	158.005	0.370	6.291	0.133	17.741	14.678	0.103	166.415	1.002	NCJM, HPMS, TESS C, K&M	No	Yes	1.021	227	100	0.1	b'AACC'	b'00nn'
53	952003729070420480	103.831	42.580	158.495	0.000	6.281	0.098	17.266	14.346	0.112	112.007	0.924	K&M, TESS C	No	Yes	0.990	218	100	0.1	b'AACB'	b'01nn'
54	2539799842150995968	16.748	3.632	159.307	0.436	6.288	0.141	17.874	14.977	0.000	80.312	0.938	NCJM, K&M, TESS C	No	Yes	1.021	2614	125	0.1	b'AACC'	b'11nn'
55	482440516581202688	72.711	66.150	159.468	0.087	6.269	0.122	18.277	15.233	0.392	86.798	1.019	K&M, TESS C	No	Yes	0.932	2622	125	0.1	b'AACC'	b'11nn'
56	3043112048663066112	118.634	-7.143	159.802	0.304	6.233	0.117	17.654	14.684	0.103	16.429	0.932	TESS	No	Yes	1.106	225	100	0.1	b'AACC'	b'10nn'
57	1023025063462941824	141.595	53.824	160.872	0.000	6.211	0.138	18.367	15.294	0.027	51.315	0.958	NCJM, K&M, TESS C	No	Yes	0.878	2887	125	0.2	b'AABB'	b'00nn'
58	4128901290300825984	254.947	-19.426	162.003	0.592	6.127	0.160	18.087	14.630	0.517	32.996	1.072	TESS	No	Yes	1.062	2617	125	0.1	b'AACC'	b'00nn'
59	4649665864475436160	79.346	-73.413	162.147	1.028	6.220	0.189	19.002	15.710	0.464	52.229	1.016	K&M, TESS	No	Yes	0.879	5023	150	0.1	b'AABC'	b'00nn'

continued . . .

	GAIA DR3 Source ID	ra	dec	Dist (pc)	AEN	para (mas)	p err (mas)	g mag	j mag	red frac	pm (mas per yr)	ruwe	Remarks	Nebu Fea-tures	DS	Gvar	Mod	T_{DS}	γ	WISE ph_qual	WISE var_flag
60	2536856105926470912	13.684	0.073	162.813	0.000	6.104	0.115	17.650	14.585	0.088	76.962	1.013	NCJM, K&M, TESS C	No	Yes	0.871	2609	125	0.1	b'AACC'	b'11nn'
61	1369633803332569088	236.577	32.445	165.820	0.639	6.013	0.168	18.807	15.467	0.070	59.031	1.002	NCJM, TESS	No	Yes	1.018	2632	125	0.1	b'AACC'	b'00nn'
62	6885510703580632576	318.162	-13.627	166.119	0.118	5.988	0.152	17.944	14.909	0.069	30.062	1.018	TESS	No	Yes	0.982	2616	125	0.1	b'AACC'	b'00nn'
63	5481309418607141888	92.585	-61.699	166.379	0.000	6.033	0.114	18.097	15.032	0.147	82.013	0.964	K&M, TESS	No	Yes	0.831	233	100	0.1	b'AACC'	b'11nn'
64	834831828618687616	156.748	49.308	166.999	0.000	5.936	0.092	17.491	14.632	0.034	88.970	1.006	K&M, TESS	No	Yes	0.950	220	100	0.1	b'AACC'	b'00nn'
65	1850962129541995648	323.232	32.297	167.374	0.000	5.940	0.095	17.811	14.755	0.190	15.014	0.998	TESS	No	Yes	1.049	225	100	0.1	b'AACC'	b'00nn'
66	1447646077468827776	198.878	25.591	167.583	0.218	5.951	0.183	18.529	15.230	0.034	86.414	0.959	NCJM, K&M, TESS	No	Yes	1.005	2626	125	0.1	b'AACC'	b'00nn'
67	3854090071297359616	144.976	7.008	168.363	0.000	5.894	0.103	17.402	14.417	0.019	15.504	0.959	TESS	No	Yes	0.923	218	100	0.1	b'AACB'	b'11nn'
68	2996292365351686144	86.498	-14.150	168.634	0.319	5.892	0.119	17.932	14.897	0.171	47.226	1.036	K&M, TESS	No	Yes	0.923	2616	125	0.1	b'AABC'	b'00nn'
69	3636165908894524544	199.359	-4.385	169.208	0.000	5.869	0.107	17.706	14.618	0.067	66.765	0.989	K&M, TESS	No	Yes	0.871	224	100	0.1	b'AACC'	b'00nn'
70	477541264565874816	73.711	61.463	169.636	0.307	5.829	0.101	17.674	14.580	0.535	79.977	0.930	K&M, TESS C	No	Yes	0.992	224	100	0.1	b'AACC'	b'00nn'
71	2344470574980336256	13.788	-25.750	170.990	0.417	5.814	0.145	17.660	14.650	0.083	31.409	1.015	TESS	No	Yes	1.156	222	100	0.1	b'AACC'	b'11nn'
72	6405584490920011648	331.399	-63.454	171.004	0.150	5.807	0.098	17.845	14.848	0.057	56.463	1.039	K&M, TESS	No	Yes	0.912	2612	125	0.1	b'AACC'	b'11nn'
73	3498693553461662208	192.333	-23.819	171.900	0.583	5.805	0.167	18.203	15.144	0.125	26.387	1.014	TESS	No	Yes	0.996	5004	150	0.1	b'AABC'	b'11nn'
74	1663135032069421056	202.039	60.202	172.047	0.434	5.808	0.113	18.001	14.989	0.037	85.056	1.080	K&M, TESS	No	Yes	1.022	231	100	0.1	b'AACC'	b'11nn'
75	647720891173924480	144.821	27.290	172.487	0.510	5.862	0.173	17.999	14.925	0.023	50.544	1.005	NCJM, K&M, TESS	No	Yes	0.877	2615	125	0.1	b'AACC'	b'00nn'

continued . . .

	GAIA DR3 Source ID	ra	dec	Dist (pc)	AEN	para (mas)	p err (mas)	g mag	j mag	red frac	pm (mas per yr)	ruwe	Remarks	Nebu Fea-tures	DS	Gvar	Mod	T_{DS}	γ	WISE ph_qual	WISE var_flag
76	4619397649388055936	48.286	-80.995	172.730	0.311	5.726	0.091	18.077	15.029	0.086	98.944	1.029	K&M, TESS	No	Yes	1.101	231	100	0.1	b'AACC'	b'11nn'
77	3646420641529967744	216.011	-2.513	173.147	0.000	5.767	0.115	17.502	14.678	0.064	23.588	0.975	NCJM, TESS	No	Yes	0.940	220	100	0.1	b'AACC'	b'00nn'
78	4784624938185655680	71.960	-50.214	173.229	0.000	5.746	0.102	18.288	15.181	0.091	37.047	0.972	TESS	No	Yes	0.877	234	100	0.1	b'AACC'	b'11nn'
79	1150574390879641472	105.397	86.256	175.013	0.508	5.664	0.101	18.050	14.806	0.071	37.986	1.018	TESS C	No	Yes	1.088	230	100	0.1	b'AACC'	b'00nn'
80	1103045771685331328	106.024	67.983	176.265	0.715	5.657	0.175	18.666	15.503	0.060	89.934	1.045	K&M, TESS	No	Yes	0.986	505	100	0.2	b'AACC'	b'00nn'
81	3595041077343698944	178.954	-7.864	178.302	0.000	5.534	0.125	18.018	14.930	0.071	23.302	0.940	TESS	No	Yes	0.968	2612	125	0.1	b'AACC'	b'00nn'
82	2789153445649630464	11.761	19.032	178.828	0.346	5.550	0.146	18.026	15.033	0.194	56.795	0.901	NCJM, K&M, TESS C	No	Yes	1.063	2616	125	0.1	b'AACC'	b'00nn'
83	4876715604017587072	74.395	-29.687	179.089	0.638	5.484	0.145	18.567	15.273	0.018	51.889	0.996	K&M, TESS	No	Yes	1.020	2626	125	0.1	b'AABC'	b'00nn'
84	4644937556449853696	38.844	-71.890	179.773	0.381	5.523	0.102	18.145	15.047	0.042	47.813	0.981	K&M, TESS	No	Yes	0.994	231	100	0.1	b'AACC'	b'11nn'
85	5631833320661544448	143.390	-32.108	180.244	0.167	5.515	0.064	17.175	14.304	0.192	40.739	1.038	K&M, TESS	No	Yes	1.027	211	100	0.1	b'AACC'	b'00nn'
86	1049350021827111808	147.766	57.727	180.860	0.289	5.477	0.119	18.181	15.081	0.026	52.145	0.904	NCJM, K&M, TESS C	No	Yes	0.908	231	100	0.1	b'AACC'	b'11nn'
87	2353610295450275968	19.781	-20.156	185.283	0.595	5.368	0.169	18.397	15.261	0.054	44.404	1.044	K&M, TESS	No	Yes	0.943	2619	125	0.1	b'AACC'	b'00nn'
88	4426899659020024192	239.052	6.096	185.514	0.000	5.351	0.047	15.997	13.345	0.078	11.031	1.040	TESS	No	Yes	0.801	187	100	0.1	b'AABB'	b'00nn'
89	6266957794311581056	237.094	-13.236	186.482	0.084	5.330	0.083	17.151	14.186	0.257	82.901	1.008	K&M, TESS	No	Yes	1.029	210	100	0.1	b'AACC'	b'00nn'
90	2798379241559922688	0.829	20.175	186.585	0.000	5.351	0.127	17.832	14.804	0.077	74.523	0.985	NCJM, K&M	No	Yes	0.915	2606	125	0.1	b'AACC'	b'00nn'
91	3683792006674301056	190.210	-0.896	189.906	0.106	5.264	0.127	17.895	15.051	0.053	80.751	1.028	K&M, TESS	No	Yes	0.852	2608	125	0.1	b'AACC'	b'01nn'

continued . . .

	GAIA DR3 Source ID	ra	dec	Dist (pc)	AEN	para (mas)	p err (mas)	g mag	j mag	red frac	pm (mas per yr)	ruwe	Remarks	Nebu Features	DS	Gvar	Mod	T_{DS}	γ	WISE ph_qual	WISE var_flag
92	2907012845810852096	81.424	-28.043	191.628	0.000	5.220	0.164	18.696	15.486	0.088	24.218	1.015	TESS	No	Yes	0.972	5007	137.5	0.1	b'AABC'	b'11nn'
93	4731386069772654720	55.511	-56.085	191.693	0.565	5.214	0.132	18.569	15.463	0.093	72.476	1.050	K&M, TESS	No	Yes	0.992	2622	125	0.1	b'AACC'	b'00nn'
94	1885602483892413440	346.598	29.430	193.661	0.000	5.126	0.114	17.706	14.773	0.066	85.287	0.945	NCJM, K&M, TESS C	No	Yes	0.929	218	100	0.1	b'AACC'	b'00nn'
95	1876027833559029632	340.893	23.816	196.086	0.260	5.113	0.144	18.163	15.105	0.049	25.878	1.042	NCJM, TESS	No	Yes	0.872	2612	112.5	0.1	b'AACC'	b'11nn'
96	1622841813561817984	238.558	57.996	196.799	0.453	5.065	0.111	18.167	15.166	0.041	44.996	1.088	NCJM, K&M, TESS C	No	Yes	0.889	227	100	0.1	b'AACC'	b'11nn'
97	2555452390900570752	9.063	5.962	201.819	0.000	4.911	0.104	17.512	14.680	0.053	73.305	0.935	NCJM, K&M, TESS C	No	Yes	0.884	2598	125	0.1	b'AACC'	b'00nn'
98	2440574312223232000	355.576	-6.039	203.896	0.000	4.925	0.137	17.999	15.142	0.156	51.485	0.965	NCJM, K&M, TESS C	No	Yes	0.962	4993	137.5	0.1	b'AACC'	b'00nn'
99	6007147938313420544	229.642	-37.912	204.501	0.000	4.832	0.120	17.768	14.803	0.160	13.742	0.878	TESS	No	Yes	0.894	216	100	0.1	b'AACC'	b'00nn'
100	6489518051784208000	352.204	-58.686	204.944	0.265	4.853	0.086	17.692	14.799	0.036	52.326	1.070	NCJM, TESS	No	Yes	0.910	2601	125	0.1	b'AABC'	b'11nn'
101	222438624003605888	53.195	36.221	205.763	0.000	4.846	0.099	16.990	14.380	0.172	63.599	0.983	K&M, TESS	No	Yes	0.826	200	100	0.1	b'AACC'	b'11nn'
102	6635616067348164224	275.678	-59.353	206.105	0.000	4.847	0.130	18.229	15.278	0.140	43.104	0.998	K&M, TESS	No	Yes	1.044	2610	125	0.1	b'AACC'	b'00nn'
103	595786357085040640	129.250	7.085	209.235	0.061	4.753	0.095	17.419	14.603	0.076	32.267	1.015	NCJM, TESS C	No	Yes	0.893	208	100	0.1	b'AACC'	b'00nn'
104	2958907320740440960	76.343	-26.718	210.575	0.422	4.809	0.131	18.467	15.462	0.155	27.083	1.006	TESS	No	Yes	0.980	2613	125	0.1	b'AACC'	b'11nn'
105	6299151559192363776	217.050	-14.751	211.345	0.000	4.715	0.145	17.957	15.124	0.049	60.477	0.947	K&M, TESS	No	Yes	1.041	2605	125	0.1	b'AABC'	b'00nn'
106	5118730826393708288	35.981	-25.798	211.444	0.091	4.691	0.099	17.567	14.569	0.048	27.954	0.972	TESS	No	Yes	1.088	214	100	0.1	b'AACC'	b'11nn'

continued . . .

	GAIA DR3 Source ID	ra	dec	Dist (pc)	AEN	para (mas)	p err (mas)	g mag	j mag	red frac	pm (mas per yr)	ruwe	Remarks	Nebu Features	DS	Gvar	Mod	T_{DS}	γ	WISE ph_qual	WISE var_flag
107	4843191593270342656	59.016	-40.530	211.900	0.000	4.681	0.077	17.713	14.928	0.048	32.280	1.064	TESS	No	Yes	0.941	63287	275	0.1	b'AAAB'	00nn
108	3543734050861649408	175.360	-18.591	216.622	0.240	4.599	0.124	17.788	14.968	0.065	9.457	1.069	TESS	No	Yes	1.017	2601	125	0.1	b'AACC'	b'00nn'
109	4226700375674235136	311.829	-1.986	217.174	0.156	4.560	0.061	16.488	13.857	0.079	72.508	1.103	K&M, TESS C	No	Yes	0.828	188	100	0.1	b'AACC'	b'00nn'
110	5065248343140177536	42.947	-29.933	217.545	0.313	4.589	0.113	17.913	14.951	0.000	33.807	1.039	TESS	No	Yes	0.919	218	100	0.1	b'AACC'	b'11nn'
111	970166080613583232	92.862	49.824	217.829	0.000	4.571	0.078	17.203	14.516	0.139	67.288	0.971	K&M, TESS	No	Yes	0.838	204	100	0.1	b'AACC'	b'00nn'
112	5441348085110168960	158.933	-38.312	218.203	0.000	4.538	0.065	17.150	14.274	0.108	62.157	0.929	K&M, TESS	No	Yes	0.888	202	100	0.1	b'AACC'	b'00nn'
113	823662302309125504	151.784	49.088	220.890	0.000	4.494	0.128	18.203	15.193	0.049	108.252	1.034	NCJM, K&M, TESS	No	Yes	0.892	2607	112.5	0.1	b'AACC'	b'00nn'
114	1106405707419734528	101.744	69.649	221.016	0.219	4.491	0.085	17.447	14.837	0.094	29.148	1.068	TESS	No	Yes	0.892	4977	162.5	0.1	b'AABC'	b'11nn'
115	5086043990671838720	51.059	-24.845	221.568	0.519	4.491	0.146	18.153	15.059	0.125	35.706	1.138	TESS	No	Yes	0.906	219	100	0.1	b'AACC'	b'11nn'
116	6817461546684629888	324.747	-22.188	221.902	0.097	4.488	0.075	16.888	14.360	0.069	75.630	1.033	K&M, TESS C	No	Yes	0.835	196	100	0.1	b'AACC'	b'11nn'
117	3634795878750939776	199.077	-5.804	221.961	0.172	4.503	0.142	17.849	14.936	0.143	58.313	1.033	TESS, K&M	No	Yes	0.960	216	100	0.1	b'AACC'	b'11nn'
118	2113794336847287040	270.844	42.592	223.214	0.123	4.472	0.100	18.057	15.171	0.088	19.966	1.020	NCJM, TESS	No	Yes	0.999	220	100	0.1	b'AACC'	b'11nn'
119	2152693481986456960	270.571	59.961	223.447	0.409	4.438	0.113	18.329	15.230	0.074	24.799	1.008	TESS	No	Yes	1.047	2609	125	0.1	b'AABB'	b'11nn'
120	2154062850702747904	280.844	57.205	231.994	0.420	4.310	0.116	18.310	15.329	0.087	26.567	1.031	TESS	No	Yes	0.906	223	100	0.1	b'AACC'	b'11nn'
121	5458954908402727936	153.397	-33.713	232.039	0.000	4.255	0.108	17.827	14.767	0.174	39.183	0.987	TESS	No	Yes	0.925	214	100	0.1	b'AACC'	b'00nn'
122	6755031658716353024	298.999	-26.020	233.059	0.000	4.275	0.122	17.665	14.993	0.117	23.437	0.968	TESS	No	Yes	0.862	2594	125	0.1	b'AACC'	b'11nn'
123	2365292026675460352	3.634	-19.493	234.597	0.000	4.221	0.083	16.969	14.166	0.037	31.769	1.006	NCJM, TESS	No	Yes	0.838	195	100	0.1	b'AACC'	b'00nn'
124	915612711689028352	126.028	42.136	235.036	0.000	4.221	0.095	17.071	14.376	0.073	65.117	0.926	K&M, TESS	No	Yes	0.953	198	100	0.1	b'AACC'	b'21nn'

continued . . .

	GAIA DR3 Source ID	ra	dec	Dist (pc)	AEN	para (mas)	p err (mas)	g mag	j mag	red frac	pm (mas per yr)	ruwe	Remarks	Nebu Fea-tures	DS	Gvar	Mod	T_{DS}	γ	WISE ph_qual	WISE var_flag
125	6294757704570139264	208.861	-16.576	235.184	0.279	4.236	0.104	17.262	14.549	0.143	34.485	1.212	TESS	No	Yes	1.087	201	100	0.1	b'AACC'	b'00nn'
126	3473317958963571840	184.297	-29.363	236.078	0.000	4.233	0.122	17.407	14.532	0.134	7.809	0.984	TESS	No	Yes	0.858	202	100	0.1	b'AACC'	b'33nn'
127	3190924756901443328	64.499	-11.189	236.138	0.000	4.213	0.119	17.590	14.651	0.070	18.925	0.988	TESS	No	Yes	1.005	205	100	0.1	b'AACC'	b'11nn'
128	6818973272093697280	331.425	-22.564	238.803	0.000	4.198	0.127	17.920	15.059	0.000	7.243	0.971	TESS	No	Yes	0.961	2601	125	0.1	b'AACC'	b'00nn'
129	4689531029378339840	5.624	-72.634	239.147	0.000	4.153	0.078	17.693	14.938	0.277	28.348	1.016	TESS	No	Yes	0.918	209	100	0.1	b'AACC'	b'01nn'
130	2435392417000825984	355.478	-10.457	239.235	0.000	4.138	0.136	17.957	14.965	0.091	29.303	0.979	NCJM, TESS	No	Yes	0.889	2600	125	0.1	b'AACC'	b'00nn'
131	6402749267044915840	327.223	-63.652	241.404	0.112	4.110	0.052	16.799	14.069	0.075	46.922	1.016	K&M, TESS	No	Yes	0.867	191	100	0.1	b'AACC'	b'11nn'
132	1005962056045974912	90.703	61.382	241.702	0.000	4.088	0.082	17.305	14.516	0.185	9.111	0.977	TESS	No	Yes	0.881	202	100	0.1	b'AACC'	b'00nn'
133	101027079730076544	34.710	23.676	243.475	0.000	4.052	0.128	17.765	14.864	0.085	25.080	0.959	TESS	No	Yes	1.101	4980	150	0.1	b'AACC'	b'00nn'
134	4674754658232078848	66.974	-66.177	243.654	0.349	4.066	0.099	18.321	15.486	0.089	14.455	0.993	TESS	No	Yes	0.957	2606	125	0.1	b'AACC'	b'00nn'
135	4714834812001755648	31.501	-59.289	247.801	0.156	3.992	0.089	17.850	14.828	0.111	61.822	1.097	K&M, TESS	No	Yes	1.039	2595	125	0.1	b'AABB'	b'00nn'
136	3176818022716814720	64.244	-13.865	249.287	0.152	3.990	0.071	17.047	14.268	0.035	54.700	1.056	TESS, K&M	No	Yes	1.001	195	100	0.1	b'AACB'	b'11nn'
137	6412717744403679744	331.949	-56.250	250.235	0.000	3.960	0.059	16.829	14.305	0.060	24.511	0.978	TESS	No	Yes	0.835	192	100	0.1	b'AACB'	b'00nn'
138	1117427693010918400	135.084	68.930	250.689	0.000	3.912	0.101	17.740	14.827	0.000	25.570	1.007	TESS	No	Yes	1.430	205	100	0.1	b'AACC'	b'00nn'
139	4898684774054542208	68.892	-21.411	251.546	0.206	3.922	0.079	17.376	14.712	0.098	7.739	1.058	TESS	No	Yes	0.898	201	100	0.1	b'AACC'	b'00nn'
140	5057336772862673152	52.250	-28.840	253.165	0.000	3.905	0.106	18.009	15.146	0.043	17.741	1.034	TESS	No	Yes	0.893	215	100	0.1	b'AACC'	b'00nn'
141	1566609769556349824	197.882	58.258	253.882	0.000	3.877	0.073	17.490	14.633	0.048	7.909	0.994	TESS	No	Yes	1.016	202	100	0.1	b'AACC'	b'01nn'
142	5083549374883972992	57.554	-25.108	256.147	0.000	3.860	0.074	17.403	14.660	0.063	24.948	1.018	TESS	No	Yes	0.901	199	100	0.1	b'AACC'	b'21nn'
143	5138097894788103424	31.127	-18.926	257.139	0.000	3.854	0.104	17.675	14.934	0.071	41.580	0.970	K&M, TESS	No	Yes	0.897	204	100	0.1	b'AACC'	b'00nn'
144	1082166694409052288	118.331	57.121	258.204	0.000	3.829	0.112	17.766	14.997	0.100	41.675	0.995	K&M, TESS	No	Yes	0.857	2591	125	0.1	b'AACC'	b'11nn'

continued . . .

	GAIA DR3 Source ID	ra	dec	Dist (pc)	AEN	para (mas)	p err (mas)	g mag	j mag	red frac	pm (mas per yr)	ruwe	Remarks	Nebu Features	DS	Gvar	Mod	T_{DS}	γ	WISE ph_qual	WISE var_flag
145	5468611605493851264	156.212	-27.707	258.610	0.000	3.868	0.123	17.991	15.278	0.167	28.624	0.980	TESS	No	Yes	0.939	2598	125	0.1	b'AACC'	b'00nn'
146	2667886899474087680	326.464	-6.459	260.751	0.337	3.786	0.123	17.527	14.646	0.118	18.743	0.951	TESS	No	Yes	0.906	203	100	0.1	b'AACC'	b'00nn'
147	1922953478004114816	359.286	44.125	262.312	0.224	3.801	0.121	17.857	14.926	0.156	31.587	1.045	TESS	No	Yes	0.852	205	100	0.1	b'AACC'	b'00nn'
148	6592971302704572288	326.779	-31.137	263.809	0.000	3.760	0.079	17.091	14.407	0.029	12.922	0.941	TESS	No	Yes	0.932	193	100	0.1	b'AACB'	b'00nn'
149	1875560270535342592	336.203	23.260	265.185	0.253	3.747	0.107	17.583	14.815	0.076	22.791	1.044	NCJM, TESS	No	Yes	0.876	203	100	0.1	b'AACC'	b'11nn'
150	133263046965499392	38.598	31.670	266.549	0.127	3.709	0.073	16.939	14.328	0.112	13.769	1.018	TESS, LAMOST	No	Yes	0.865	188	100	0.1	b'AACC'	b'00nn'
151	858610318053921920	176.861	59.892	268.280	0.436	3.646	0.082	17.413	14.640	0.073	23.045	1.085	TESS	No	Yes	1.006	198	100	0.1	b'AACC'	b'11nn'
152	1623882363879075200	245.566	58.807	269.360	0.244	3.669	0.109	18.446	15.422	0.093	10.242	0.988	TESS	No	Yes	0.890	218	100	0.1	b'AACC'	b'00nn'
153	2480882305418201856	23.396	-4.029	270.901	0.418	3.688	0.122	17.534	14.711	0.025	62.976	1.132	K&M, TESS C	No	Yes	0.953	199	100	0.1	b'AACC'	b'11nn'
154	2437221214075471744	354.011	-9.333	272.107	0.210	3.681	0.112	17.312	14.765	0.000	28.321	1.014	TESS	No	Yes	0.875	2582	125	0.1	b'AACB'	b'00nn'
155	1390217593013664512	234.411	41.442	272.428	0.459	3.624	0.119	18.204	15.302	0.089	22.269	1.034	TESS	No	Yes	0.998	215	100	0.1	b'AACC'	b'01nn'
156	4851401543515220736	49.477	-41.304	274.254	0.000	3.593	0.095	18.008	15.018	0.093	17.698	0.988	TESS	No	Yes	0.849	2595	137.5	0.1	b'AABB'	b'11nn'
157	6783520279866548480	322.007	-31.786	274.906	0.000	3.597	0.093	16.902	14.217	0.029	32.911	0.976	TESS	No	Yes	0.833	187	100	0.1	b'AACB'	b'11nn'
158	4932875462509521280	13.405	-48.492	275.717	0.000	3.597	0.076	17.474	14.720	0.030	82.362	0.972	K&M, TESS	No	Yes	0.986	198	100	0.1	b'AACC'	b'11nn'
159	3929437305341869056	194.689	12.620	275.741	0.000	3.548	0.083	16.998	14.249	0.000	41.018	0.989	K&M, TESS	No	Yes	0.921	190	100	0.1	b'AACC'	b'11nn'
160	2478471596110203008	20.161	-7.177	278.444	0.000	3.524	0.087	17.137	14.349	0.138	51.926	1.022	NCJM, K&M, TESS	No	Yes	1.123	2575	125	0.1	b'AABB'	b'11nn'
161	2966133315455819648	86.805	-20.128	283.725	0.000	3.454	0.068	17.149	14.358	0.099	18.139	0.987	TESS	No	Yes	0.878	190	100	0.1	b'AACC'	b'00nn'
162	5112579608592599680	55.008	-14.308	284.664	0.000	3.469	0.059	16.860	14.259	0.032	25.304	0.947	TESS	No	Yes	0.864	85782	325	0.1	b'ABCC'	b'0nnn'
163	1050495536848847360	145.782	59.436	286.832	0.260	3.439	0.076	17.229	14.632	0.026	21.279	1.097	TESS	No	Yes	0.822	192	100	0.1	b'AACC'	b'00nn'

continued . . .

	GAIA DR3 Source ID	ra	dec	Dist (pc)	AEN	para (mas)	p err (mas)	g mag	j mag	red frac	pm (mas per yr)	ruwe	Remarks	Nebu Features	DS	Gvar	Mod	T_{DS}	γ	WISE ph_qual	WISE var_flag
164	2159638130570202880	278.512	61.584	290.555	0.311	3.359	0.100	18.021	15.183	0.102	22.791	1.017	TESS	No	Yes	0.917	205	100	0.1	b'AACB'	b'11nn'
165	2903767607178651776	85.357	-30.960	290.673	0.089	3.441	0.113	18.185	15.440	0.045	23.408	1.031	TESS	No	Yes	0.937	473	100	0.2	b'AACB'	b'11nn'
166	1020168880146788736	145.222	52.265	296.473	0.000	3.317	0.081	17.329	14.683	0.023	25.186	0.964	TESS	No	Yes	0.827	191	100	0.1	b'AACC'	b'11nn'